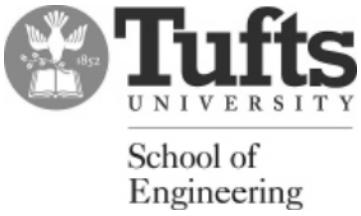

INVESTIGATION OF MICROPUNCHING HOLES IN ARTICULAR CARTILAGE FOR APPLICATIONS IN TISSUE ENGINEERING

A thesis submitted by

Theodore W. Vandenberg

In partial fulfillment of the requirements

for the degree of

Master of Science

In

Bioengineering

TUFTS UNIVERSITY

May 2015

Adviser:

Thomas P. James

Associate Professor of Mechanical Engineering

Abstract

Articular cartilage degeneration is a central pathological feature of osteoarthritis. Cartilage in the adult does not regenerate *in vivo* and, as a result, cartilage damage in osteoarthritis is irreversible. With our ever-aging population, osteoarthritis has become a leading cause of disability and unfortunately, no optimal treatments for osteoarthritis are currently available. To address this problem, a research community is focused on the development of both natural and synthetic biodegradable tissue scaffolds. The scaffolds must contain depressions or holes for the purpose of chondrocyte seeding and growth in order to create an implantable construct. Scaffolds also contain artificial microtubules to enhance nutrient diffusion during early cellular development.

In addition to chondrocytes, cartilage tissue consists of the extracellular matrix (ECM). Studies of many tissue types have established that ECM plays an important role in regulating cell behavior and controlling processes such as tissue differentiation and tumor progression. Unlike most natural tissues, adult cartilage ECM is exceptionally dense and lacking in vascularity, which makes it difficult for chondrocytes to be transplanted directly into the matrix. Current methods of creating cell home sites through chemical decellularization of the ECM degrade the mechanical integrity of the cartilage tissue.

The research conducted in this study used a mechanical, rather than chemical, method to create cell home sites. A novel micropunching machine was developed to fabricate 200 μm diameter holes in cartilage, thereby creating a porous natural scaffold while maintaining a healthy ECM. Equine articular cartilage slices were harvested from the cadaver's back knee joint and cryo-sectioned into 100 μm thick slices. Using various die clearances and hydration levels, micro-scale holes were mechanically punched in cartilage tissue.

The maximum force required to punch a hole in the cartilage sample was shown to have a relationship to both clearance of the die and hydration level of the sample. As the die clearance increased, the maximum punching force (MPF) decreased. In addition, as a sample dried out the MPF increased. However, the failure mechanism changed for the different levels of hydration. Saturated samples failed in tension, while dry samples failed in shear, producing larger resulting hole sizes. Upon inspection, a 200 μm punch produced 50 μm holes in saturated and hydrated samples, with fibers extending into the hole. In dry samples, a 200 μm punch produced 200 μm holes with smooth hole walls. An analytical model was developed to predict MPF based on the hydration level of the sample and the diameter of the male punch.

The Young's moduli of both porous (micropunched) and nonporous samples were not found to be significantly different at 4% porosity. Yield occurred at strain levels much higher than those encountered for in vivo cartilage. Therefore, results indicate that porous samples maintain their mechanical properties for successful cell culture and integration in vivo.

A preliminary cell culture study indicated that seeded cells can position themselves in the micro-holes and along the walls of the holes to successfully take advantage of the three-dimensional architecture. The results of this research indicate that a micropunching process is adequate to create holes in natural cartilage tissue for the purpose of seeding progenitor cells and eventual fabrication of a tissue implant.

Acknowledgements

First and foremost I would like to thank my family for their support and guidance throughout my life. I would like to thank my thesis advisor, Professor Thomas James. His guidance and advice have made this research possible. I also want to thank Eric Schmitt; he along with Professor James created the micropunching machine that was the key to this project. I owe Dr. Li Zeng and Roshni Rainbow much thanks for leading the research in cell seeding. I would like to thank Professor Lauren Black for allowing me access to his lab and Lauren Baugh for helping with the sectioning of the cartilage samples. I want to thank Dr. Jason Moore for his guidance in the modeling of the punching force of cartilage and hosting me in his lab. Andrew Barnett also was of huge help in developing this model and performing the literature search. Chris Nehme was immensely helpful in conducting the force measurement trials, taking SEM pictures, and providing overall guidance and support throughout the research. Finally, I want to thank David Sutherland for his help in the preliminary research in the feasibility of micropunching the cartilage samples and the best choice of materials.

Contents

List of Figures

List of Tables

1 Introduction

1.1 Background:

Articular cartilage degeneration is a central pathological feature of osteoarthritis [1]. Cartilage is an avascular tissue in mature animals and as a result it is unable to regenerate, causing cartilage damage associated with osteoarthritis to be irreversible [2, 3]. As the median population of the United States ages, the number of cases of osteoarthritis and associated primary total knee arthroplasty (total joint replacement) is increasing [3]. An intervention to replace worn cartilage could prevent or delay the need for arthroplasty as the condition worsens.

Tissue engineering is a field of research that focuses on regenerative medicine [4]. A longstanding goal of tissue engineering is to develop and grow implantable tissue *in vitro* (outside of the human body) that is indistinguishable from native tissue. Previous efforts to engineer cartilage through seeding cells in a natural or synthetic scaffold have had varying degrees of success, but to date none of the methods has consistently created a durable articular surface [5].

Cartilage repairs are currently attempted by a variety of implant methods, such as perichondrial or osteochondral autografts (derived for the patient's own tissue) or by implanting osteochondral allografts (tissue taken from another person). In addition, repairs can be made by biopsy of healthy cartilage to isolate chondrocytes (cartilage forming cells) that are subsequently cultivated and replicated prior to implanting for regeneration of damaged sites. However, there are many issues associated with each of these contemporary methods of cartilage repair: (1) cartilage implants, including perichondrial and osteochondral grafts, are difficult to affix to the repair site, (2) chondrocytes taken from autografts produce a second defect at the donor site, (3) perichondrial autografts initiate the production of a fibrous replacement tissue, which is

unlike native cartilage, (4) chondrocytes implanted alone have a 28-61% failure rate, and (5) repairs by each of these methods have been shown to degenerate over time [6]. Thus, research is required to invent new methods of cartilage repair.

The research challenge is to engineer a cartilage implant that contains living chondrocytes and is capable of integrating and adapting to surrounding native cartilage. The implant must be composed of materials that will promote the formation of cartilage tissue, such as natural extracellular matrix (ECM), and initially contain sufficient micro-vascularity to provide the diffusion of oxygen and nutrients to promote cellular growth.

1.2 Structure of Cartilage

Cartilage is a viscoelastic composite material with varying micro-scale characteristics. It provides excellent load carrying capability and low friction between mating joint surfaces. The complexity of the porous structure makes it difficult to create an artificial matrix that mimics the mechanical properties of native tissue. Therefore, natural cartilage ECM is an attractive material to be used as a tissue scaffold when engineering an implantable construct. In addition, natural ECM provides the correct three-dimensional micro-architecture and biochemical composition for growing cells [7].

Saturated cartilage is approximately 70% water. The remaining ECM consists of Type II collagen and proteoglycans, with a low concentration of chondrocytes. The chondrocytes reside in spherical voids (lacunae). Presently, a chemical process is used to remove chondrocytes from their lacunae to prepare new home sites for cell seeding and to prevent a host immunological response. Unfortunately, the chemical process is not 100% effective and it degrades the collagen matrix, generally compromising its mechanical properties [8,9,10].

1.3 Problem Statement

Cartilage ECM is comparatively dense and uniquely avascular, resulting in a low rate of diffusion of nutrients and waste products. For this reason, *in vitro* growth of thickened sections (three dimensional) has been a persistent challenge. Cells on the surface of a tissue scaffold are normally healthy, but cells within the center of a thickened scaffold are difficult to keep alive due to a lack of nutrient diffusion. Thus, it would be advantageous to culture cells in thin scaffolds that provide a three dimensional environment for cell adhesion and growth while providing sufficient nutrient diffusion.

An approach taken by Schmitt et al. was to use a micropunching machine to create porous 2D membranes from biocompatible, biodegradable polymers that can be aligned, stacked, and bonded to create 3D tissue scaffolds. The engineered scaffolds are designed to contain sufficient home sites for cell seeding and microtubules for nutrient diffusion [11]. Schmitt demonstrated that 200 μm diameter holes could be punched in 30-40 μm thick polycaprolactone (PCL) membranes by a new cryogenic micropunching process [12].

The aim of this thesis is to repurpose the micropunching machine developed by Schmitt to create micro-holes in natural, cartilage ECM. These micro-holes will be used for home sites for chondrocyte seeding and growth. In addition, the mechanics of the punching process will be investigated.

1.4 Research Objectives

i) Utilizing a steel gage pin for a male punch and a female die with laser cut holes, investigate the ability to micropunch 200 μm holes in slices of cartilage ECM with a thickness of 100 μm;

ii) Determine the force-stroke profile and peak punching force during micropunching 200 μm holes in cartilage ECM with various die clearances;

iii) Determine peak punching force during micropunching 200 μm holes in cartilage ECM during various states of water hydration (dry, hydrated, and saturated states);

iv) Develop an analytical model to predict peak micropunching forces at each hydration level and make comparisons to experimental results (determine a sample size for statistical significance);

v) Compare the mechanical properties of punched cartilage ECM with those of unpunched ECM using compression testing; and

vi) Investigate the ability of current seeding methods to position chondrocytes in punched cartilage ECM's micro-holes and along the walls of these holes.

2 Survey of Literature

2.1 Micropunching

Punching is a process that has been researched in depth at the macro-scale. However, micropunching is a new field in which few studies have been conducted examining the fabrication of micro-holes, which in general is defined to mean holes with a diameter less than half a millimeter (500 μm). A typical setup to punch a single round hole has a male punch and a female die arranged as shown in Fig. 2.1. The difference in radii between the female die hole and the male punch is defined as die clearance. The percent die clearance is defined as radial die clearance divided by workpiece thickness.

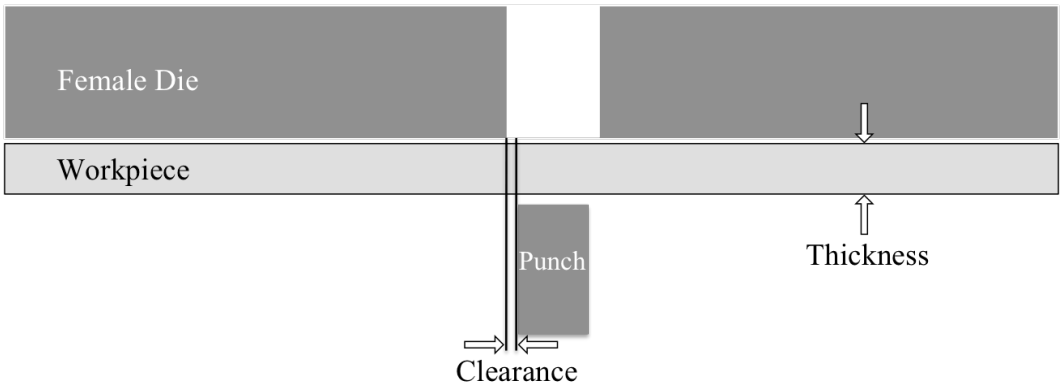

Figure 2.1: Micropunching setup and terminology

In 2001, Joo et al. designed a micro-punching system capable of successfully creating 100 μm diameter holes in 100 μm thick brass foil [13]. They used tungsten carbide for the male punch, machined by a grinding process, and the female die was made using micro-electro-discharge machining (micro-EDM). In addition to the punch and die, Joo included a stripper plate, which is a part of the die tooling that surrounds the punch and helps to align and guide it into the female die hole while holding the workpiece in place [13]. While there are benefits in using a stripper plate to align the die sets, it increases the effective length of the punch. This is undesirable as it is challenging

to manufacture high aspect ratio micro-punches, where punch length is sufficiently larger than the punch diameter.

Joo et al. extended their research in 2005 by removing the stripper plate, and instead used high precision linear motors to guide the male punch into the hole of the female die. To ensure that the punch was aligned with the hole, a mirror was placed at an angle to the side of the machine, allowing a microscope to view the alignment process, Fig. 2.2. With this arrangement, they successfully punched 25 μm, 50 μm, and 100 μm diameter holes in brass and stainless steel foils from 25 μm to 100 μm thick, keeping the thickness to hole diameter ratio equal to 1.0 [14].

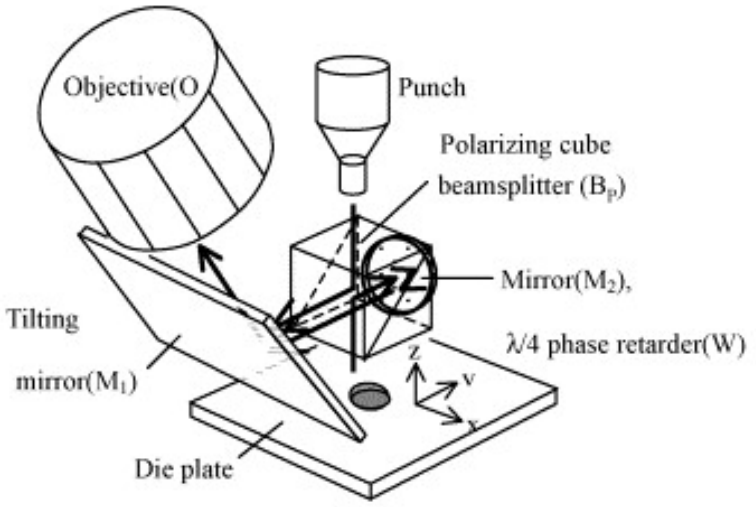

Figure 2.2: Mirror and microscope setup to ensure alignment of male punch in micropunching machine designed by Joo et al. [14]

A novel micropunching machine, designed by Schmitt [15] in 2013, inverts the typical die arrangement, fixing the female die in place above the male die. This allows direct alignment by utilizing a microscope without a mirror to align the male and female die halves by peering through the hole in the female die as the male punch is raised into position, Fig. 2.3.

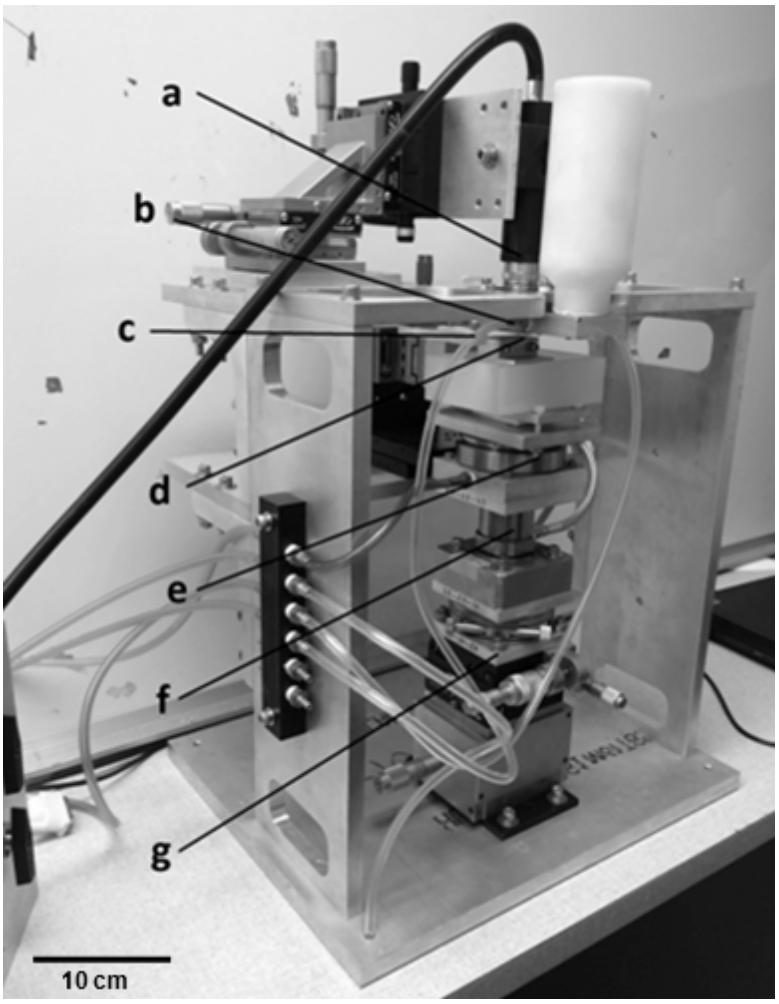

Figure 2.3: Custom micropunching machine used to create holes in cartilage tissue (a) Microscope, (b) Female die holder, (c) Vacuum tube, (d) Male punch holder, (e) Spherical bearing, (f) Force dynamometer, (g) X, Y, Z and θ staging

In the research by Schmitt, 30-40 μm thick polycaprolactone (PCL) membranes were punched with a 200 μm diameter stainless steel gage pin (punch). The female dies were fabricated by laser cutting a 150 μm stainless steel sheet. Typically, an array of 16 progressively larger holes was cut to investigate the effect of die clearance on hole quality.

2.2 Tissue Engineering

Tissue engineering is a rapidly growing field of research that focuses on regenerative medicine. The longstanding goal of tissue engineering is to develop and grow an implantable tissue *in vitro* that is indistinguishable from native tissue, in order to restore, repair, or replace degraded tissues in the body [15,16]. The first attempt at tissue engineering occurred in the 1980's. Eugene Bell first created a bi-layered skin graft. His approach was to use a collagen matrix, seeded with autologous skin fibroblasts. It was not successful when used as a skin graft, but it was and is currently used to treat venous ulcers. Bell, as a result, established the field of tissue engineering [17].

Many approaches have previously been used, but the most common method involves a scaffold, cells, and a bioreactor. Cells are seeded in a scaffold and cultured in a bioreactor *in vitro* before being implanted in a patient. This process is depicted in Fig. 2.6 [18]. A scaffold is a material that can act as an artificial ECM to hold the implanted cells while they differentiate and begin to produce native ECM. It provides attachment sites and mechanical support for cells while they grow and develop [17,19].

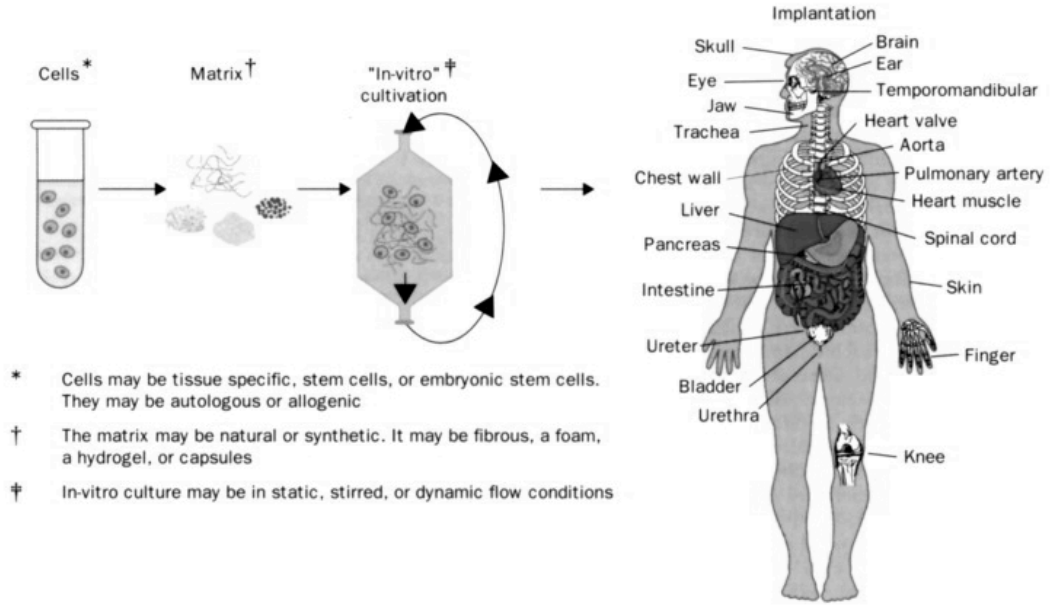

Figure 2.4: Tissue engineering overview [18]

The ideal scaffold would have an identical three-dimensional micro-architecture and biochemical composition as the tissues native ECM [7]. Part of the micro-architecture includes having an interconnected porous network to facilitate transportation of nutrients and metabolic waste. Next, the scaffold must be biodegradable and bioresorbable without causing an adverse immune response so that host cells can safely digest the scaffold as fresh ECM is produced. Finally, the scaffold must have identical mechanical properties to that of the native tissue at the implant site in order to provide sufficient temporary mechanical support for the cells until they deposit enough natural ECM to support their growth [15,17,19,20,21].

Most contemporary scaffolds have been made from synthetic materials, mainly polymers, such as poly(ethylene glycol) (PEG), polylactic acid (PLA), polyglycolic acid (PGA), polylactic-co-glycolic acid (PLGA), and poly(ethylene glycol)-diacrylate (PEGDA) [15,17,20,22]. Recently, however, many researchers are moving away from synthetic scaffolds and focusing on natural materials, including collagen, hyaluronic acid, and silk [23]. A benefit of scaffolds made from natural materials is they typically do not have the issue of biocompatibility.

2.3 Structure of Cartilage

Cartilage is a structural tissue found throughout the bodies of all animals. There are many different kinds, but the focus of this research is on hyaline articular cartilage, which covers the ends, or articular surfaces, of the bones in synovial joints. Synovial joints are characterized by being enclosed in a fibrous tissue capsule, which is filled with synovial fluid, Fig. 2.7 [24]. Hips, knees, and elbows are all examples synovial joints [10].

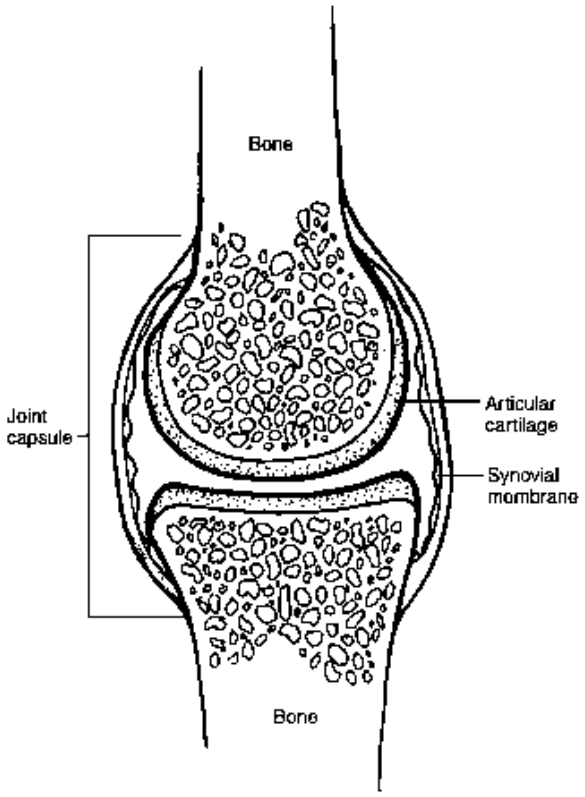

Figure 2.5: Cross-section of a synovial joint, showing the articular cartilage-bone interface [10]

The articular cartilage covering the medial femoral condyle of an adult, human knee is approximately 2.2 mm thick [25]. Its main function is to distribute loads on the joint in order to prevent injury to the underlying bone. It also aids in the smooth sliding motion between the bones as joint movement occurs. Articular cartilage must be durable to withstand the constant sliding motion as well as the constant loading of the knee [26]. In addition, it must be pliable in compression to distribute the load. A unique aspect of cartilage is that it demonstrates anisotropic properties in tension. Cartilage is strong in tension when it is pulled parallel to the collagen fibers, the major component of its ECM. However, when pulled perpendicular to the collagen fibers, cartilage is much weaker [10,27,28].

Cartilage ECM is a composite material that gives the tissue its mechanical properties [26]. Approximately 70% to 85% of cartilage weight is water, but the water concentration varies with the depth, from the surface of the tissue. Once the water is removed, about 60% to 70% of the dry weight is collagen. Of the many different types of collagen, cartilage consists of Type II, Type VI, Type IX, and Type XI, though Type II makes up about 90-95% of the collagen in articular cartilage. It is responsible for providing the mechanical strength of the ECM.

The collagen fibers grow in layers called leaves, which vary in orientation from the surface to the subchondral layer [21,26,29]. At the deep layers of cartilage, near the cartilage-bone transition, the collagen leaves are oriented perpendicular to the surface of the bone, but near the articular surface, the leaves curve and begin to grow parallel to the surface. The boundaries between the collagen leaves are known as split lines and are depicted in Fig. 2.8 [30]. The orientation of the collagen leaves parallel to the surface provides the compressive characteristics of cartilage and the perpendicular orientation of the leaves in the deeper levels gives cartilage its resistance to shear at the cartilage-bone interface.

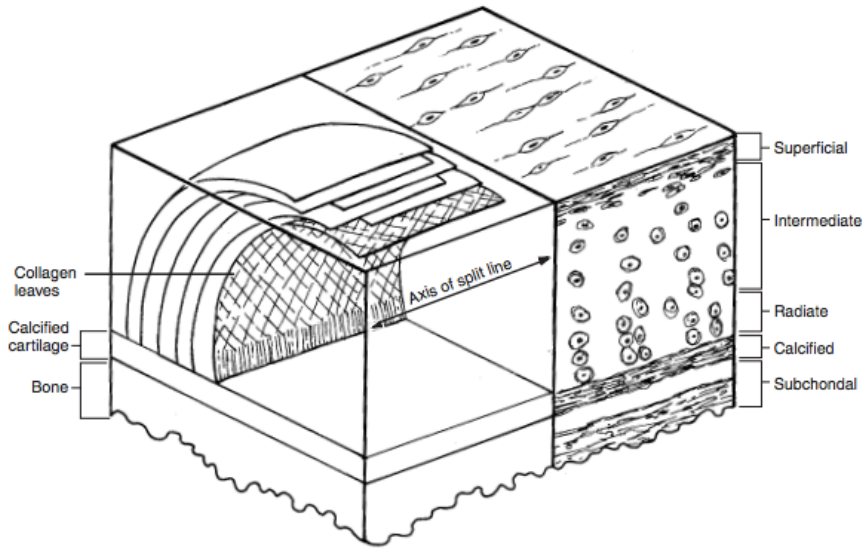

Figure 2.6: Cross-section of articular cartilage demonstrating cell density and collagen leaf orientation for the different zones [10]

The final major component of articular cartilage is proteoglycans. They make up about 30% of the dry weight. Proteoglycans consist of a protein core with glycosamioglycans (GAGs) attached to the core. The GAGs' negative charges are responsible for the binding of growth factors and the high levels of hydration throughout the tissue by promoting the retention of water [21,24].

Chondrocytes are the only type of cell present in cartilage tissue. The tissue as a whole has a low level of metabolic activity due to low cell density (only about 1% of the volume of the tissue), but each chondrocyte has a high metabolic rate, similar to that of cells in vascular tissue [19,26]. The chondrocytes are responsible for generating and maintaining the proteins that form cartilage ECM. The ECM of cartilage is extremely dense and surrounds the cells, thus there is no cell-to-cell contact throughout the tissue. The ECM also protects the chondrocytes during normal tissue use [26].

Mature cartilage is an avascular tissue, thus the chondrocytes depend on diffusion to receive the nutrients needed. Convection is caused by tissue deformation from joint loads, which aids the diffusion process, but diffusion distances can still be up to several millimeters. However, immature, developing cartilage has a higher need for nutrients and has been found to contain vessels, called cartilage canals, that originate from the abaxial perichondrium and curve upwards towards the articular surface. Ytrehus et al. found that cartilage canals were present in juvenile porcines [2]. They took cross sections of the articular cartilage in porcines at ages 7, 11, 13, and 15 weeks. As can be seen in Fig. 2.9, cartilage canals are clearly present in porcines at 7 weeks, and have noticeably regressed by 15 weeks. This study found that the regression of the cartilage canals is solely age-dependent.

As discussed, the microstructure and biochemical composition of cartilage vary with depth. Thus, it is convenient to refer to cartilage as being composed of different zones. The four zones, starting from the articular surface and moving towards the

underlying bone, are the superficial zone, the middle or intermediate zone, the deep or radial zone, and the calcified cartilage zone [26]. These zones are shown in Fig. 2.8.

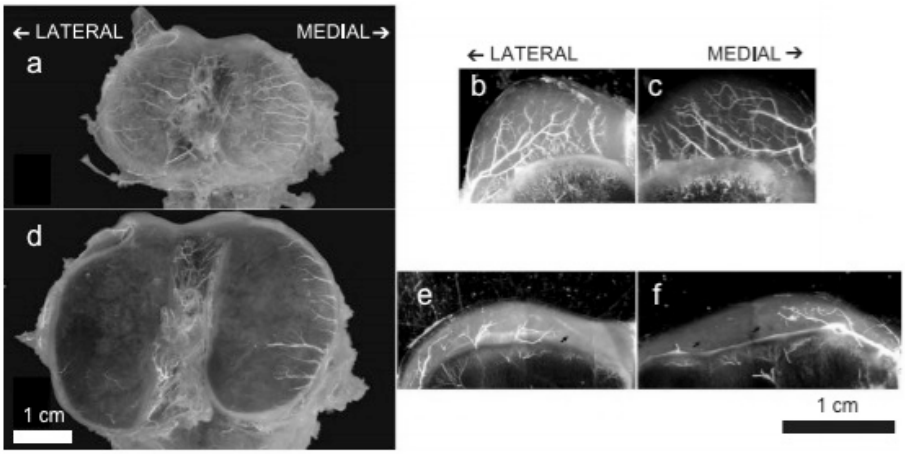

Figure 2.7: Views of cartilage canals (a and d) Femoral articular surface of 7 and 15 week old porcine respectively, (b, c and e, f). Cross sectional view of femoral condyles in a 7 and 15 week old porcine respectively [2].

Though cartilage is described as being in zones, there are no distinct boundaries between each. Instead, it is a more gradual transition from one to the next. The first zone, at the articular surface, is the superficial zone. It is the thinnest zone, but it is responsible for the specialized mechanical properties of cartilage. Cartilage shows greater tensile stiffness and strength at the superficial zone than at the deeper zones [26]. At this zone, the collagen fibers are much finer than in the deeper zones and the split lines are oriented parallel to the articular surface [30]. The collagen leaves actually form two layers within the superficial zone. The top layer, called the lamina splendens, is a thin layer of fine collagen fibrils that covers the articular surface and contains no cells. The second layer contains chondrocytes that are flattened to an ellipsoid shape and lay parallel to the surface, as can be seen in Fig. 2.8 [26]. The ECM as a whole in the superficial zone has the highest water content and the highest permeability. This allows

for the water in the matrix to be squeezed out easily during an impact load to aid in the lubrication of the joint [31].

The next zone is the intermediate zone. According to Mansour, the orientation of the collagen fibers in this zone remains controversial [10]. However, it is established that the morphology and biochemical composition of this zone are between those of the superficial zone and the next zone, the radial zone.

In the radial zone, the collagen fibrils have the largest diameter and are packed in tight bundles. They form a network that surrounds the chondrocytes [30]. In this zone the concentration of water is the lowest throughout the tissue. The chondrocytes are spheroidal and oriented perpendicularly to the articular surface, and they are much more active in producing collagen and proteoglycans than in the superficial zone [26]. The permeability in the radial zone is also much lower than in the superficial zone [31].

The final zone is the calcified cartilage zone. This region acts as a transition between the radial zone and the subchondral bone. The chondrocytes in this zone are smaller in volume than in the radial zone and have a very low metabolic rate [26]. The collagen leaves are oriented perpendicularly to the articular surface, like in the radial zone, and the collagen fibers are also packed in tight bundles [30].

Most of the defects in cartilage occur at the superficial zone or at the surface, thus the focus of this research and the cartilage harvested for micropunching is in the superficial zone. Adult articular cartilage does not have the ability to repair any significant structural damage [16]. One reason is that mature cartilage is avascular. Lesions fail to heal because of a lack of blood supply and because of a lack of self-repair capacity [15]. It has been shown that if a defect encompasses a major portion (an area with a diameter greater than 3 mm) of the articular surface, it may progress further to degeneration of the joint and osteoarthritis [32].

2.4 Osteoarthritis

Osteoarthritis is the degeneration of articular cartilage, leading to pain and loss of normal joint function [10,16]. It is one of the leading causes of disability in developed countries [33]. In the United States, it is only behind cardiovascular disease for the most common cause of disability [34]. Studies have shown that it is most prevalent in the elderly population; about 80% of people over 65 years old report having osteoarthritis, and nearly 100% of people over 80 report having it. However, it is uncommon to be found in people under 40 years old [35,36].

Osteoarthritis progresses over three stages, taking several years to develop. First, the cartilage matrix is disrupted or altered due to abnormal loading of the joint, such as a high impact or torsional loading, or the repetitive loading over many years. This causes the water content to rise, thus increasing the permeability and decreasing the stiffness of the matrix, making the tissue more vulnerable to additional mechanical damage [16]. Next, the chondrocytes respond to the damaged tissue. They begin to proliferate and generate and degrade ECM macromolecules to remodel the matrix. This can last for years and sometimes restores the tissue back to health or maintains the level of damage without further degeneration. However, frequently the chondrocytes are not able to achieve this, leading to the third stage. This stage is marked by a decline in the response from chondrocytes. The rate of their synthesis of macromolecules decreases and there is progressive loss of tissue. This could be a result of the matrix being damaged and not protecting the chondrocytes, causing them to die. The treatment of isolated initial defects may help delay or prevent the development of osteoarthritis [10,16].

Currently, the best methods for cartilage defect repair have only been able to produce tissue that resembles but does not duplicate the structure, composition, or function of natural cartilage. This has been achieved by helping the chondrocytes restore the matrix through a few different methods: (i) the subchondral bone can be penetrated to

release blood and growth factors, (ii) a tissue graft taken from cartilage in another area of the joint, or another person, can be used, and (iii) chondrocytes can be taken from cartilage in another area of the joint, proliferated in vitro, and then implanted into the legion [6,16]. These methods have been shown to decrease the symptoms of osteoarthritis and improve joint function, but they do not provide a complete and permanent solution.

In addition to these attempts to repair cartilage, there have also been many attempts at tissue engineering cartilage. Most of these attempts use artificial polymeric scaffolds seeded with stem cells or chondrocytes. Many are then subjected to various mechanical stimulations, such as compression, while being cultured in bioreactors. However, none of these methods have been able to predictably restore a durable articular surface [16]. The issue is that cartilage is a complex tissue with a highly dense ECM, low cellular density, and no vascularization. Therefore, it is difficult to culture a three-dimensional tissue in vitro without the cells in the center of the scaffold dying due to insufficient nutrient and waste diffusion.

2.5 Comparison of Two and Three-Dimensional Matrices for Tissue Growth

In nature, cells grow in a three-dimensional ECM, but in many early tissue engineering attempts, cells were grown on flat two-dimensional collagen gels. Two-dimensional cell cultures have been studied extensively, as they are used for many purposes including cell culture and proliferation. Though cells can survive and expand on a two-dimensional polymer gel, issues arise. Normally, spherical cells flatten themselves on 2D cultures to attach to as much of the surface as possible. This behavior causes the cells to have an artificial polarity between the lower and upper surfaces of the normally non-polar cells [37]. There has been a recent move to create three-dimensional

scaffolds for tissue engineering purposes, but little is known about cell-matrix adhesions in three-dimensional matrices in vivo [37,38].

Three-dimensional cell culture conditions have been studied in vitro, and have been shown to provide attachment sites for the cells that more closely resemble the cell environment of developing tissues in vivo [15,20,37]. Hwang et al. compared embryonic stem cell cultures in various two-dimensional and three-dimensional matrices [20]. They found that Type IIA collagen was predominantly expressed in monolayer cultures, while Type IIB collagen was predominant in three-dimensional hydrogel matrices. Type II collagen is expressed in two forms, IIA and IIB. Type IIA collagen is synthesized in juvenile or prechondrogenic cells while Type IIB is expressed in adult or differentiated chondrocytes. Thus, these results suggest that three-dimensional cell cultures promote chondrogenic differentiation of embryonic stem cells [20]. Three-dimensional matrices have also been shown to increase the entrapment of ECM created by the developing cells in addition to enhancing cellular functional activities of cells when compared to 2D cultures, including cellular migration [15,20,37].

One of the most important roles of the ECM is to provide mechanical cues to the cells, whether it is to chondrocytes in cartilage tissue under compression, or to embryonic stem cells to cue their differentiation [26]. Hwang et al. reported that three-dimensional scaffolds transmit these signals to the cells, while two-dimensional scaffolds do not [15]. Therefore, 3D scaffolds appear to be more advantageous for tissue engineering cartilage.

2.6 Developing Three-Dimensional Tissue Scaffolds

Many techniques exist to design and fabricate a three-dimensional scaffold. Photomask-based and micromold-based methods involve cross-linking prepolymer solutions using various methods such as select exposure to UV light. Rapid prototyping-based methods involve creating a computer aided design (CAD) model that is then

created by various methods layer by layer; 3D printing can be used to achieve this. Finally, pores in polymer gels can be created by gas foaming: a process where a gas is introduced in the matrix and once the polymer solidifies, the gas diffuses out, leaving behind an interconnected pore network. Though all of these methods are capable of creating controlled microarchitectures, they all require the use of artificial polymers that subsequently biodegrade into biocompatible monomers [39].

Despite the fact that thick, three-dimensional scaffolds have been successfully created, it is not possible to culture chondrocytes in a thick scaffold. Newly developing chondrocytes need more nutrients than mature chondrocytes that have a lower level of cellular function. But due to the vascularity of cartilage, the newly developing chondrocytes in the center of the scaffold cannot obtain enough nutrients, leading to necrosis. Thus, a method must be created to provide a three-dimensional scaffold that allows all cells access to sufficient nutrients for development.

Bian et al. conducted a study examining different methods to decrease the diffusion distance required of nutrients for three-dimensional constructs [40]. Thick agarose hydrogel constructs, 2.34 mm thick, and thin constructs, 0.78 mm thick, were cultured under the same conditions. Thin constructs were found to have Young's and dynamic moduli twice that of thick constructs, significantly higher GAG and collagen content, and greater DNA content. In addition, the thin constructs had uniform mechanical properties throughout the depth of the tissue while the thick constructs had a softer central core. The uniform composition throughout the depth of the thin samples and the varying composition of the thick samples can be seen in Fig. 2.10 [40].

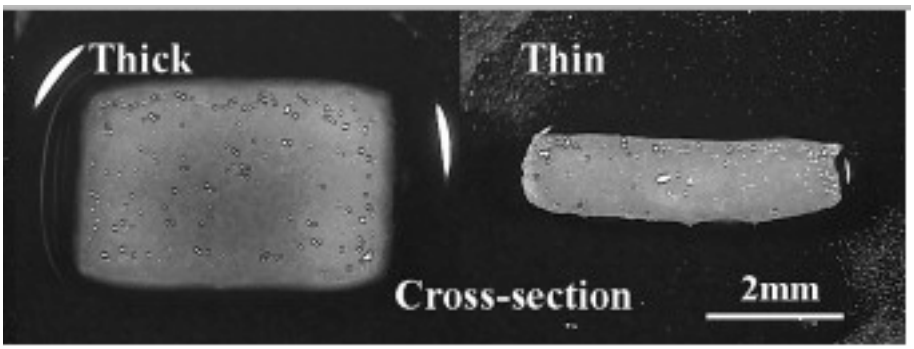

Figure 2.8: Cross-sectional view of thick and thin constructs on day 48 of culture [40]

Bian et al. also examined the influence of introducing 1.0 mm diameter channels, with a biopsy punch, through the thickness of 4.0 mm diameter cylindrical constructs, 2.34 mm thick. The channels increased the Young's and dynamic moduli significantly from day 28 of culture onward. When thick constructs were cultured without a channel, the mechanical properties reached a plateau after 28 days. This is because the chondrocytes produced matrix that hindered nutrient diffusion to the center of the construct. The mechanical properties of the constructs with channels were uniform throughout the thickness, unlike the constructs without channels. Also, the introduction of channels did not adversely affect cell viability at the cutting surface or other areas in the construct. Bian et al. found that channels smaller than 1.0 mm in diameter were filled in by deposited matrix within the first week of culture, while channels larger than 1.0 mm in diameter remained completely unfilled after 28 days of culture. Thus, it was determined that 1.0 mm is the ideal diameter of a channel intended for extended access of nutrients.

In addition to macro-channels, 1.0 mm in diameter, micro-channels have been investigated. Choi et al. observed the effect of micro-channels on diffusion rates in a calcium alginate hydrogel construct. They created square channels, 0.1 mm high and 0.1 mm wide, through lithography. The introduction of these micro-channels resulted in an

increase in diffusion rate of nutrients needed by the cells. However, this method was only conducted on constructs made of artificial materials [41].

2.7 Natural Extracellular Matrices

Though the three-dimensionality of a scaffold has a significant input on developing cells, the material or materials of which the scaffold is made also plays a vital role in cell attachment, migration, and proliferation [21]. Cartilage is a composite of materials with widely differing properties, making it very difficult to mimic in an artificial scaffold [10]. Using a cell-derived ECM provides the natural composition and ultrastructure of the tissue, which is responsible for directing cell attachment and differentiation to the desired tissue [7,9]. The difference between a natural ECM and a synthetic scaffold is the structural and functional proteins that make up the ECM and their three-dimensional organization. The organization of these proteins can lead to the difference between the cells constructively remodeling the ECM or creating scar tissue [21].

When cells are seeded in any scaffold, they begin to remodel the matrix by degrading the existing ECM and concurrently deposit their own neomatrix. The products of the degraded matrix produce biologic signals that play an important role in cellular activity and tissue remodeling [9]. Thus, it is important that what is being degraded can be recognized by the cells and contains the correct biochemical signals.

Natural ECMs have been implanted into patients for tissue regeneration purposes. The presence of a natural scaffold has been shown to have a positive effect on the regeneration process [42]. However, any implanted material that is not derived from the patient must have all cellular components removed to prevent an adverse host response. This involves an intense chemical decellularization process that leaves the remaining matrix mechanically compromised, and in a tissue like cartilage, the

mechanical properties of the ECM are an essential aspect to proper function [8-10]. Cartilage ECM is also very difficult to fully decellularize due to its high density. The decellularization process does, however, leave growth factors present in the ECM biologically active [21].

Once the natural ECM has been effectively decellularized, it can either be implanted into the body with or without being recellularized in vitro. If a scaffold is placed in the patient without being recellularized, host cells infiltrate it upon implantation and begin the remodeling process [19,21]. Cartilage, however, must be recellularized before being implanted because it is avascular and the matrix is too dense for cells to be able to infiltrate the center of the scaffold.

The use of natural ECMs for tissue regeneration is becoming a more widely use method. More than 200,000 human patients had been implanted with xenogeneic ECM scaffolds (tissue taken from a species other than human) by 2004 [21]. In addition, multilayered ECM scaffolds from porcine small intestinal submucosa (SIS) and human urinary bladder submucosa (UBS) have been successfully used in more than 150,000 human patients [43]. However, all of these uses are for tissues with a simple microstructure, such as skin epidermis [39]. Thus, the next step is to produce a method to use cell-derived ECMs for more complex tissues to improve the current strategies of using artificial matrices.

Many researchers have begun this work by studying the effects of cell-derived ECM on cell culture versus artificial scaffolds. Hwang et al. found that embryonic stem cells did not consistently undergo chondrogenesis in PEG hydrogels, indicating an issue with artificial matrices [20]. Cukierman et al. conducted a study comparing fibroblast culture on different natural and artificial scaffolds [37]. The experimental matrices used were a tissue-derived 3D matrix, which was detergent-extracted mouse embryo sections, and a cell-derived 3D matrix, which was ECM naturally deposited by fibroblasts with the

original cells removed. In addition, a set of control matrices including 2D matrices of fibronectin, laminin, and collagen I, a 3D collagen gel, and a 2D matrix, which was a cell-derived 3D matrix that was mechanically compressed to make it two-dimensional. After comparing the cell cultures on each matrix, Cukierman et al. found that cellular adhesions were most prevalent in cell-derived 3D matrices and tissue-derived 3D matrices. They also found that 3D collagen gels did not have the same rate of cell attachment, migration, or proliferation as cell-derived or tissue-derived 3D matrices [37]. Thus, it appears that the ideal scaffold for tissue engineering purposes should be three-dimensional as well as from a natural cell source [22].

2.8 Needle Insertion in Tissue

One method that is investigated here is to create three dimensional porous tissue scaffolds by punching holes in tissue constructs. It is important, however, to be able to predict the force required to punch these holes for manufacturing purposes.

Many studies have been conducted examining the forces needed to insert various sharp needles and flat punches, most commonly a hypodermic needle, into skin tissue or a rubber substitute [44]. Models have been created to analyze the mechanisms and predict the forces required, varying parameters such as the needle or punch shape, the material being punched, the velocity of penetrator, and the degree of pre-stretch. The mechanics of punching with flat-bottomed punches will be explained in detail, as these punches will be the focus of this thesis.

The mechanisms of penetrating soft solids are different from the commonly studied strong, ductile solids like metals and polymers. The first step in the process is deformation of the tissue. As the punch begins to make contact with the sample, it deforms the material in the direction of the advancing punch without breaking the surface. For cartilage, the punch squeezes the water out of the extracellular matrix as it is

compressed. Next, as the punch continues to advance, a crack, smaller than the size of the punch, forms on the surface of contact. The crack propagates through the tissue, with the mode of the cracking dependent on the geometry of the needle. In addition to crack propagation, the punch causes reversible deformation in the surrounding material by expanding the hole created by the crack. The punch expands the hole to the circumference of the punch, but once the punch is removed, the hole returns to its original size [45-48].

The geometry of the crack created depends on the geometry of the needle as well. A sharp-tipped punch, such as a hypodermic needle, creates a planar crack; when the needle is removed, a linear wound is left in the skin [45]. Figure 2.11 depicts the insertion of a sharp-tipped punch, the elastic deformation of the punch widening the crack, and the remaining planar wound after the punch has been removed. However, with a flat-bottomed cylindrical punch, a ring crack is created and a circular wound is left in the skin when the punch is removed. A circular crack created by a flat-bottomed punch is depicted in Fig. 2.12. Stevenson et al. determined that a ring crack created by a flat-bottomed punch propagates by a Mode II method. The punch head compresses a column of the material, causing the crack to propagate ahead of the punch, as is depicted in Fig. 2.13 [49]. The material in the column slides past the material remaining outside of the crack diameter. Shergold and Fleck observed that in human skin and a rubber substitute, the diameter of the ring crack remaining, after the punch was removed, was significantly smaller than the diameter of the punch [45]. Thus, the material must elastically deform around the edges of the crack.

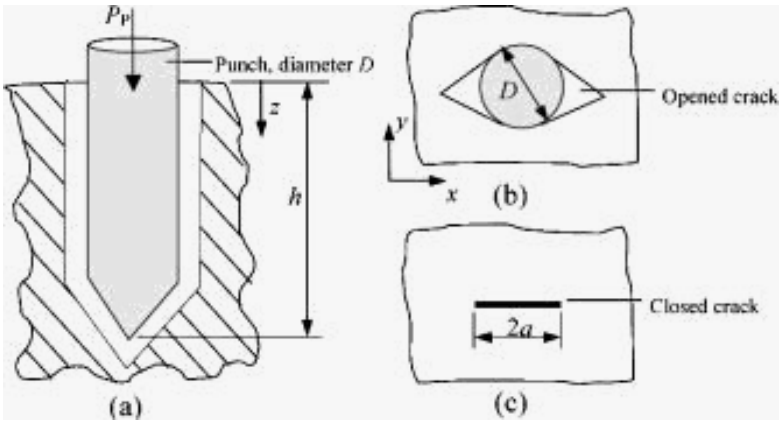

Figure 2.9: (a) Sharp-tipped punch penetrating a soft solid, (b) Sharp-tipped punch expanding a planar crack, (c) Planar crack closed after sharp-tipped punch is removed [45]

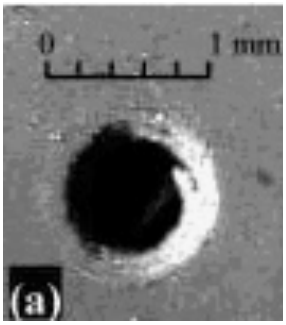

Figure 2.10: Surface of Sil8800 rubber penetrated by a flat-bottomed punch with 1 mm diameter [45]

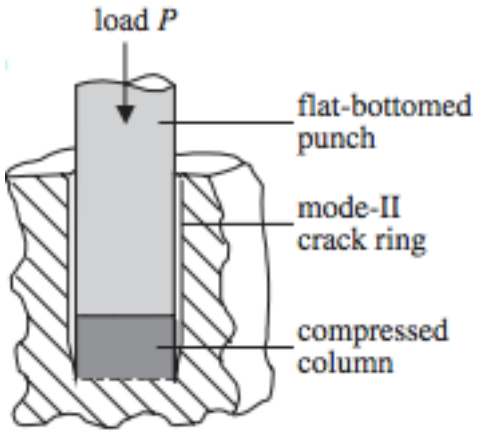

Figure 2.11: Penetration of a soft solid by a flat-bottomed punch [46]

Many factors have been found to contribute to the total force required to penetrate a substance with a punch. First is the geometry of the tip of the punch. Shergold et al. found that as the sharpness of the tip increases, the maximum force on the punch decreases. A flat-bottomed punch requires about two to three times the force of a sharp-tipped needle [46]. In addition to the maximum force, the sharpness of the punch tip changes the profile of the force measurement. After the initial penetration of the top surface, a sharp-tipped punch advances smoothly, with the force on the punch steadily increasing as the depth of the punch increases due to increasing friction. However, for a flat-bottomed punch, the load on the punch is unsteady and oscillates. This has been attributed to the incremental propagation of the ring crack [45]. Fig. 2.14 shows a typical force profile for a sharp-tipped punch and a flat-bottomed punch, highlighting the unsteady load on a flat-bottomed punch. Another factor of the geometry that affects the maximum force required is the diameter of the punch; as the diameter increases, so does the force exhibited [45].

Some of the relationships between punch geometry and penetration force can be explained by the material properties. The properties that have a relation to the punching force are the fracture toughness, the shear modulus, and the strain-hardening exponent. The fracture toughness is specific to the material and to the mode by which the crack is formed. A material's Mode II (sliding crack propagation) fracture toughness is greater than that of Mode I (tearing crack propagation). As the fracture toughness of the material increases, the penetration force also increases. This explains the greater force required for a flat-bottomed punch, which creates a crack by Mode II and thus has greater fracture toughness, compared to a sharp-tipped punch, which creates a crack by Mode I, introducing lower fracture toughness. In cartilage, the fracture toughness, as well as many other properties, is dependent on the direction of the collagen fibers. Mode I cracks propagate more easily in the direction parallel to the collagen fibers [50].

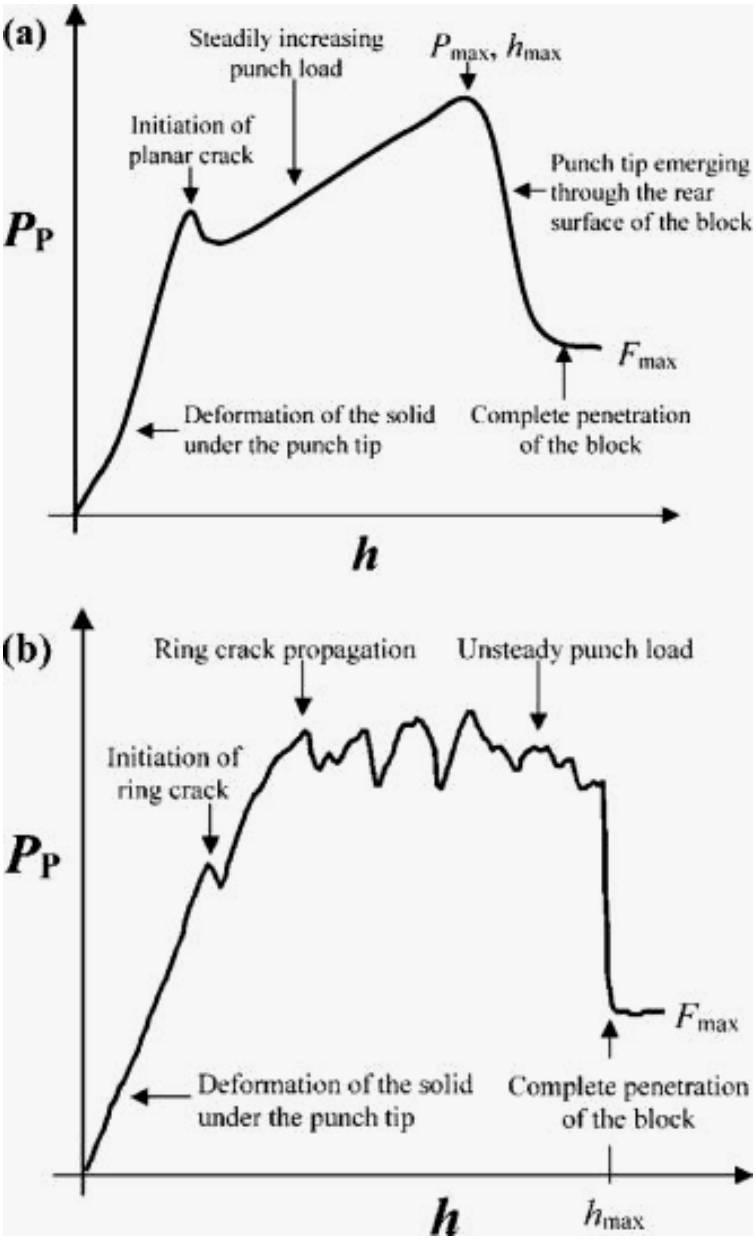

Figure 2.12: Characteristics of the force to penetrate a soft solid on (a) a sharp-tipped punch and (b) a flat-bottomed punch versus displacement of the punch [45]

There are three methods used to measure the fracture toughness of a material, all of which give different values for the same material [45,48]. First, is the scissor test: the material is cut with a pair of sharp scissors, and the force required to do the cutting is measured. This method is good for defining the fracture toughness for Mode I cracking, due to the sharp edges of the scissors. The next method is the trouser test. A small

incision is made in a material. Then each side of the incision is pulled in opposite directions and the force needed to tear the material is determined. This method determines a good representation of the fracture toughness for blunt-tip penetrating or tearing of the material. Both of these methods are illustrated in Fig. 2.15 [45,46]. However, a better method has been developed to measure the fracture toughness for penetrating a material.

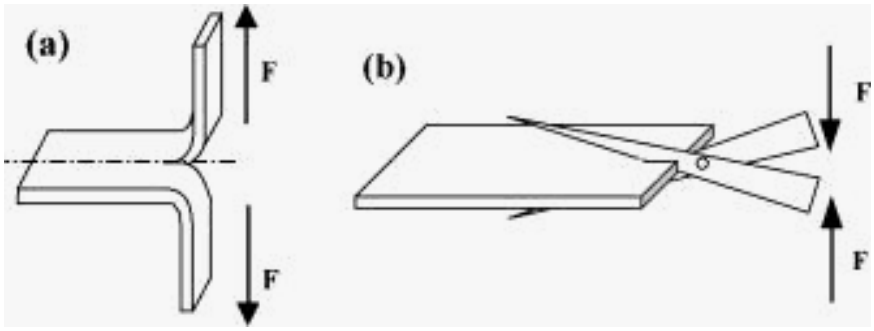

Figure 2.13: (a) Trouser test, (b) Scissor test [45]

Azar et al. developed a method to determine the fracture toughness of a material involving punch or needle insertion [48]. The punch is inserted into the thick material, and the penetration force required is measured against the position of the punch. The contributions to the total penetration force will be the force required to create and propagate the crack, the force to expand the hole to the circumference of the punch, and the friction force on the edge of the punch. Next, the punch is again inserted into the same location of the material, measuring the force as this occurs. The contributions to the force in this trial will be only the force required to expand the hole and the friction force. Thus by subtracting the total force profile of the second trial from the total force profile of the first trial, only the force required to create and propagate the crack will be remaining. The fracture toughness can then be determined from this remaining force profile. [48].

The shear modulus and the strain-hardening exponent also affect the force on a penetrating punch. They can be determined from a stress strain curve of a standard compression or tension test [51,52]. It is unclear what the effect of each parameter has individually on the penetration force because both tend to change from one material to the next. However, analytically, it can be shown that as the shear modulus increases and as the strain-hardening exponent decreases, the penetration force increases [46].

When working with a biological tissue, however, there is variability within the tissue that cannot be quantified in simple parameters. Azar et al. found slightly inconsistent force readings when punching liver tissue. They attributed this to the non-homogeneity of liver [48].

Other experimental factors contributing to the penetration force on the punch are the degree of pre-stretch on the material and the velocity of the penetrator [45,46]. However, the effects of these two parameters are unclear. Frick et al. reported that the force required to penetrate tissue with a suture needle increased with increasing pre-tension in the tissue [53]. On the other hand, Figge and Barnet found that less force is required to penetrate stretched skin than loose skin [54]. Frick et al. also found that when needle velocity was increased, the penetration force did not change [53]. Yet, when Brett et al. increased the insertion speed, they found that the penetration force decreased [55]. This could be explained by the fact that strain rate causes slight effects on toughness but not significant, as reported by Chin-Purcell et al. [56].

A model to predict the forces required to penetrate soft tissues was developed by Mooney et al., but this model is inappropriate for describing constitutive responses that have a strong strain-hardening characteristic, such as skin and cartilage [46,57]. Thus, Ogden generated a model to encompass materials with these properties [58]. His model was based on the strain energy function, Equation (2.1),

$$\phi = \frac{2\mu}{\alpha^2}\left(\lambda_1^\alpha + \lambda_2^\alpha + \lambda_3^\alpha - 3\right) \tag{2.1}$$

where ϕ is the strain-energy density per undeformed unit volume, α is the strain-hardening exponent, μ is the shear modulus under infinitesimal straining, and λ_i are the principal stretch ratios. Shergold et al. used the Ogden model, Eq. (2.1), to characterize skin and rubbers to analytically determine penetration forces [46]. They defined the work done by a flat-bottomed rigid cylindrical punch on the workpiece,

$$P_F \delta h = 2\pi b J_{IIC} \delta\ell + \frac{\partial S_C}{\partial \ell}\delta\ell + \frac{\partial S_H}{\partial \ell}\delta\ell \tag{2.2}$$

where P_F is the load on the punch, $P_F \delta h$ is the incremental work done by the punch upon advancing by δh into the workpiece, *b* is the radius of the crack formed, J_{IIC} is the fracture toughness of the material for a Mode II crack propagation, ℓ is the undeformed length of the column of material below the punch head, and $\delta\ell$ is the incremental increase of the length of the column of the material compressed below the punch, Fig. 2.14. The quantity $\frac{\partial S_C}{\partial \ell}$ is the work done per unit depth in order to compress the column beneath the punch, and $\frac{\partial S_H}{\partial \ell}$ is the energy stored within the solid external to the hole due to the hole expansion by the punch. The contributions to the work done by the punch from each component of the total force required were summed, except for friction, which was neglected [46].

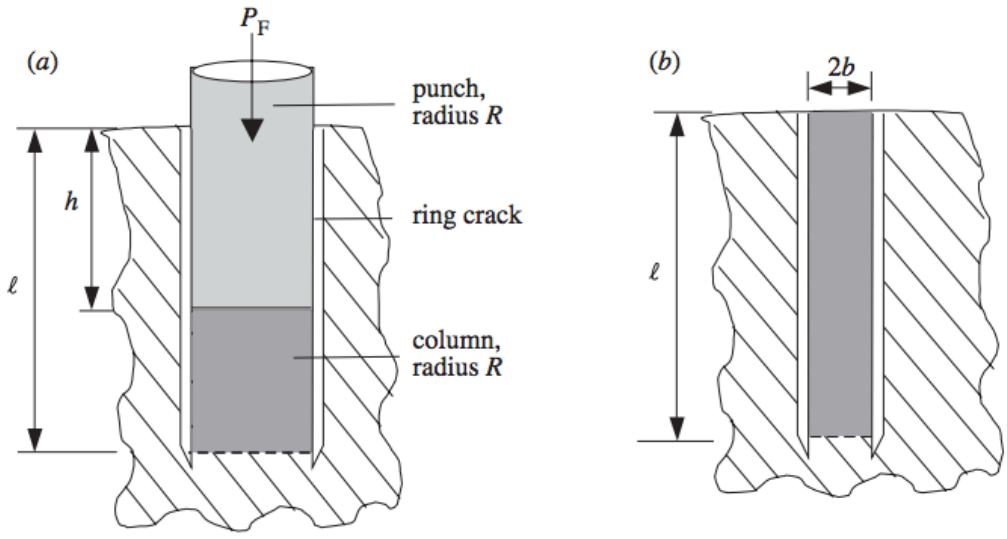

Figure 2.14: (a) Propagation of a ring crack in a soft solid ahead of a flat-bottomed rigid cylindrical punch and (b) Ring crack in a soft solid after punch removal [46]

Some assumptions must be made for these models to hold true. First, the material must be assumed to be incompressible to allow for a strain energy function to be defined [57]. Many investigators have reported justification that skin can be considered incompressible [46]. On the other hand, even though cartilage is mostly water, which is incompressible, it does not act as an incompressible substance. When a load is applied to cartilage, the water flows out of the matrix to improve impact resistance properties and to aid in lubrication, reducing the volume of the tissue [10]. However, once the water has been squeezed out, cartilage can be assumed to be incompressible due to the fact that all of its solid components can be modeled as incompressible [59].

The next assumption is to neglect the friction on the punch. Shergold et al. assumed that the friction was negligible compared to the contributions of the other factors on the penetration force [45]. Finally, the material must be assumed to be isotropic and hyperelastic [46]. Cartilage is not isotropic; its properties are very dependent on the direction of the load with respect to the orientation of the collagen fibers. But, as the authors made this assumption for skin, though it is also not entirely accurate, it can be used to determine punching forces to a first approximation. Sanjeevi et al. performed a

uniaxial tensile test on human tendons, which are composed of aligned collagen fibers, and determined that collagen fibers can be considered elastic [60]. In addition, shear tests performed on cartilage show that the matrix behaves as a viscoelastic solid [61]. Thus, it is valid to model cartilage as hyperelastic.

3 Effect of Die Clearance on Punching Force Measurements

3.1 Introduction

The aim of this thesis is to investigate the feasibility of using a mechanical punch to create micro-scale holes in 100 μm thick cartilage. The holes are intended to be home sites for cell seeding, providing alternative three-dimensional adhesion cites to decellularized lacunae, in a thin scaffold providing adequate nutrient diffusion. The thin, punched ECM scaffold will allow for a more gentle and effective decellularization process, with the intent to preserve mechanical integrity of the seeded construct.

The approach taken is to use a micropunching machine developed by Schmitt et al. [11]. Schmitt demonstrated that 200 μm diameter holes could be punched in 30-40 μm thick polycaprolactone (PCL), a biodegradable polymer used for cell scaffolds in tissue engineering applications.

Initial studies were conducted to determine the feasibility of repurposing the micropunching machine developed by Schmitt [12]. Micro-holes were punched in cartilage ECM samples ranging in thickness from 50 μm to 200 μm with male punches of diameter 100 μm and 200 μm. A novel method was developed, in which the thin cartilage samples were placed between two pieces of wax paper. The two layers of wax paper and the cartilage sample are then punched together. Using this method, holes ranging from 46 μm to 186 μm can be created using a 200 μm male gauge pin as a punch, a female die hole between 204 and 223 μm, and a cartilage sample 100 μm in thickness.

In this research, the new micropunching machine was employed to examine the effect of die clearance on maximum punching force (MPF) when using a 201 μm diameter punch to create holes in thin sections of cartilage.

3.2 Materials and Methods

3.2.1 Micropunching Machine

A micropunching machine designed by Schmitt [11] utilizes a microscope to align the male and female die halves by peering through the hole in the female die as the male punch is raised into position, Fig. 3.1. The female die is fixed in place, while the male die is positioned by precision X-Y-θ micrometer controlled staging, Fig. 3.1(g).

The machine is capable of utilizing a variety of die sets. The dies can be fabricated from silicon by lithographic processing, micromachining, laser cutting, or more conventionally as pins in die blocks, depending on the desired scale and feature shape. The die sets are secured in place by using a vacuum system, Fig. 3.1(c). Parallelism between the male and female dies is obtained through a spherical bearing. The bearing is locked in place by vacuum after mating contact is made between the die halves, Fig. 3.1(e).

Punching force is measured in real-time with an inline 3-component quartz dynamometer (9047C, Kistler Instruments, Switzerland), Fig. 3.1(f). The dynamometer has a dynamic range of 30kN in the punching direction with a measurement sensitivity of 3.7 pC/N. Data from the dynamometer is transmitted to a charge amplifier (ICAM 5073, Kistler Instrument Corp., Amherst, NY), which has a sensitivity of 1+/- 0.5% pC/mV. High speed data acquisition is achieved with a multifunction data acquisition board (PCI 6132, National Instruments, Austin, TX), which has a simultaneous sampling rate of 2.5×10^6 samples per second. A LabVIEW (National Instruments, Austin, TX) virtual instrument was written to stream the sampled data to a series of CSV (comma separated values) files, at which point they were imported into Matlab (MathWorks, Natick, MA) for analysis.

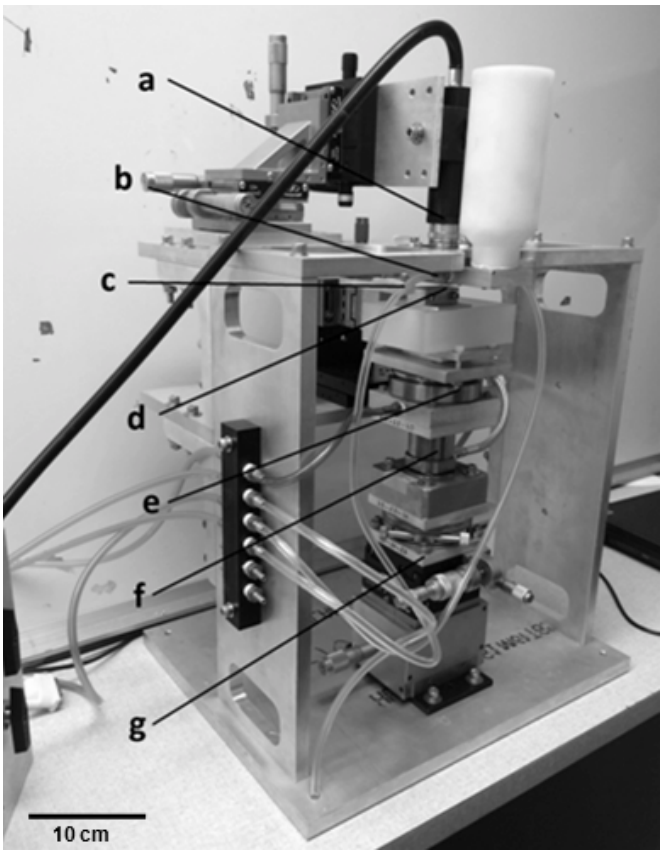

Figure 3.1: Custom micropunching machine used to create holes in cartilage tissue (a) Microscope, (b) Female die holder, (c) Vacuum tube, (d) Male punch holder, (e) Spherical bearing, (f) Force dynamometer, (g) X, Y, Z and θ staging

During experiments, the punch is raised and lowered quasi-statically by hand turning a micrometer driven high capacity stage (Maximum capacity = 111 N, Model MVN80, Newport Corporation, Irvine, CA, USA). For a full description of the micropunching machine see [12].

3.2.2 Die Sets

The male die (punch) is a nominal 200 μm steel, flat-bottomed, gage pin with a Rockwell C hardness of 60-62 (Model 21135A71, McMaster- Carr, Princeton, NJ, USA). The actual punch diameter as measured is 201 μm. The end of the punch was used in the as- received condition, Fig. 3.2.

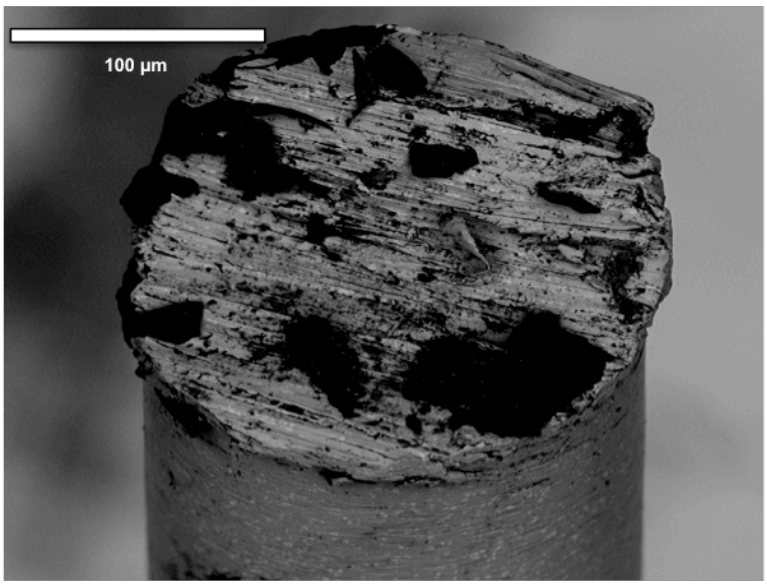

Figure 3.2: SEM picture of the male punch in the as-received condition (diameter = 201 µm)

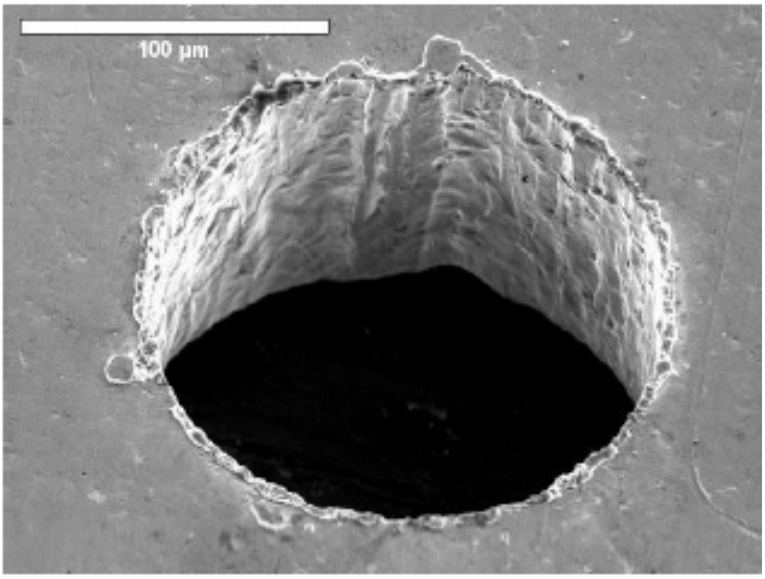

Figure 3.3: SEM picture of the female die manufactured by laser cutting 150 µm stainless steel (diameter = 208 µm)

The female die was manufactured by laser cutting holes in a 150 µm thick, ground stainless steel plate (Photo Etch Technology, Lowell, MA, USA), Fig. 3.3. Attenuation of the laser results in a tapered hole, where the entrance side of the laser creates a larger hole than the exit side. The female dies were oriented within the press so the smaller hole was facing the male punch. Laser cut holes of three diameters were

manufactured (208 μm, 214 μm, and 218 μm) to investigate the effect of die clearance on the punching force profile. The diameters refer to the entrance side of the female die.

3.2.3 Cartilage Sample Preparation

Articular cartilage is scraped from the medial and lateral condyles of the femur of a rear leg of an equine between the 24th and 36th months of age, obtained from the Cummings School of Veterinary Medicine, North Grafton, MA, USA. Samples approximately 2.0 mm in depth and 50 mm^2 are taken from both condyles. The samples are fixed in 10% formalin for 24 hours. Next, the samples are placed in optimum cutting temperature (OCT) compound, which is a medium for frozen tissue specimens (Sakura Finetek USA, Inc., Torrance, CA, USA). Embedded samples are frozen on dry ice for further processing. The samples are sectioned to 100 μm thick slices with a cryostat-microtome (Leica CM1950, Leica Biosystems, Wetzlar, Germany). The samples are then placed in a non-sterile phosphate buffered saline (PBS) bath and maintained at 4°C.

3.2.4 Experimental Design

A series of punching experiments are performed to determine the effect of die clearance on MPF. Given a punch diameter of 201 μm, the difference in diameters between the punch and the female die sets are 7 μm, 13 μm, and 17 μm. In a saturated state, the thickness of the cartilage sample measures approximately 95 μm. This results in a theoretical die clearance of 3.7%, 6.8%, and 8.9% (die clearance = radial clearance / sample thickness), respectively.

For each die clearance, 15 holes are punched in the cartilage sample. During punching, the cartilage is placed between two sheets of 30 μm thick wax paper (Reynolds, Lake Forest, Illinois). The wax paper is secured in a material fork and positioned between the die sets with X-Y- Z precision staging, Fig. 3.4. After punching every five holes, the sample is rehydrated by submerging it in a non-sterile PBS bath for

15 seconds. Trials during which the punch contacts the female die are removed before analysis.

3.2.5 Data Analysis

Amplified output of the dynamometer is recorded as volts in proportion to the load. Voltage is then converted to force in Newtons by multiplying the data set by a calibration factor. Noise in the raw data is filtered by weighted local linear regression, with the heaviest weighting at points closest to the data set of interest (Matlab, MathWorks, Natick, MA, USA). Drift in the data, which is an attribute of a quartz dynamometer, is removed by subtracting the linear regressed drift curve. The MPF is determined from the filtered data after accounting for drift. The Matlab code used for this analysis is shown in Appendix A.

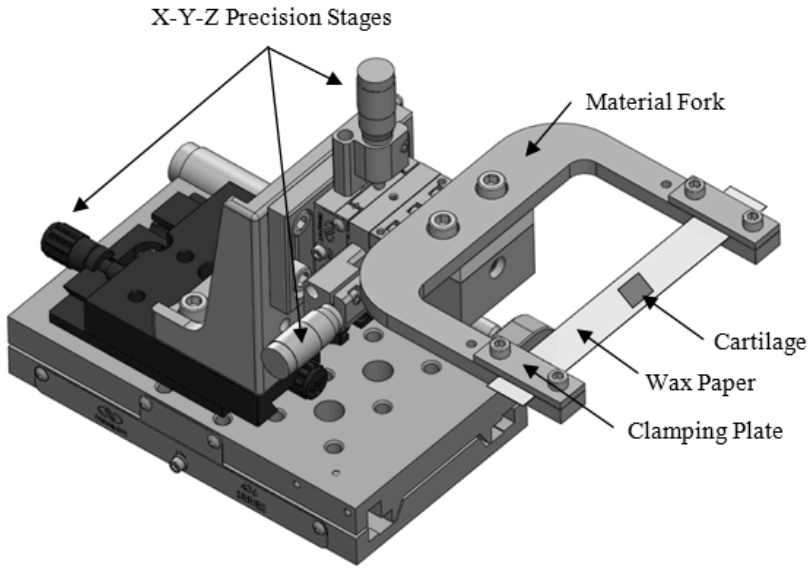

Figure 3.4: Material holder for positioning the cartilage sample between the male and female die sets

3.2.6 Statistical Analysis

An Anderson-Darling test is executed to confirm the data follows a normalized distribution and a two sample t-test is performed to determine significance ($p < 0.050$)

when comparing MPF of the three combinations of die clearance. Minitab 16 (Minitab, State College, PA, USA) is used for statistical analysis.

3.3 Results

Experiments were conducted to determine the effect of die clearance on the MPF of cartilage between wax paper. A typical punching force curve is shown in Fig. 3.5 for a die clearance of 6.8%.

The maximum force to punch a hole in cartilage between two pieces of wax paper has a high degree of variation for the smallest die clearance, 3.7%, but has a relatively low standard deviation for the two larger die clearances, 6.8% and 8.9%, Fig. 3.6. The MPFs range from 2.4 N to 4.7 N for a 3.7% die clearance, Fig. 3.7.

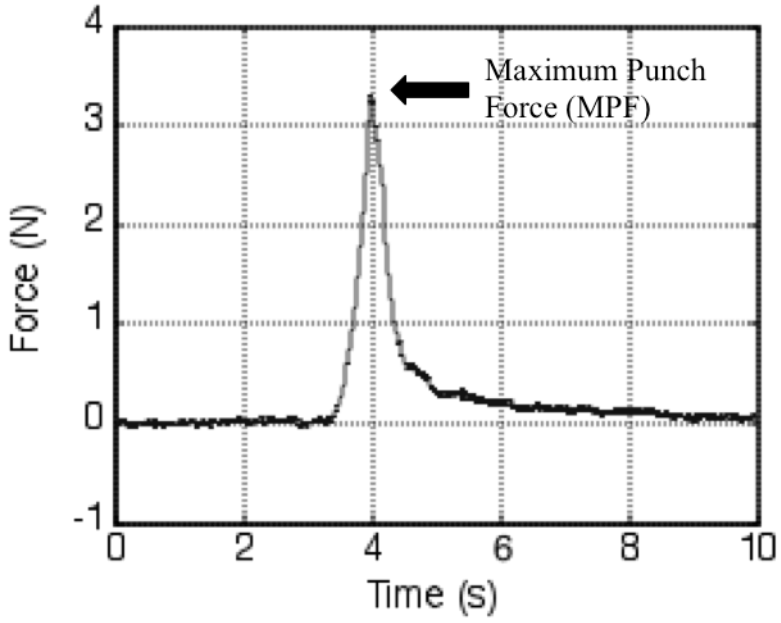

Figure 3.5: Dynamometer data showing the punching force curve after filtering and drift correction (201 µm punch; 6.8% die clearance; 95 µm thick cartilage, saturated)

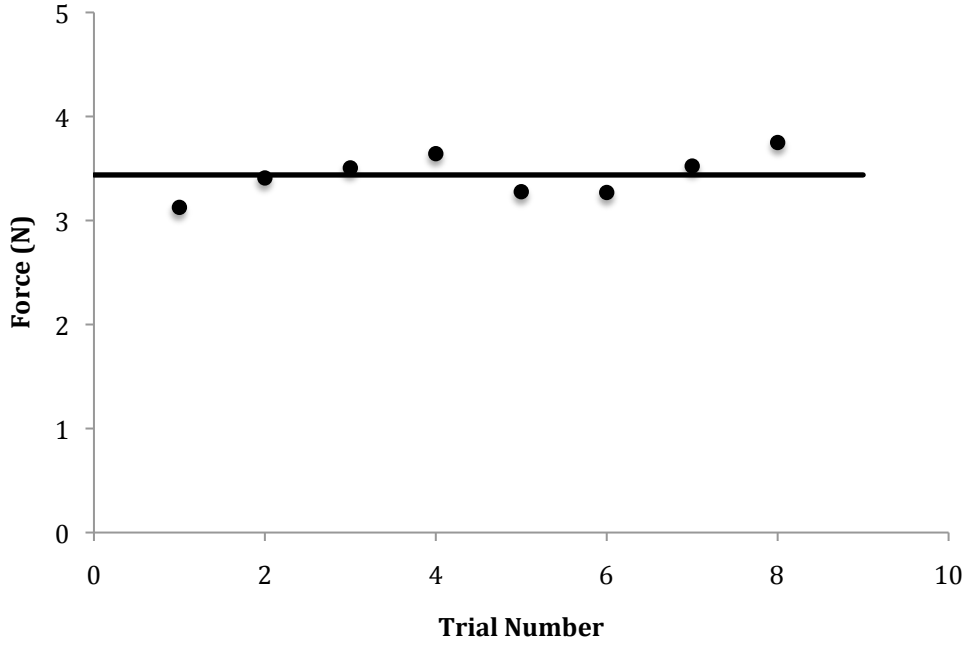

Figure 3.6: Maximum punching force of cartilage sample between wax paper punched with die clearance of 6.8% (Punch diameter = 201 µm, 6.8% die clearance, 95 µm thick cartilage, saturated). Line indicates mean of 3.44 N, st. dev. = 0.21 N.

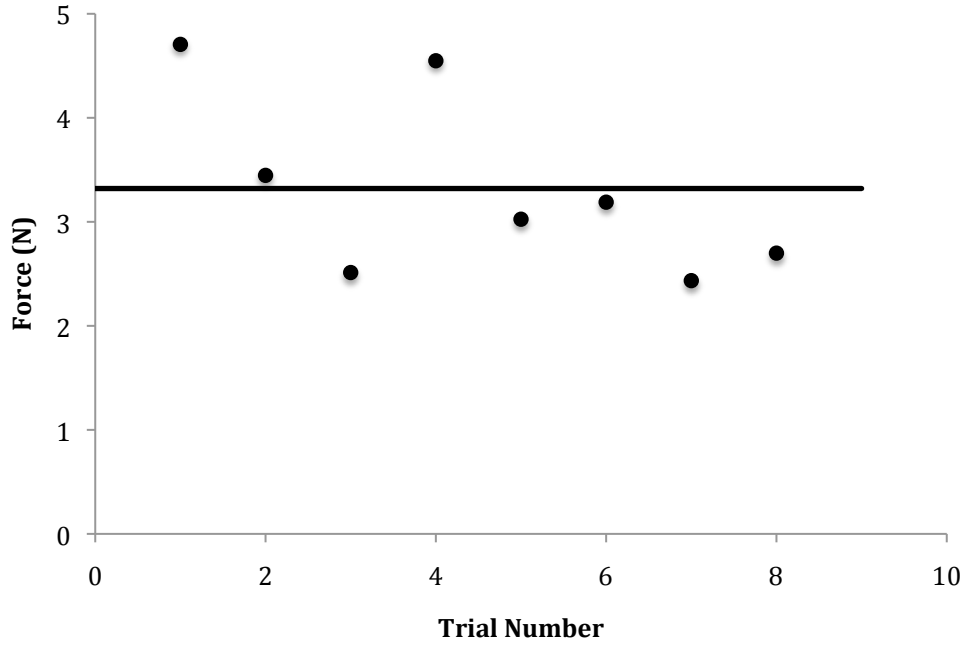

Figure 3.7: Maximum punching force of cartilage sample between wax paper punched with 3.7% die clearance (Punch diameter = 201 µm, 3.7% die clearance, 95 µm thick cartilage sample, saturated). Line indicates mean of 3.32 N, st. dev. = 0.88 N.

The mean MPF as a function of die clearance is shown in Fig. 3.8. The relatively high standard deviation of the 3.7% die clearance, Table 3.1, is attributable to the punch contacting the edge of the female die hole during punching, creating a frictional force, as well as variations within each sample. This is likely unavoidable for small die clearances because the punch deflects slightly as water is squeezed from the samples, causing interference and a resulting change in measured punching force. The small variations in data for the larger die clearances are likely attributed to variations within each sample.

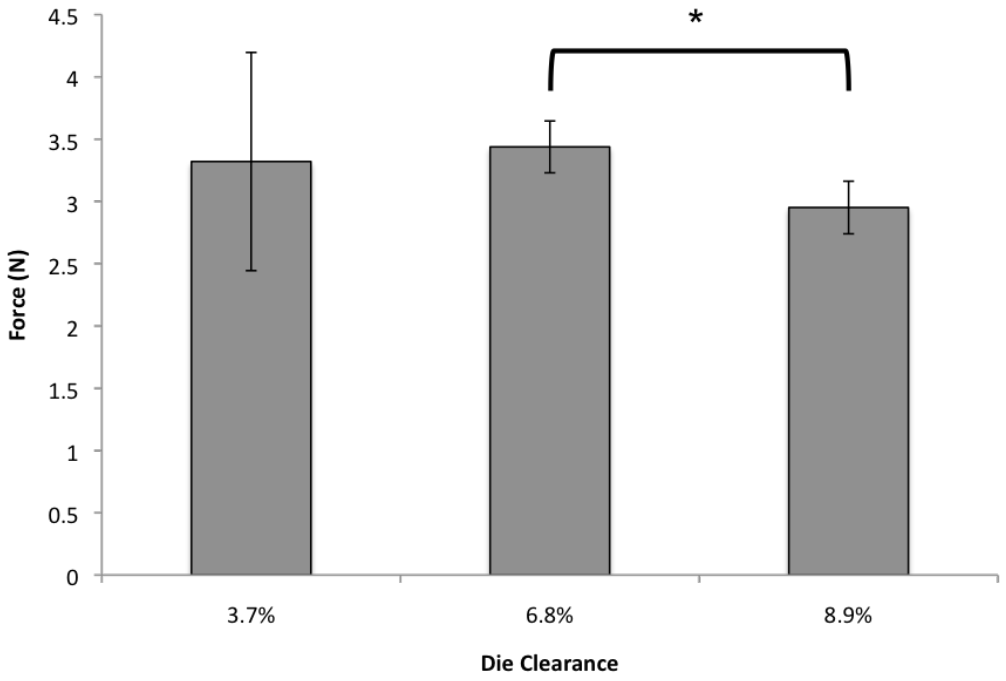

Figure 3.8: Mean maximum punching force of cartilage sample between wax paper as a function of die clearance for a saturated cartilage sample between two pieces of wax paper (bars indicate +/- one st. dev.) (201 µm punch, 95 µm thick cartilage sample). * Statistically significant ($p < 0.05$).

Table 3.1: Mean maximum punching force of a saturated cartilage sample between wax paper as a function of die clearance (n=8 for each die clearance)

Difference between Punch and Die Dia. (μm)[1]	Die Clearance (%)[2]	Mean Maximum Punching Force (N)	Standard Deviation (N)	Coefficient of Variation (%)
7 (n=8)	3.7	3.32	0.88	26.5
13 (n-8)	6.8	3.44	0.21	6.1
17 (n=6)	8.9	2.95	0.21	7.1

[1] Punch diameter: 201 μm; Cartilage thickness: 95 μm
[2] % Die clearance = (radial die clearance / cartilage thickness) x 100

Table 3.2: Significance of mean maximum punching force as a function of die clearance for a saturated sample

t-test	p-value
$3.7 < 6.8$[1]	0.369
$3.7 > 8.9$	0.142
$6.8 > 8.9$	< 0.001

[1] Test for significance: Is the punching force for a die clearance of 3.7% less than the punching force measured for a die clearance of 6.8%?

An Anderson-Darling test was performed to confirm that the data follows a normalized distribution ($p > 0.050$). The force measurements at 3.7% ($p = 0.176$), 6.8% ($p = 0.902$), and 8.9% clearances ($p = 0.346$) all follow a normalized distribution, indicating two-sample t-tests can be executed.

A two sample t-test was used to determine if the change in mean MPF, as a function of die clearance, is significant ($p < 0.050$), Table 3.2. The results show a trend that the MPF decreases as the die clearance increases. However, the increase in MPF is not statistically significant when comparing a die clearance of 3.7% to the other die clearances due to the high standard deviation and coefficient of variation caused by the variations of measurements.

3.4 Discussion

The investigation of die clearance on MPF of cartilage between wax paper revealed a trend of the force decreasing with increased clearance. The results had high

coefficients of variation for 3.7% die clearance caused by natural variations in the samples as well as the punch coming in contact with the female die. The water in the samples appears to cause the punch to move out of alignment during each stroke, causing the punch to hit the edge of the die hole, increasing the measured MPF. The trials during which the punch clearly hit the bottom of the female die were removed from the data, however some of the remaining values might be greater than the true punching force due to a frictional force of the punch contacting in the inside of the female die hole. The results for 6.8% and 8.9% die clearance, on the other hand, had low coefficients of variation, giving more reliable data. Thus, for future experiments, female die holes in the range of 214 μm to 218 μm should be used to ensure low levels of variation in the results.

The data show a significant trend toward an increase in force as the die clearance decreases for 6.8% and 8.9% die clearances. However this trend is not statistically significant when considering the 3.7% die clearance due to the high degree of uncertainty in the measurements. Therefore, it can be concluded that as die clearance decreases, MPF increases as long as the punch does not contact the female die. This conclusion would follow the trend of metals and polymers, which also have increasing MPFs as die clearance decreases [62].

To our knowledge, this is the first reporting of a mechanical punching process utilized to create home sites for cell seeding in cartilage ECM. It is hypothesized that the holes punched in the cartilage tissue achieved in this study will provide implanted cells with three-dimensional adhesion cites in a thin scaffold, promoting chondrogenic differentiation of embryonic stem cells while allowing sufficient nutrient diffusion [12].

To access the significance of this research, additional experiments are required to confirm these results for more die clearances, as well as to compare cell differentiation and growth for cartilage scaffolds prepared by mechanical punching to those prepared by chemical decellularization, which only provides a two-dimensional surface on which the

cells can grow. In addition, experiments must be conducted to determine the effects of the punching process on the mechanical properties of the sample by conducting deformation tests on samples before holes have been punched in them, and after. Finally, the impact of fixation of the samples on their mechanical properties and their ability to promote chondrogenic differentiation must be investigated.

3.5 Conclusion

This study was the first to show that holes can be punched in cartilage ECM using a micropunching machine. MPF measurements have a high degree of variation for low die clearances, but appear to have a significant dependence on die clearance. MPF of a cartilage sample between wax paper was approximately 2 N to 5 N for a 201 μm punch in 95 μm thick equine articular cartilage.

4 Effect of Hydration on Punching Force Measurements

4.1 Introduction

In the previous research, a relationship existed between die clearance and maximum punching force (MPF). In addition to die clearance, hydration level of the samples may play a role in fracture mechanics as well as the resulting hole size. This too must be investigated.

In this research, the micropunching machine is employed to examine the effect of hydration level on maximum punch force and resulting hole size when using a nominal die clearance of approximately 7.5% to create holes in thin sections of cartilage. Three terms are used herein to describe the hydration level of cartilage samples: (1) *Saturated*, which is the hydration level during the first three holes punched or the first two minutes of being removed from its phosphate buffered saline solution (PBS) bath, resulting in approximately 90-100% of its mass when removed from the PBS bath, (2) *Hydrated*, which is the state after three holes are punched in the sample, or after being compressed between two pieces of wax paper by a 500 g compression weight and dried for ten minutes at 21°C, resulting in approximately 30% of its saturated mass, and (3) *Dry*, which is when the sample is placed between two pieces of wax paper and a 500 g mass is applied for eight hours, resulting in approximately 15% of its saturated mass.

4.2 Materials and Methods

4.2.1 Punching Force for Cartilage in Wax Paper

Twelve equine samples are removed from their PBS baths, weighed (HR-200, A&D Engineering, San Jose, CA, USA), and their approximate thicknesses are measured using a micrometer (293-344, Mitutoyo Corporation, Kawasaki, Kanagawa, Japan). Three samples are dried for 8 hours between two pieces of wax paper, comprising the dry

samples. Three additional samples are dried to 30% of their saturated mass to be hydrated samples, and finally, three samples are left in a PBS bath to be saturated samples. The hydrated and saturated cartilage samples are placed between two sheets of 30 μm thick wax paper prior to punching.

Four holes are then punched in each hydrated and dry sample (n=10, die interference on 2 points), and three holes are punched in each saturated sample (n=5, die interference on 4 points) using a punch diameter of 201 μm and a female die hole of 216 μm, resulting in a die clearance approximately 8.5%. In each case, the force on the punch is measured as it advances through the material.

After each hole is punched in the hydrated and dry samples, and the force on the punch is measured, the punch is advanced through the same hole in the same location and the force is measured again. This is referred to as the "two-punch test". The punch is only advanced through the sample once in each location for saturated samples. After the four holes have been punched in each sample, the radii of the resulting holes are measured using a confocal microscope (Model 82026-620, VWR International, Radnor, PA, USA) and camera (D3000, Nikon Inc., Melville, NY, USA) and are recorded along with the corresponding force profiles. Hole sizes are measured by calibrating the pixel size and measuring the diameter of each hole by the number of pixels. The average of three diameters is reported.

4.2.2 Punching Force of Wax Paper

The micropunching machine is used to measure the force required to punch two layers of 30 μm thick wax paper at three different hydration levels to determine the contribution to the measured MPFs of cartilage in wax paper. By subtracting the force required to punch wax paper from the total MPF of wax paper and cartilage, the force required to punch cartilage can be determined.

4.2.2.1 Sample Preparation

Three samples, 1.6 cm by 30.5 cm, are cut from commercially available wax paper that is 30 μm thick (Reynolds, Lake Forest, Illinois). Three test groups are used. One sample is soaked in PBS at room temperature (21°C) until it is saturated and then left out until it has completely dried; this sample is called the *PBS Dry Sample*. Another sample is left "as is" after it is cut; this sample is the *Dry Sample*. The last sample is soaked in PBS just before testing; this sample is the *PBS Sample*.

Before punching, the wax paper samples are folded in half to make 1.6 cm by 15.25 cm strips that are two layers thick, as is done in previous experiments when a sample of cartilage is trapped between two pieces of wax paper.

4.2.2.2 Experimental Design

A series of punching experiments are performed to determine the effect of hydration level on the maximum force required to punch two layers of wax paper. Using a punch diameter of 201 μm and a female die hole of 217 μm, 20 holes are punched in a total of 60 μm thick samples of wax paper at each hydration level, creating a die clearance of 13.3% (die clearance = radial clearance / sample thickness). The centers of holes were 1000 μm apart to ensure that adjacent holes would not compromise the strength of the wax paper. Mean values for each hydration level are calculated, and the results are statistically compared.

4.2.3 Final Hole Size Investigation

The diameter of each hole punched in the cartilage samples is measured to determine the effect of hydration level on final hole size. Cartilage samples punched while saturated or hydrated are measured in the saturated state, and cartilage samples punched while dry are measured in the dry state.

The diameters of the final holes from the force measurements at each hydration level are measured and used for this investigation. In addition, holes are punched in an

equine sample that is 84.6 ± 2.3 μm thick (mean +/- SD; n = 10), with a 208 μm female die (4.1% die clearance). Holes are punched when the sample is saturated and also in the dry state. The saturated sample is dried, compressed between two pieces of wax paper, and the hole sizes are measured. Then the saturated sample is rehydrated and the hole sizes are measured in the saturated state. The hole sizes of the dry sample are also measured in the dry state, and then rehydrated and measured in the saturated state. The results are statistically compared.

4.2.4 Scanning Electron Microscopy

Four holes are punched in samples at dry, hydrated, and saturated hydration levels with a 201 μm punch and a 208 μm female die hole (nominal die clearance = 3.5%). The samples are then left to dry between two pieces of wax paper, which are compressed by a 500 g mass for 24 hours to ensure they are fully dry. The samples are then sputtered with gold and imaged in a scanning electron microscope (SEM) at 5 kV.

4.3 Results

4.3.1 Maximum Punching Force

4.3.1.1 Cartilage in Wax Paper

Experiments were conducted to determine the effect of hydration on the punching parameters of cartilage samples. The MPF and resulting hole diameters were measured for ten locations at the saturated, hydrated, and dry hydration levels. The normalized MPF was calculated by dividing the MPF by the circumference of the resulting hole for a given location. For the hydrated and dry samples, the "two-punch test" was performed and the second stroke maximum force was measured. The "two-punch test" was not performed on saturated samples because it squeezes the water out of the samples, lowering the hydration level beyond the saturated threshold during the second punch stroke. The data from the "two-punch tests" are used in the calculation of

the fracture toughness of the cartilage samples in Chapter 5. All data are presented in Appendix B.

The resulting MPFs ranged from 1.89 N to 2.87 N for saturated samples, 2.49 to 4.50 N for hydrated samples, and from 3.44 N to 4.50 N for dry samples, Table B.1-B.3. The mean MPF, second stroke force, resulting hole radius, and normalized MPF are shown as a function of hydration level in Table 4.1. There is a significant increase in MPF as the sample dries out ($p < 0.050$), Table 4.2. The mean MPF of dry samples is significantly greater than that of hydrated and saturated samples, and the mean MPF of hydrated samples is significantly greater than that of saturated samples. The higher standard deviation values of MPF and second stroke force for hydrated samples can be attributed to the slight variations in hydration level for each sample measured. There was less of a variation in hydration level for saturated and dry samples.

Table 4.1: Punching results for cartilage between wax paper at various levels of hydration (mean +/- st. dev.)

Hydration Level	Mean Maximum Punching Force (N)	Mean Second Stroke Force (N)	Mean Final Hole Diameter (μm)[2,3]	Mean Normalized Max Force (N/mm)[1]
Saturated (n = 5)	2.46 ± 0.39	N/A	51.30 ± 13.08	15.92 ± 4.05
Hydrated (n = 10)	3.18 ± 0.63	0.55 ± 0.22	50.24 ± 12.34	21.12 ± 5.88
Dry (n = 10)	4.01 ± 0.37	0.27 ± 0.04	191.64 ± 10.16	6.68 ± 0.63

[1]Normalized Max Force = Maximum Punching Force/Hole Circumference
[2]Punch Diameter = 201 μm
[3]Saturated and hydrated samples measured while saturated, dry samples measured while dry

Table 4.2: Significance of mean maximum punching force as a function of hydration level

t-test	p-value
Saturated < Hydrated	0.019
Saturated < Dry	< 0.001
Hydrated < Dry	< 0.001

When the forces are normalized by dividing by the final hole circumference, hydrated samples have the greatest normalized MPFs, Fig. 4.1. The mean normalized MPF of hydrated samples is significantly greater than that of saturated and dry samples, and the mean normalized MPF of saturated samples is significantly greater than that of dry samples, Table 4.3.

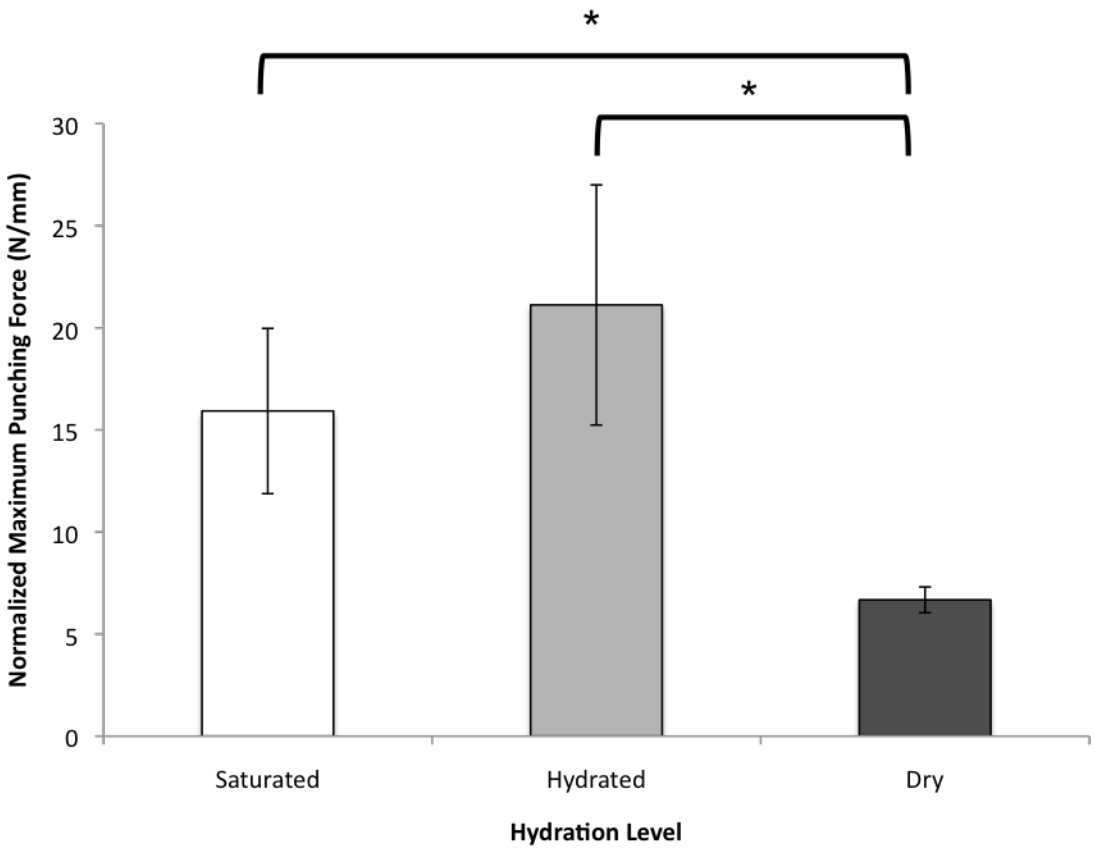

Figure 4.1: Mean normalized maximum punching force of cartilage at each hydration level (bars indicate +/- one st. dev.) (saturated samples n=5, hydrated and dry samples n=10, 201 µm punch, 216 µm die, 8.5% nominal die clearance; Normalized Force = Maximum Punching Force/Resulting Hole Circumference). * Statistically significant ($p < 0.05$).

Table 4.3: Significance of mean normalized maximum punching force as a function of hydration level

t-test (n=10)	p-value
Saturated < Hydrated	0.051
Saturated > Dry	0.003
Hydrated > Dry	< 0.001

The mean second stroke force of hydrated samples is significantly greater than that of dry samples ($p = 0.016$), Fig. 4.2. The greater second stroke force for hydrated samples is likely due to the smaller resulting hole radii for these samples. Similarly, the hydrated samples have a higher standard deviation, which is likely the result of a larger range in resulting hole size than found in dry samples. The punch must elastically expand the hole more if the hole radii are smaller.

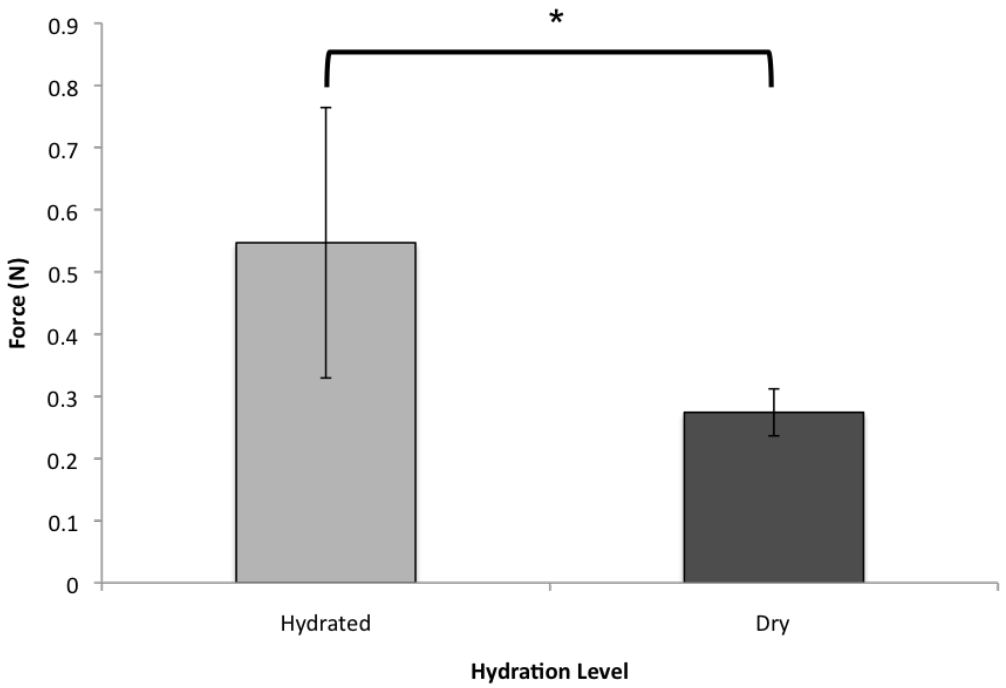

Figure 4.2: Second stroke punch force for hydrated and dry samples of cartilage (n=10, 201 µm punch, 216 µm die, 8.5% nominal die clearance). * Statistically significant ($p < 0.05$).

4.3.1.2 Wax Paper

Experiments were conducted to determine the punching force of wax paper at different hydration levels. A typical punching force curve of two layers of PBS Dry wax paper is shown in Fig. 4.3.

Results indicate that the maximum force to punch a hole in two layers of wax paper is dependent on the hydration of the sample, Table 4.4. The MPF and standard deviation increase when the wax paper is soaked in PBS, whether it is still wet or after drying.

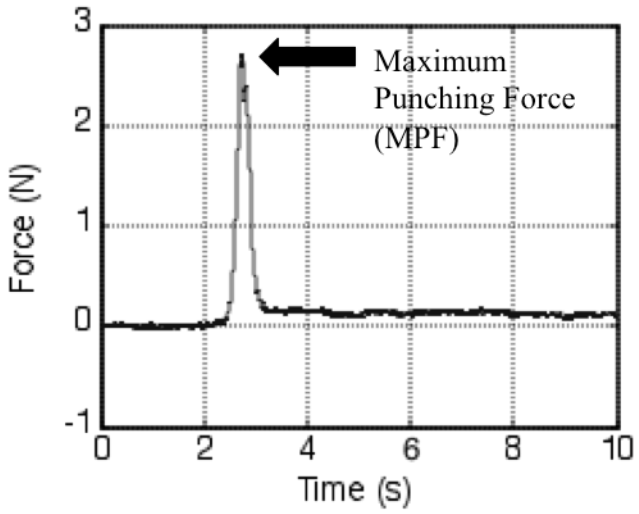

Figure 4.3: Dynamometer data showing the punching force curve of two layers of PBS Dry wax paper (201 µm punch; 216 µm die, 13.3% die clearance; two layers of 30 µm thick wax paper)

Table 4.4: Mean maximum punching force as a function of hydration for two layers of wax paper. PBS = sample soaked in PBS; Dry = sample left dry; PBS Dry = sample soaked in PBS and then dried.

Hydration	Mean Maximum Punching Force (N)[1]	Standard Deviation (N)	Coefficient of Variation (%)
PBS	2.60	0.38	14.6
Dry	2.06	0.14	6.8
PBS Dry	2.46	0.38	15.4

[1]Punch diameter: 201 µm; Female die hole diameter: 217 µm; Sample thickness: 60 µm; Die clearance: 13.3%

A two sample t-test is used to determine if the change in mean MPF of wax paper, as a function of hydration, is significant ($p < 0.050$), Table 4.5. The results show that the mean MPF is greater if the sample is still wet with PBS (PBS sample) or was soaked in PBS and then dried (PBS Dry sample), than if it was never soaked in PBS (Dry sample), but there is no significant difference between PBS and PBS Dry samples.

Table 4.5: Significance of mean maximum punching force as a function of hydration

t-test (n = 14)	p-value
PBS > Dry[1]	< 0.001
PBS Dry > Dry	< 0.001
PBS > PBS Dry	0.161

[1]Test for significance: Is the punching force of a wet sample greater than the punching force measured for a dry sample?

These results indicate that for saturated and hydrated cartilage samples, a value of 2.60 ± 0.38 N (mean +/- standard deviation) should be subtracted from the total force measurements. Also, 2.46 ± 0.38 N should be subtracted from the total force measurements of dry cartilage samples.

4.3.1.3 Cartilage

The MPF of cartilage samples can be determined by subtracting the MPF of two layers of wax paper from the MPF of cartilage and wax paper punched together, Table 4.6. The mean MPF of PBS wax paper determined previously is subtracted from the mean MPF of saturated and hydrated cartilage samples punched in wax paper to determine the true MPF of the cartilage samples. The mean MPF of PBS Dry wax paper is subtracted from the mean MPF of dry cartilage samples.

Table 4.6: Mean maximum punching force of cartilage between wax paper, wax paper, and cartilage at each hydration level (mean +/- st. dev.)

Hydration Level	Cartilage in Wax Paper (N)	Wax Paper (N)	Cartilage[1] (N)
Saturated[2]	2.46 ± 0.39	2.60 ± 0.38	- 0.14 ± 0.54
Hydrated[2]	3.18 ± 0.63	2.60 ± 0.38	0.58 ± 0.74
Dry[3]	4.01 ± 0.37	2.46 ± 0.38	1.55 ± 0.53

[1]Calculated by subtracting the mean maximum punching force of wax paper from that of cartilage in wax paper
[2]PBS wax paper
[3]PBS Dry wax paper

4.3.2 Final Hole Size

When punching holes in cartilage, the size of the final hole is generally smaller than the punch diameter and the holes tend to be slightly non-circular. Figure 4.4 shows a sample of cartilage that was punched while saturated. The punch diameter is 201 μm, but the resulting hole size is approximately one half to one fourth the punch diameter, Fig. 4.4(a).

Table 4.7 shows that final hole size is a function of sample hydration during punching and during measurement. The punch diameter and the die clearance were held constant at 201 μm and 3.7% respectively, and the final hole diameters are presented. For all comparisons in Table 4.7, the results are significant ($p < 0.050$). In general, a hole punched in dry cartilage will be larger than a hole punched in saturated cartilage.

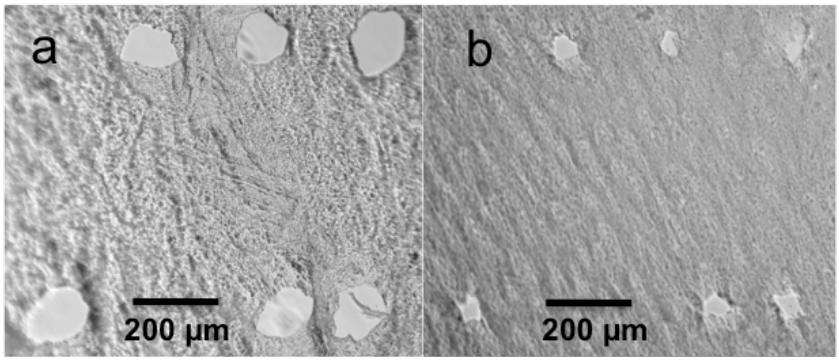

Figure 4.4: Holes punched in saturated cartilage. (a) The picture was taken while the sample was dry. (b) The picture was taken while the sample was saturated (201 μm punch, 208 μm die, 3.7% die clearance).

Table 4.7: Comparison of average final hole diameter (μm) for dry and saturated conditions (mean +/- SD; n=6)

	Punching Condition[1]	
Sample Condition During Measurement	Dry (12 hours)	Saturated
Dry	143 +/- 12	105 +/- 8
Saturated	176 +/- 10	50 +/- 4

[1]Punch diameter = 201 μm; Die clearance = 3.7%; 95 μm thick cartilage

The final hole diameters are measured after the force measurement trials are completed. Hole diameters were measured in the saturated state for samples punched while saturated or hydrated, while hole diameters were measured in the dry state for samples punched while dry. The mean final hole diameters are presented for each hydration level in Table 4.8. The mean final hole diameter of saturated and hydrated samples are not significantly different, however the hole diameter of dry samples is significantly greater than saturated and hydrated samples ($p < 0.050$). The mean hole diameter of dry samples is nearly four times larger than that of saturated and hydrated samples, Fig. 4.4. The coefficients of variation of saturated and hydrated samples are larger than that of dry samples.

Table 4.8: Mean final hole radius for each hydration level (n=10)

Level of Hydration	Mean Final Hole Diameter (μm)[1]	Standard Deviation (μm)	Coefficient of Variation (%)
Saturated	51	13	25.5
Hydrated	50	12	24.0
Dry	192	10	5.2

[1]Measured while saturated; Punch diameter: 201 μm; Female die hole diameter: 216 μm

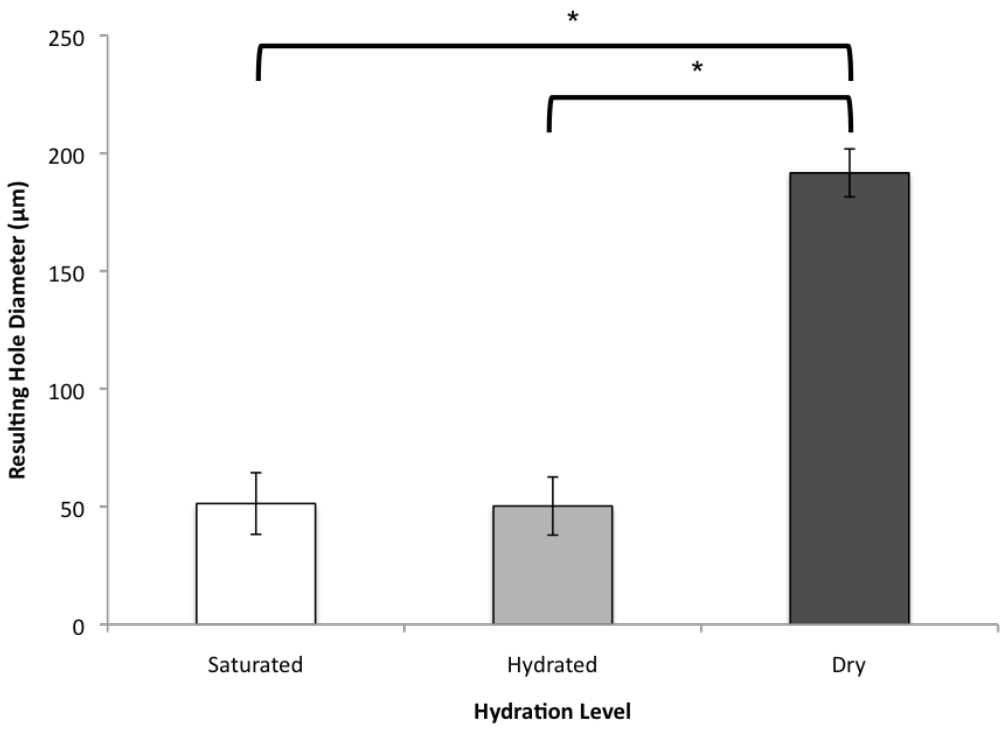

Figure 4.5: Mean resulting hole diameter in cartilage for each hydration level (bars indicate +/- one st. dev.). Sample measured while saturated (n=10, 201 µm punch, 216 µm die, 8.5% nominal die clearance). * Statistically significant ($p < 0.05$).

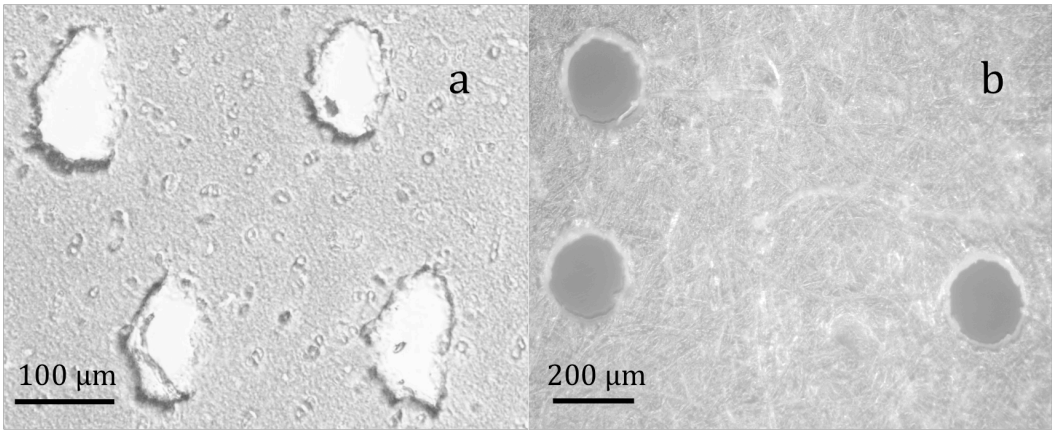

Figure 4.6: Comparison of hole shape for micro-holes punched in cartilage samples: (a) saturated and (b) dry. Saturated samples have irregularly shaped holes and dry samples have round shaped holes (201 µm punch, 216 µm die, 8.5% nominal die clearance).

In addition, holes punched in dry samples are round, but in saturated samples the holes are irregular, with hydrated samples also being irregular in shape, Fig. 4.6.

4.3.3 SEM Photos

Holes were punched in samples at each hydration level and then dried and imaged with a SEM. Figures 4.7-4.9 present the SEM images of samples punched while saturated, hydrated, and dry respectively.

The inside edges of the holes punched in the saturated sample have noticeable fibers extending into the hole, Fig. 4.7. One fiber, in fact, stretches across the diameter of the hole, unbroken. The fibers appear to have been stretched and broken during the punching process.

On the other hand, the inside edges of the holes punched in the dry sample are very smooth with no collagen fibers extending into the hole, Fig. 4.9. The collagen fibers do not appear to have been stretched during the punching process.

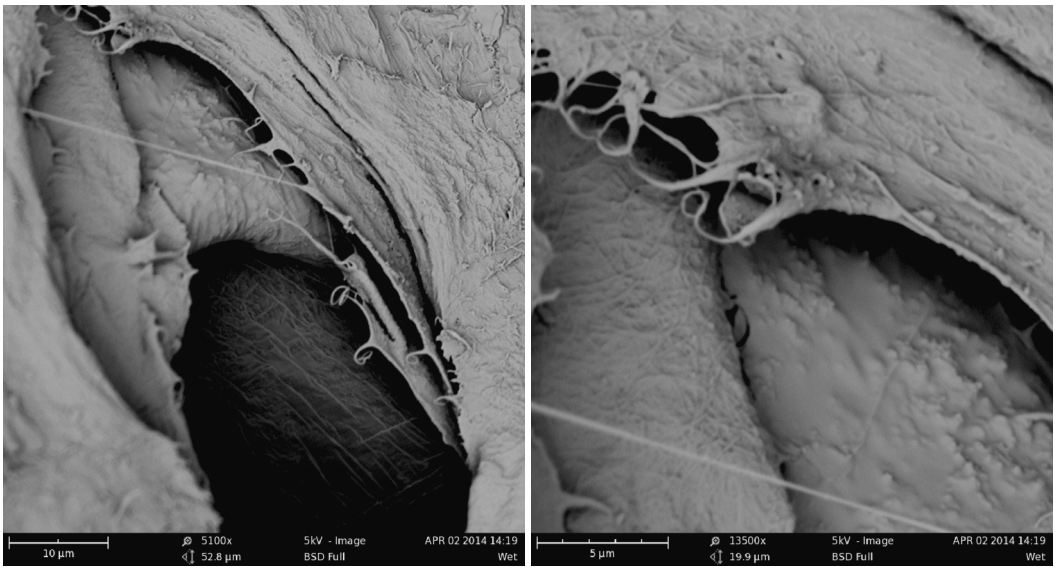

Figure 4.7: Scanning electron microscopy image of a hole punched in a saturated sample of cartilage (201 µm punch, 208 µm die, 3.7% die clearance; view of hole at 45°, SEM voltage: 5 kV, (a) 5,100X (b) 13,500X)

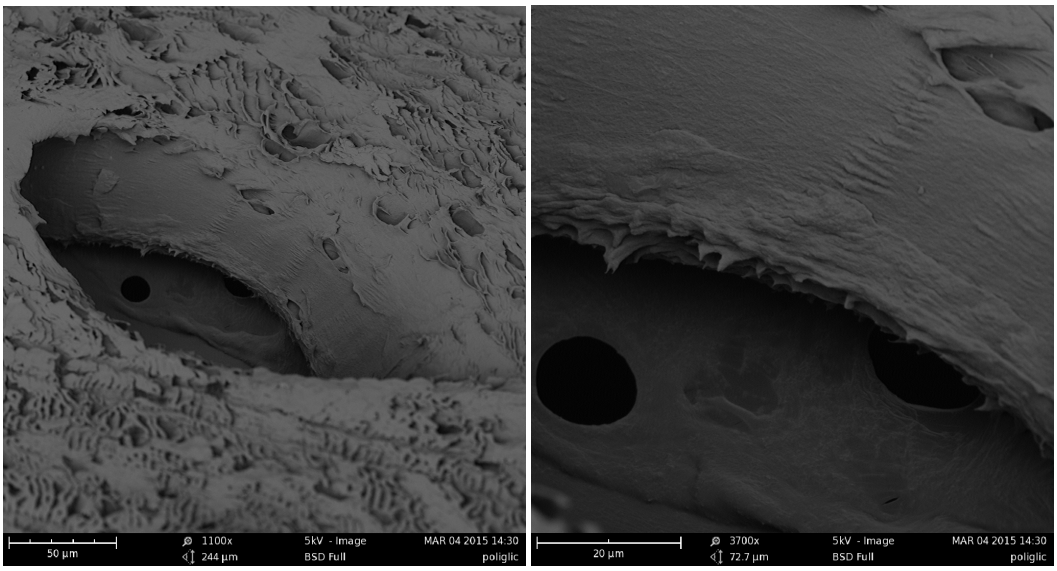

Figure 4.8: Scanning electron microscopy image of a hole punched in a hydrated sample of cartilage (201 µm punch, 208 µm die, 3.7% die clearance; view of hole at 45°, SEM voltage: 5 kV, (a) 1,100X (b) 3,700X)

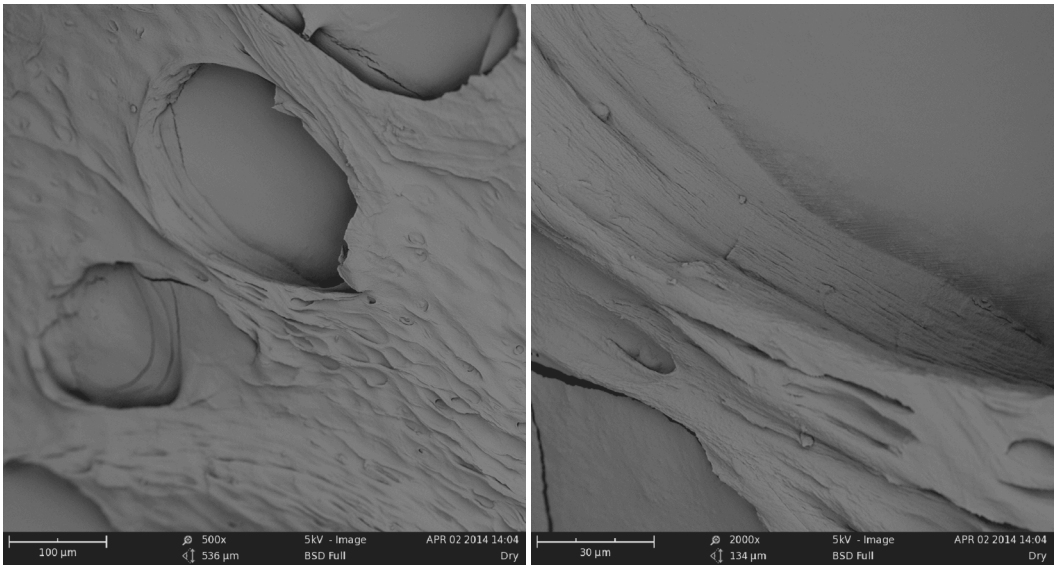

Figure 4.9: Scanning electron microscopy image of holes punched in a dry sample of cartilage (201 µm punch, 208 µm die, 3.7% die clearance; view of holes at 45°, SEM voltage: 5 kV, (a) 500X (b) 2,000X)

The holes punched in the hydrated sample, Fig. 4.8, appear to have characteristics between those of the saturated and dry sample. Fibers slightly protrude into the center of the holes on one side of the sample, but are much less pronounced than the fibers of the saturated sample, and the rest of the inside of the hole appears smooth

like the holes in the dry sample. This indicates that fibers were stretched slightly during the punching process, but not as much as those in the saturated sample.

4.4 Discussion

4.4.1 Effect of Hydration on Maximum Punching Force

The investigation of hydration level on MPF revealed a significant trend of the force increasing as the hydration level decreased (as the sampled dried out). Saturated samples had the lowest mean MPF and dry samples had the highest MPF, with hydrated samples' mean MPF being between the two, but slightly closer to that of saturated samples. Hydrated samples had the highest coefficient of variation due to biological variation and slight differences in hydration level at each hole location. Saturated and dry samples had lower coefficients of variation, caused only by slight biological variation and any error in dynamometer measurement.

The force measurements taken while punching wax paper indicated that PBS and PBS Dry samples had higher standard deviations than samples that were never soaked in PBS. Thus, the wax paper introduces additional uncertainty in the maximum punching force measurements of cartilage between wax paper, increasing the standard deviations.

Given that the resulting hole size varies greatly with hydration level and slightly within each sample, force measurements were normalized by dividing the MPF by the final hole circumference when measured in the saturated state for saturated and dry samples and in the dry state for dry samples. This resulted in the hydrated samples having the greatest normalized MPF and dry samples having the lowest normalized MPF. The mean normalized MPF of dry samples has a very low coefficient of variation because the force measurements and resulting hole sizes of dry samples have very small variations. Hydrated and saturated samples, however, both had large coefficients of variation for normalized MPF, with hydrated samples having the highest.

Dry cartilage requires the most force to punch and saturated samples require the least force to punch. However, due to the variations of resulting hole size with changes in hydration level, dry samples require the lowest normalized force to punch, or the least amount of force per unit length of the circumference of the hole. The hydrated samples require the greatest normalized force to punch and saturated samples are in the middle. This means that dry samples are fractured more easily than hydrated and saturated samples, but more material is sheared or torn in dry samples, due to the larger hole sizes, than saturated and hydrated samples, resulting in higher MPFs.

The true punching force of cartilage was calculated by subtracting the maximum force required to punch wax paper from the MPF of cartilage and wax paper together. The results indicate that dry cartilage samples require approximately 1.55 N to punch. However, hydrated and saturated samples have very low force requirements that fall within the variability of the experimental parameters. The standard deviations of hydrated and saturated samples were greater than the calculated MPFs of only cartilage, thus these calculated MPFs are within the uncertainty of the measurements and could be due to noise in the dynamometer and the data smoothing process. Therefore, hydrated and saturated cartilage samples (100 μm in thickness) require negligible force to punch.

This method used for calculating MPF of cartilage samples i.e., by subtracting the MPF of wax paper from the MPF of cartilage between wax paper, should be confirmed by experimentally measuring the force required to punch only cartilage. The standard deviations of measuring the punching force of cartilage samples and wax paper contribute to high levels of uncertainty when calculating the MPF of cartilage. Thus, more accurate equipment and setup are necessary to measure these low punching forces.

4.4.2 Effect of Hydration on Resulting Hole Size

The investigation of the effect of hydration level on resulting hole size revealed that saturated and hydrated samples had nearly identical hole sizes of about one quarter

the size of the male punch, while dry samples had much larger resulting holes, nearly equal to the punch diameter.

Under SEM examination, edges of the holes that were punched while saturated or hydrated appeared to have a more ragged appearance than equivalent holes punched when the cartilage is dry. The holes punched in saturated and hydrated samples also have more irregular shapes while the holes in dry samples are nearly round. When the cartilage is saturated or hydrated, it is hypothesized that collagen fibers are stretched into the clearance gap between the male and female dies, resulting in a tensile failure mode. This would explain the higher normalized punching force and the resulting hole diameter being much smaller than the punch diameter. In comparison, the edges of holes punched when the cartilage is dry appeared to be smooth, indicating that collagen fibers were likely fractured by shear. This would explain the larger hole size and lower normalized punching force.

The samples had significantly larger holes when punched while dry as compared to punching while saturated. This is true whether the samples were saturated or dry when the pictures were taken, supporting the hypothesis that during punching saturated samples stretch into the female die before tearing, while dry samples are sheared. However, when the dry punched sample is rehydrated, average hole size increases, but when the saturated punched samples are rehydrated, average hole size decreases. Generally, as a sample is rehydrated, it expands and as it dries out it contracts. This explains why the hole sizes of dry punched samples were smaller when dry. It is hypothesized that as the saturated punched sample dries out, the collagen fibers that are extending into the hole contract, which makes the hole size appear larger.

From this research, it is clear that the edge quality, shape, and diameter of the holes is affected by the hydration level of the cartilage while micropunching. If larger, smooth, round holes are desired (nutrient channels), samples can be punched in a dry

state, and if smaller, ragged, irregular holes are desired (wells for cell seeding/lacunae alternatives), the samples can be punched while saturated or hydrated.

4.5 Conclusion

For the design of die sets, results from this study indicate that the expected MPF should range from approximately 2 N to 4.5 N for samples of approximately 100 μm thickness, and will not exceed 5 N. If the measured force on the male punch exceeds 5 N, it can be assumed that the punch is in contact with the hole in the female die. Though hydration level has a statistically significant effect on MPF, all measurements are in a similar range so the same maximum expected force can be used for all hydration levels.

Hole size and quality are also greatly affected by hydration level. Therefore, the hydration level of the sample can be used to control these parameters based on the desired outcome. If holes are desired to act as nutrient channels, they can be punched in dry samples so that they are larger, round, and smooth. However, if holes are desired for wells to seed cells for culture, samples can be punched in saturated or hydrated states so the holes are smaller, irregular, and ragged, which may result in better cell adhesion. With further investigation, hole size can be correlated to exact hydration level and the resulting hole sizes can be predicted a priori.

5 Analytical Model to Predict Maximum Punching Force

5.1 Introduction

Understanding the mechanics involved in punching holes in cartilage extracellular matrix (ECM) is important during the design of die sets. Determining the maximum punching force (MPF) is necessary for designing both die sets and a machine capable of creating large matrices of holes in a single stroke of the punch press. The stroke-force profile is useful in material selection for dies and can also provide insight into the alignment process where punch deflection is a concern. For example, if the force on a punch is significantly greater than the MPF calculated, then it can be assumed that the punch is misaligned and interfering with the female die. Also, long punches that are small in diameter may be susceptible to buckling.

The literature provides a starting point for an evaluation of punching mechanics. Shergold et al. modeled the puncture of elastic solids using the Ogden strain energy density function [45, 46, 57]. The model predicts the total punching force as a combination of three forces: (1) the force needed to produce a crack in the solid, (2) the force needed to compress a column of the material below the head of the punch, and (3) the force needed to elastically expand the circumference of the crack to the size of the circumference of the punch. Research here was undertaken to test the application of a modified version of Shergold et al.'s force prediction model to micropunching holes in thin slices of cartilage ECM.

Shergold's model utilizes some assumptions to simplify the model and to validate the use of the Ogden function. First, one requirement for the Ogden strain energy density function to be valid is that the solid must be incompressible. If the water in cartilage has mostly or completely evaporated from the matrix, it can be assumed that cartilage ECM acts as an incompressible solid because the constitutive components are

incompressible. Thus, at hydrated and dry hydration levels, the incompressibility assumption is largely valid. When punching holes for cell seeding purposes, nearly all of the holes punched are in the hydrated or dry hydration levels, so these are the most important levels to be able to predict the maximum punching force.

To simplify the forces contributing to the maximum punching force, the friction on the punch as it slides against the sides of the hole is neglected. This is an acceptable assumption because the cartilage samples being punched are quite thin, approximately 100 µm. In addition, Shergold et al. made this assumption for thick solids because the contribution of the friction force is negligible compared to the other factors contributing to the penetration force [46].

In the modified version of the Shergold model used in this research, the force required to compress a column of the material below the head of the punch is neglected. This is a valid assumption due to the small thickness of cartilage samples. Thus, the remaining contributions to the maximum punching force are the force required to create a crack in the solid and the force required to elastically expand the radius of the crack.

Following the Shergold model, the work done by the punch is equal to the sum of the work done to create the crack and the work done to elastically expand the hole,

$$F_{total}\delta h = 2\pi b J_{IIC}\delta\ell + \frac{\partial S_H}{\partial \ell}\delta\ell \tag{5.1}$$

where F_{total} is the total punching force, δh is the increment by which the head of the punch is advanced, b is the radius of the hole after the punch has been removed, J_{IIC} is the Mode II fracture toughness of the material, $\delta\ell$ is the instantaneous vertical distance of the advancement of the column of compressed material, and $\frac{\partial S_H}{\partial \ell}$ is the energy stored in the solid, radially around the hole. Shergold et al. derived the mathematical calculation of each component [46]. Following this derivation, the version of the force equation used is

$$\frac{F_{total}}{\pi\mu R^2} = \left[\frac{2b}{R}\frac{J_{IIC}}{\mu R}\right] + \left[\frac{2}{\alpha^2}\int_1^{\infty}\left[\left(1-\frac{\left(\frac{b}{R}\right)^2}{\eta}\right)^{-\alpha/2} - 2\right]d\eta\right] \tag{5.2}$$

where $\eta = \left(\frac{r}{R}\right)^2$, r is the instantaneous radial position, and R is the punch radius. Equation (5.2) utilizes the shear modulus, μ, the strain-hardening exponent, α, and the mode II fracture toughness, J_{IIC}, of the cartilage samples in wax paper. These parameters are determined experimentally. A complete derivation of Eq. (5.2) is shown in Appendix C.

5.2 Materials and Methods

5.2.1 Compression Testing

The parameters of the force prediction model must be determined for cartilage samples in wax paper at hydrated and dry hydration levels. Compression testing is performed to determine the shear modulus, μ, and strain-hardening exponent, α, at each hydration level.

For each trial, equine cartilage samples are selected from the superficial layer that was previously sectioned (see Section 3.2.3). A 5 mm diameter biopsy punch (33-35, Integra Miltex, York, PA, USA) is used to extract uniformly cylindrical samples with an approximate thickness of 100 μm.

Three cylindrical samples are concentrically stacked for each compression test. The stack of cartilage is placed between two pieces of 30 μm thick wax paper, compressed by a 500 g weight, and left to dry for the allotted amount of time: minimum of eight hours for dry samples and ten minutes for hydrated samples, forming the *Dry* and *Hydrated Stack Samples*, respectively. The dry stack samples shrink in diameter during the drying process. Thus, the diameter of the dry stack samples are measured again once they have reached the desired hydration level.

An unconfined compression test is performed on each of the dry and hydrated stack samples (3366 Load Frame, Instron, Norwood, MA, USA), Fig. 5.1. A varying load is automatically applied to the samples to attain a quasi-static compression rate of 4 μm/s. The hydrated and dry stack samples in wax paper are placed on the lower platen and compressed immediately after they reach their desired levels of hydration, Fig. 5.2. The resulting force vs. extension data is recorded. From these data, an engineering stress vs. engineering strain plot is created. This process is repeated so that a total of five hydrated and five dry stack samples are compressed.

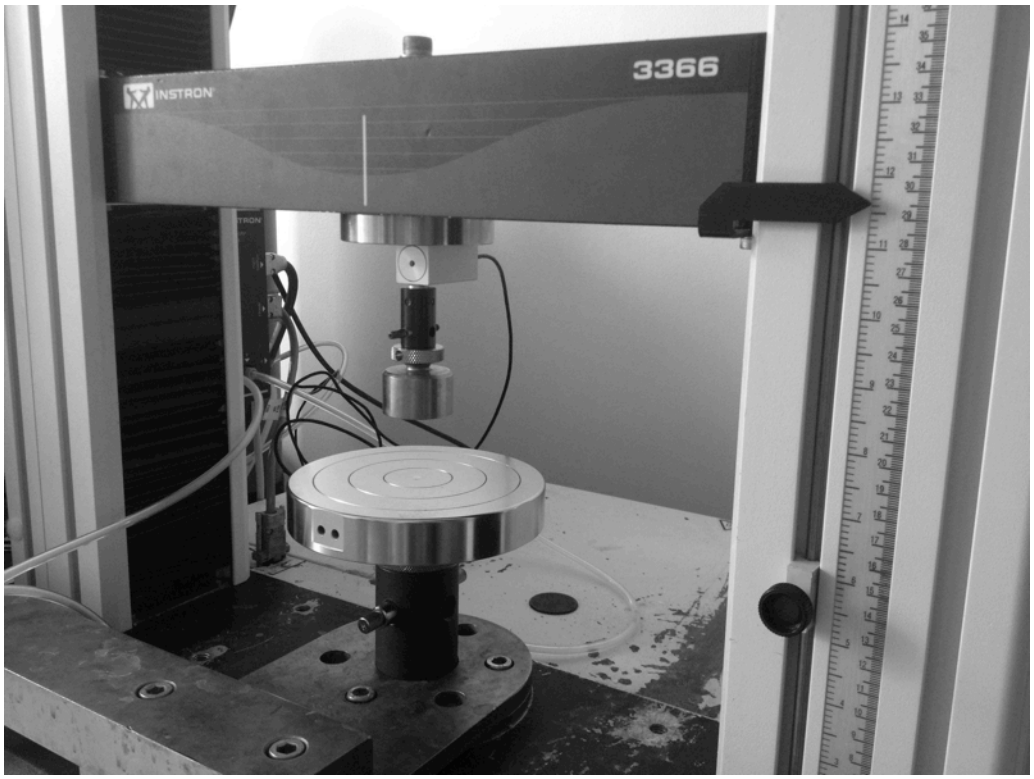

Figure 5.1: Compression testing setup

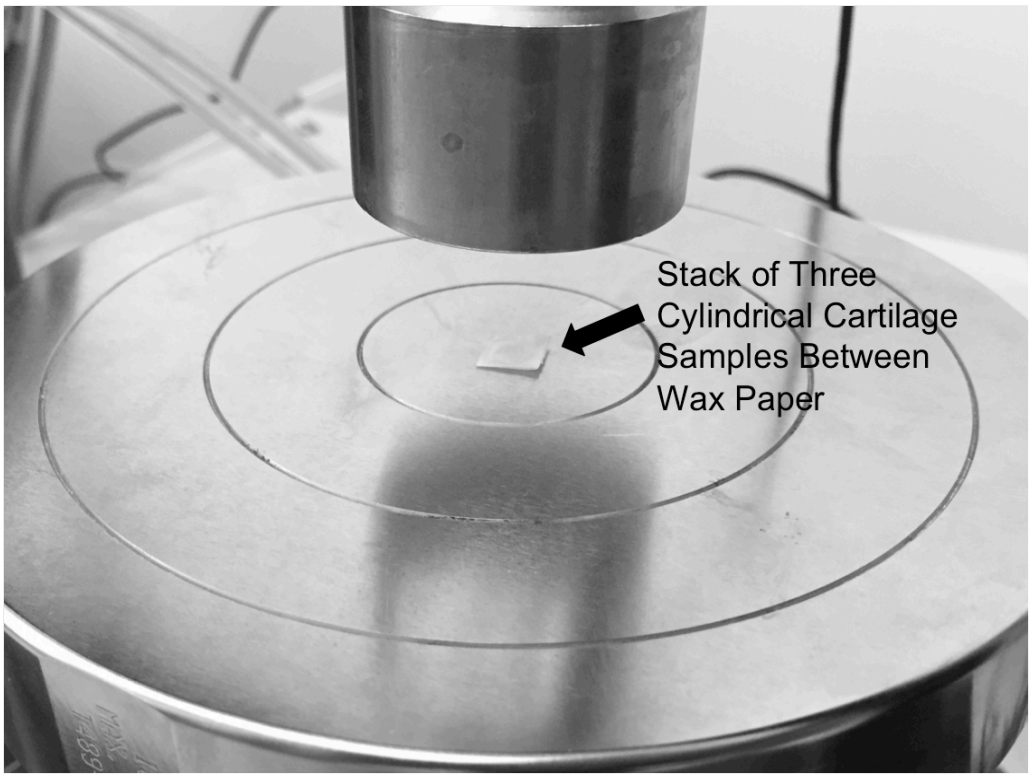

Figure 5.2: Stacked hydrated sample, in wax paper, on lower platen before compression testing

The gage length of each cartilage stack is calculated by extending the steepest straight portion of the elastic region of the load-deflection curve, until it intersects with the x-axis at zero stress. The intersection point is defined as zero strain, denoting the upper platen location at the gage length of the sample, point A, Fig. 5.3 [63]. All engineering strain calculations are taken from this intersection point.

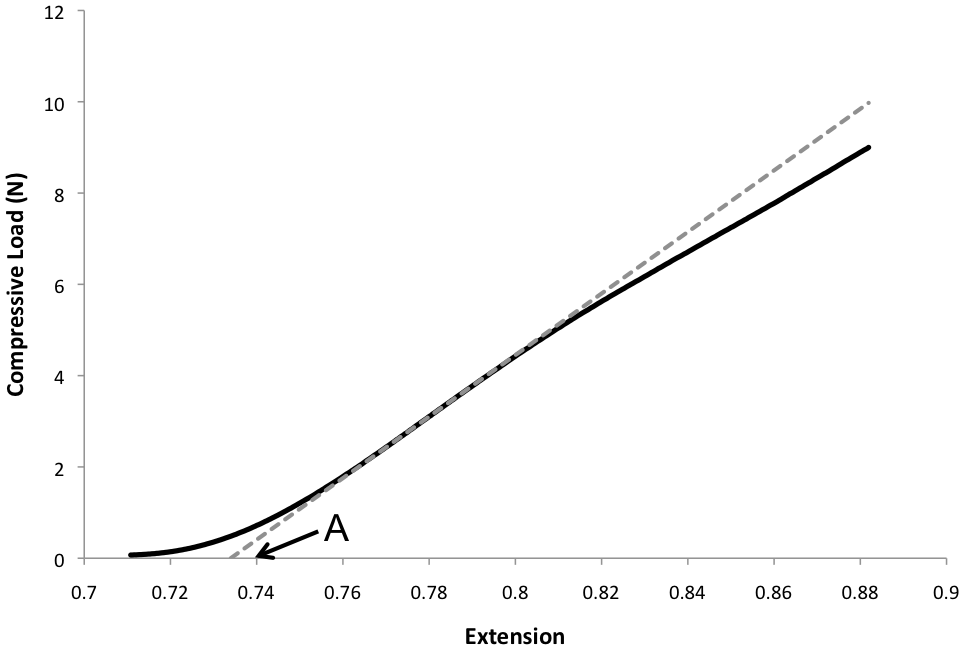

Figure 5.3: Compressive Load vs. Extension curve of a hydrated stacked sample with (A) upper platen position at gage length

The engineering stress is calculated by dividing the load on the sample by the nominal area of the sample. The nominal area of the hydrated samples is the area of the 5 mm diameter circular cross-sectional area and the nominal area of the dry samples is measured before compression.

5.2.2 Calculation of Shear Modulus and Strain-Hardening Exponent

Using data obtained from compression tests on cartilage, the shear modulus, μ, and the strain-hardening exponent, α, are calculated for hydrated and dry samples. The

stretch ratio, λ_z, of the samples is needed for these calculations. This ratio is defined as the compressed thickness of the sample at each moment, divided by the gage length of the sample. Thus, the stretch ratio is calculated by

$$\lambda_z = \frac{L - \left[x(t) - x(0)\right]}{L} \tag{5.3}$$

where L is the gage length, x(t) is the position of the compressing platen at time t, and x(0) is the position of the compressing platen when it is at the gage length, or point A on the sample load-extension curve, Fig. 5.3.

The stress on the sample in the direction of compression is computed by dividing the load on the sample by its nominal area. The stress can also be calculated analytically by taking the derivative of the Ogden strain energy function with respect to the stretch ratio in that direction and subtracting hydrostatic pressure, p, [57], Eq. (5.4),

$$\hat{\sigma}_z = \frac{d\phi}{d\lambda_z} - p \tag{5.4}$$

where $\hat{\sigma}_z$ is the calculated stress in the direction of compression and $\frac{d\phi}{d\lambda_z}$ is the derivative of the Ogden strain energy function with respect to the stretch ratio in the direction of the compression, λ_z. The hydrostatic pressure is introduced due to the assumption of incompressibility [58]; there will be an internal hydrostatic pressure in the sample causing it to expand radially when compressed axially. This hydrostatic pressure, however, is small in comparison to the stress due to the compression, so it can be assumed to be zero.

The Ogden strain energy function, ϕ, in terms of the coordinate stretch ratios is written as,

$$\phi = \frac{2\mu}{\alpha^2}\left(\lambda_x^\alpha + \lambda_y^\alpha + \lambda_z^\alpha - 3\right) \tag{5.5}$$

where λ_x, λ_y, and λ_z are the stretch ratios in the x, y, and z directions, respectively (z is the direction of compression). By assuming that the material is incompressible, the product of the three stretch ratios must equal 1.0. This allows the three stretch ratios to be related in one equation [58]. Therefore, according to Shergold et al. [57] it can be stated that

$$\lambda_x = \lambda_y = \frac{1}{\sqrt{\lambda_z}} \tag{5.6}$$

when z is the direction of compression. The result of the differentiation of the Ogden strain energy function is the analytically calculated stress [57],

$$\hat{\sigma}_z = \frac{d\phi}{d\lambda_z} = \frac{2\mu}{\alpha}\left(\lambda_z^{\alpha-1} - \lambda_z^{-1-\alpha/2}\right) \tag{5.7}$$

The full derivation of Eq. (5.7) is shown in Appendix D.

The relative least squares error of the analytically calculated stress is given by

$$S = \left(\sigma_z - \hat{\sigma}_z\right)^2 \tag{5.8}$$

where $\hat{\sigma}_z$ is the analytically calculated stress from Eq. (5.7) and σ_z is the engineering stress measured from the compression test. The results of the compression tests and the analytical representation of the stress on the sample from Eq. (5.7) are combined with Eq. (5.8) to produce Eq. (5.9).

$$S = \left[\sigma_z - \frac{2\mu}{\alpha}\left(\lambda_z^{\alpha-1} - \lambda_z^{-1-\alpha/2}\right)\right]^2 \tag{5.9}$$

The variables μ and α are determined by numerically minimizing the error function, Eq. (5.9). The least squares error, S, is computed for each data point by calculating the analytical stress at each point and comparing it to the measured stress at said point. The average of all values of S is then minimized by finding the ideal values of μ and α in the admissible range. Equations (5.8) and (5.9) are derived in Appendix E.

5.2.3 Calculation of Fracture Toughness

Mode II fracture toughness, J_{IIC}, for each hydration level is calculated with data from the "two-punch tests", Table 4.1. Since the samples used are approximately 100 μm thick, it can be assumed that the two surfaces contacting the male and female dies will crack simultaneously. Thus, the peak forces of each trial can be used rather than integrating over the distance that the punch travels from the crack forming at the punch face and the crack forming in proximity to the hole in the female die. The peak force of the first trial of the "two-punch test" is recorded and the same is done with the second trial. The second peak force is then subtracted from the first.

Since the top and bottom surfaces are assumed to crack simultaneously, the simplified version of the fracture toughness equation is applicable,

$$J_{IIC} = \frac{F_{total,1} - F_{total,2}}{2\pi b} \tag{5.10}$$

where J_{IIC} is the Mode II fracture toughness of the material, $F_{total,1}$ is the peak force on the punch during the first trial, $F_{total,2}$ is the peak force on the punch during the second trial (after a hole is formed), and *b* is the radius of the hole after the punch is removed. A full derivation of Eq. (5.10) is shown in Appendix F.

The fracture toughness is calculated at each punching location for cartilage samples between wax paper because the fracture toughness could differ at each location within a sample due to natural variations in biological tissues. Refer to Section 4.2.1 for a review of the procedure.

5.2.4 Prediction of Punching Force

The force on the punch is predicted using the fracture toughness, the shear modulus, and the strain-hardening exponent. Recall that Eq. (5.2) is modified from the original equation used by Shergold et al. [57] for the samples used in this study.

Specifically, the force needed to compress the column of material below the punch is neglected because it is insignificant compared to the other factors due to the small thickness of the samples. Therefore, the only components of total force that are considered are: (1) force required to create and propagate the crack in the material, and (2) expanding of the hole to the size of the punch. The predicted force, Eq. (5.2), is computed numerically (Matlab, MathWorks, Natick, MA, USA) due to the integral.

5.3 Results

5.3.1 Analysis of Compression Testing

Compression tests were conducted on five Hydrated and five dry stack samples in wax paper. An engineering stress-engineering strain curve obtained from a typical compression test on a hydrated and a dry stack sample is shown in Fig. 5.4.

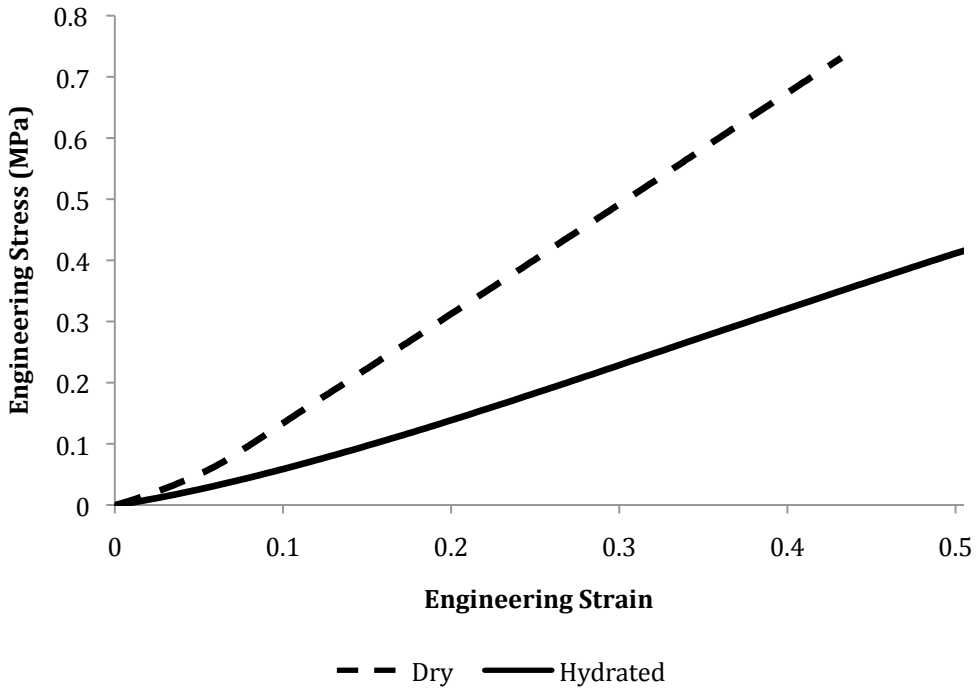

Figure 5.4: Engineering stress-engineering strain curves of Dry and Hydrated stack samples between wax paper

Table 5.1: Shear modulus and strain-hardening exponent determined from compression testing for cartilage samples at hydrated and dry hydration levels

Hydration Level	Shear Modulus (μ) (MPa)	Strain-Hardening Exponent (α)
Hydrated (n=5)	0.15	1.49
Dry (n=5)	0.49	2.45
B452 Silicone Rubber Skin Substitute [45, 46]	0.40	3.0
Human Skin [45, 46]	0.11	9.0

Data from compression tests is used to calculate the shear modulus, μ, and strain-hardening exponents, α, of hydrated and dry cartilage samples in wax paper. The measured stress values and the calculated predicted stress values from Eq. (5.7) are used with Eq. (5.9) to determine μ and α for each trial. The average μ and α values of the five trials are then calculated for each hydration level, Table 5.1. For reference, values of μ and α are also shown for human skin and a silicone rubber skin substitute. The values of μ and α for each compression trial are reported in Appendix G.

5.3.2 Calculating Fracture Toughness

Mode II fracture toughness for each hole punched in hydrated and dry samples in wax paper is calculated according to Eq. (5.10).

The "two-punch test" is performed for four holes in three different equine samples at hydrated and dry hydration levels. These data are taken from the previous chapter on the effect of hydration on maximum punching force, Table 4.1. The data for hydrated samples are presented in Table 5.2 and the data for dry samples are presented in Table 5.3.

Table 5.2: Data from "two-punch test" on hydrated samples (201 μm punch, 216 μm die, 7.47% nominal die clearance)

Measured Maximum Punching Force (N)	Second Stroke Punch Force (N)	Resulting Hole Radius (μm)	Fracture Toughness (N/m)
3.78	0.41	19.93	26922
3.01	0.29	36.27	11934
2.61	0.66	30.26	10288
3.10	0.40	27.50	15667
2.91	0.72	26.71	13069
2.49	0.33	22.49	15269
3.17	0.33	18.44	24538
4.50	0.80	29.63	19850
3.62	0.65	23.99	19697
2.56	0.88	15.97	16778

Table 5.3: Data from "two-punch test" on dry samples (201 μm punch, 216 μm die, 11.71% nominal die clearance)

Measured Maximum Punching Force (N)	Second Stroke Punch Force (N)	Resulting Hole Radius (μm)	Fracture Toughness (N/m)
3.62	0.28	94.93	5594
3.55	0.20	98.44	5414
4.50	0.28	99.54	6756
4.17	0.30	95.66	6444
3.44	0.25	86.36	5894
4.32	0.34	89.43	7081
4.33	0.27	92.29	7002
4.12	0.30	100.39	6053
3.90	0.28	99.62	5789
4.18	0.25	101.53	6164

Table 5.4: Average fracture toughness of hydrated and dry samples in wax paper

Hydration Level	Average Fracture Toughness (N/m)	Standard Deviation (N/m)	Coefficient of Variation (%)
Hydrated	17401	5375	30.9
Dry	6219	583	9.4

The average fracture toughness determined by micropunching cartilage in wax paper at each hydration level is summarized in Table 5.4. The average fracture toughness

of hydrated samples is nearly three times greater than that of dry samples. This supports the results of the previously calculated normalized MPF, which revealed that dry samples had a much lower normalized mean MPF than hydrated samples, indicating that dry samples require less force to fracture.

5.3.3 Punching Force Prediction

Using the average shear modulus and strain-hardening exponent for each hydration level and the fracture toughness at each hole location, the MPFs at those locations were predicted using Eq. (5.2). The results of the predicted force calculations and the measured MPFs, as well as the percent difference between the two, at each location are presented in Tables 5.5 and 5.6 for hydrated and dry samples, respectively.

Table 5.5: Measured and predicted maximum punching forces for hydrated samples of cartilage in wax paper

Measured Maximum Punching Force (N)	Predicted Punching Force (N)[1]	Percent Difference
3.78	4.62	22.2%
3.01	3.51	16.4%
2.61	2.85	8.9%
3.10	3.66	18.9%
2.91	3.17	8.9%
2.49	3.28	31.8%
3.17	4.18	31.7%
4.50	4.60	2.3%
3.62	4.03	11.4%
2.56	3.22	25.9%

[1] $\mu = 0.15$ MPa; $\alpha = 1.49$ (Table 5.1)

Table 5.6: Measured and predicted maximum punching forces for dry samples of cartilage in wax paper

Measured Maximum Punching Force (N)	Predicted Punching Force (N)[1]	Percent Difference
3.62	3.92	8.4%
3.55	3.91	10.3%
4.50	4.78	6.2%
4.17	4.46	6.8%
3.44	3.85	11.7%

4.32	4.60	6.7%
4.33	4.67	7.7%
4.12	4.37	6.0%
3.90	4.18	9.7%
4.18	4.48	7.1%

[1] $\mu = 0.49$ MPa; $\alpha = 2.45$ (Table 5.1)

A two sample t-test was performed to determine if the average predicted and measured MPFs were significantly different ($p < 0.050$) for each hydration level. The results show the predicted MPFs are not significantly different from the measured MPFs for both hydrated ($p = 0.071$) and dry samples ($p = 0.058$). However, the predicted MPFs are almost significantly different from the measured MPFs, so caution must be used when making conclusions. In addition, the predicted and measured values for hydrated samples differ by an average of 17.8%, with a max percent error of 31.8%, Table 5.5, and dry samples differ by an average of 8.1%, with a max percent error of 11.7%.

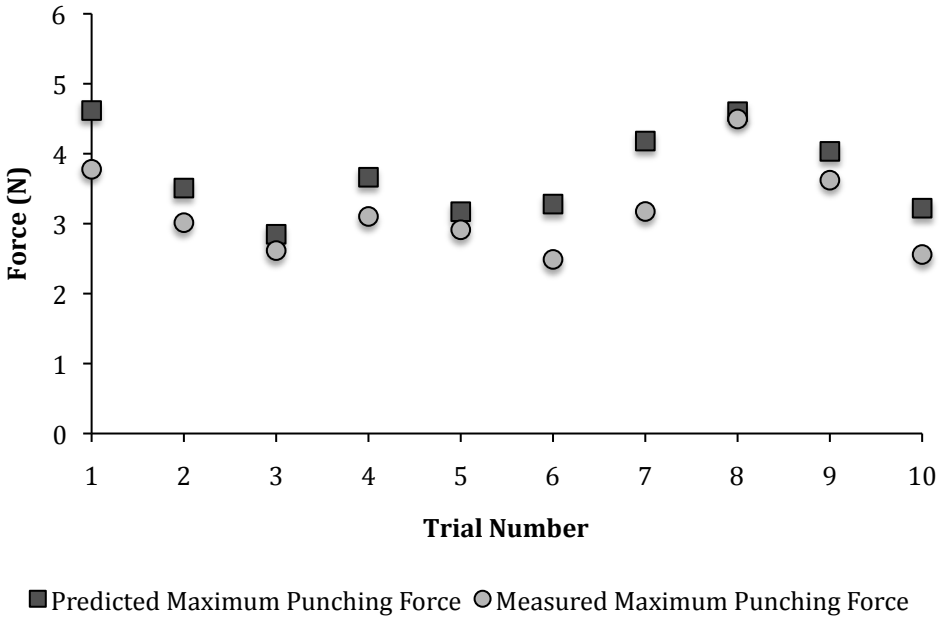

Figure 5.5: Comparison of measured and predicted maximum punching forces for each trial of hydrated samples

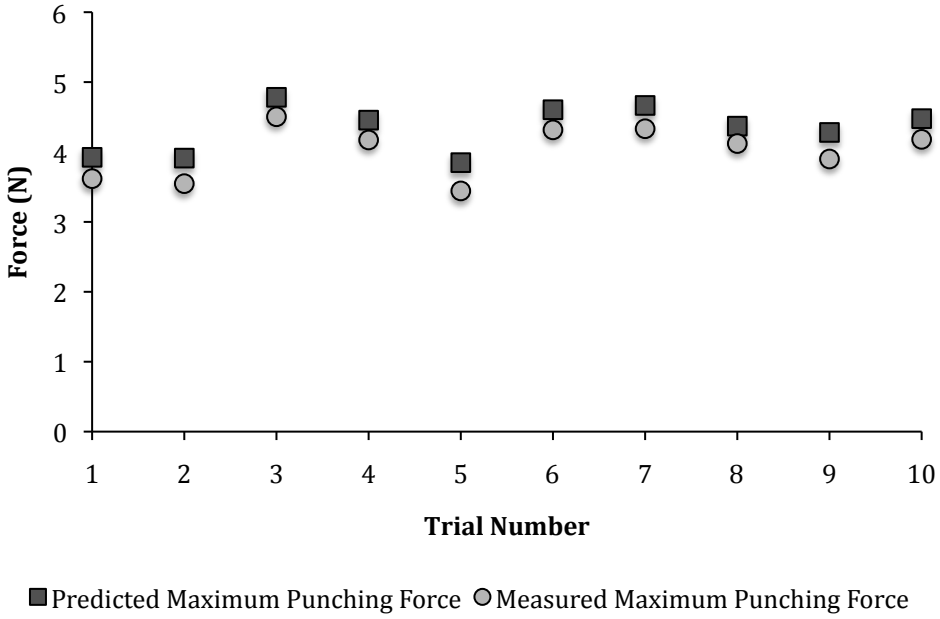

Figure 5.6: Comparison of measured and predicted maximum punching forces for each trial of dry samples

The predicted MPFs follow the same trend of results as the measured values. When a higher force is recorded during punching, the predicted force reflects this trend. The trend is followed by the predictions for hydrated samples as well, but the level of accuracy varied with each hole location. One predicted value differed from the measured MPF by only two percent while others differed by over thirty percent, but all predicted values were greater than their respective measured values for both states of hydration. Still, when comparing the average for all measurements and predictions, the predicted values are not significantly different than the measured MPFs. In general, the level of accuracy of the predicted values for dry samples was much greater than that of hydrated samples. The predicted MPFs for dry samples varied from their respective measured value by between 6% and 12%.

The predicted force, Eq. (5.2), takes into consideration the radius of the male punch, the radius of the resulting hole, shear modulus, strain-hardening exponent, and

fracture toughness for a combination of wax paper and cartilage. Thus, a predicted MPF can be calculated for any cartilage sample in wax paper at hydrated and dry hydration levels using the average shear modulus, strain-hardening exponent, Table 5.1, fracture toughness, Table 5.4, and resulting hole radius, Table 4.1, for each hydration level. This predicted MPF and the average measured MPF for each hydration level are presented in Table 5.7.

Table 5.7: Comparison of average measured and predicted maximum punching force for any hydrated sample and any dry cartilage sample in wax paper. Predicted maximum punching force was calculated using average shear modulus, strain-hardening exponent, fracture toughness, and resulting hole size at each hydration level.

Hydration Level	Mean Measured Maximum Punching Force (N)	Predicted Maximum Punching Force (N)	Percent Difference
Hydrated	3.18	3.77	18.8%
Dry	4.01	4.33	8.0%

The predicted MPFs of any hydrated sample and any dry sample are both reasonably accurate, with the dry MPF prediction being slightly more accurate. Both predictions, however, are greater than the measured mean MPF. This is beneficial because it creates a factor of safety when predicting the required MPFs. In addition, the predicted MPF of both a hydrated sample and a dry sample fall within one standard deviation of the mean measured MPF.

5.4 Discussion

The MPFs of hydrated and dry samples in wax paper were successfully predicted using a modified version of Shergold's model. An original method of compression testing thin cartilage slices by stacking multiple samples was performed as well as the "two-punch test" developed by Azar et al. [48] to determine the shear modulus, strain hardening exponent, and fracture toughness in the modified model.

The predicted MPFs were slightly higher than the measured MPFs for both hydrated and dry samples in wax paper, but followed the trend of the measured values closely. Predicted MPFs for hydrated samples had a lower degree of accuracy than that of dry samples. Yet, there was no significant difference between the predicted and measured forces for both hydrated and dry samples. In addition, the predicted MPFs of any hydrated sample and any dry sample only differed from the average MPFs measured by 18.8% and 8.0%, respectively.

These results confirm that the Ogden model is useful when predicting the punching force for hydrated and dry cartilage samples in wax paper. Dry cartilage samples have been shown to shear when they are punched, following a Mode II fracture failure method. Hydrated cartilage samples, however, appear to fail in tension, contrary to the Mode II fracture assumed in the modified Shergold model. Despite this contradiction, the model still appears to accurately predict the MPF of hydrated samples due to the assumption of an incompressible, elastic material and the contribution of wax paper to the fracture toughness calculation.

Thus, the modified Shergold model used provides a method to analytically predict the MPF of a thin cartilage sample based on hydration level and punch diameter for a micropunching process where wax paper is used to capture and position the cartilage for processing.

6 Comparing the Compressive Mechanical Properties of Porous and Nonporous Cartilage Samples

6.1 Introduction

When implanting a micropunched, porous, cartilage sample in vivo, it is important to know its mechanical properties in accordance with the degree of porosity. To promote integration, it is desirable for the mechanical properties of the implanted construct of an engineered tissue to match that of the native tissue as closely as possible. This is especially true for a tissue whose major function is providing mechanical support, such as articular cartilage. If the construct is not adequately stiff, it can be targeted by neighboring tissue for remodeling or fail under physiological loads. Where as if it is too stiff, it may lack the elasticity needed to mimic native tissue and could cause stress shielding, resulting in the degradation of the surrounding native tissue [64].

Punching micro-holes in the cartilage samples creates more surface area for cell adhesion and permits water inside the sample to escape more easily. The combination of a change in area and hydration under load may affect the mechanical integrity of the cartilage sample.

It is desirable to determine if the micropunching process significantly affects the mechanical properties of a cartilage sample. The stress-strain curves of samples that have not been punched, referred to here as nonporous, and samples that have been punched, so called porous, are compared. Specifically, the Young's moduli, compressive strengths, strains at yield, and stresses at yield are analyzed. If there is no significant difference between the mechanical properties of porous and nonporous samples, then it can be assumed that micropunching at the porosity level tested does not adversely affect the mechanical properties of the cartilage samples under compressive loading.

6.2 Materials and Methods

6.2.1 Cartilage Sample Preparation

Cartilage samples were micropunched to determine the effect of porosity on compressive Young's modulus and yield point. For each trial, six equine cartilage samples are selected with an approximate thickness of 100 μm. Three of the cartilage samples are chosen to be micropunched. These samples are placed between two pieces of 30 μm thick wax paper with two pieces of Kimwipes (Kimberly-Clark Professional, Roswell, GA, USA), 2.5 cm by 1.25 cm, folded four layers thick and soaked in phosphate buffered saline solution (PBS). The Kimwipes are placed in contact with the edges of the cartilage samples to help maintain hydration during punching. A square matrix of 100 holes is punched in three of the samples with a 201 μm diameter punch and a 216 μm diameter female die hole. The punch is moved laterally 250 μm between each stroke of the punch, leaving a nominal web of approximately 50 μm between the closest edges of the punch when forming adjacent holes. This creates a matrix of 100 holes in approximately a 2.5 mm x 2.5 mm square, Fig. 6.1. The remaining three equine samples are left unpunched as a control. A 5.0 mm diameter biopsy punch (33-35, Integra Miltex, York, PA, USA) is used to remove cylindrical samples from the porous and nonporous cartilage. The 100 hole matrix of the porous samples is centered in the cylinder, and the nonporous cylindrical punch-out is obtained from the center of the nonporous samples, or another undamaged section if the center appears compromised.

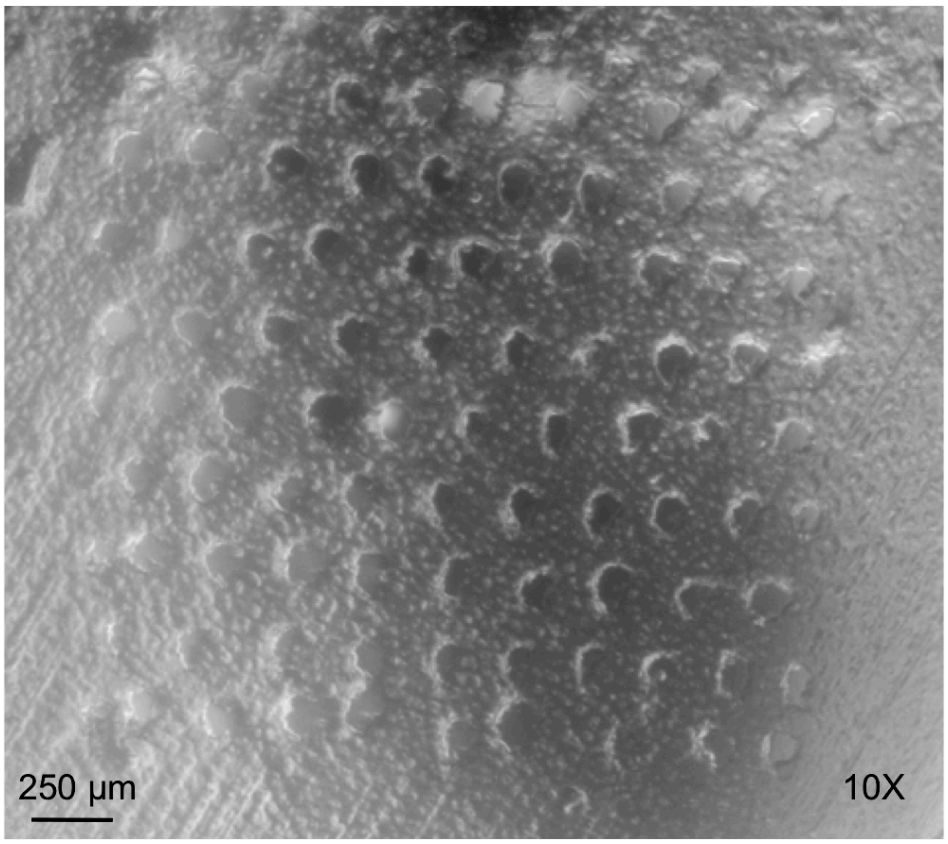

Figure 6.1: Micropunched porous sample for compression testing. 100 micro-holes punched (201 µm punch, 216 µm die, 8.5% nominal die clearance).

One of the porous samples is selected and the porous surface area is calculated using image analysis. The average diameter of the micro-holes in this sample is calculated by calibrating pixels to length while the sample is in a saturated state. The combined hole area is then calculated by determining the area of an average hole, and multiplying the value by the number of holes in the sample. The level of porosity of the samples is calculated by dividing the combined surface area of the micro-holes by the surface area of the sample prior to micropunching.

6.2.2 Compression Testing

An unconfined compression test is performed on each of the porous and non-porous stacked samples (3366 Load Frame, Instron, Norwood, MA, USA), which are each comprised of three cylindrical punch-outs that are stacked concentrically. A varying load is applied to the stacked samples to attain a quasi-static compression rate of 4 µm/s.

Once the nonporous and porous stacked samples are placed on the lower platen, a single drop of room temperature (22°C) PBS is placed on top of the sample to maintain hydration, Fig. 6.2. The samples are then compressed. The resulting load vs. extension data are recorded. From these data, engineering stress vs. engineering strain plots are created.

The thickness of each sample is calculated by extending the steepest straight portion of the elastic region of the load-deflection curve to the zero load line (x-axis). The point where this line crosses the x-axis is the point of zero strain, marking the upper platen position at the initial thickness or gage length of the sample [63]. All engineering strain calculations are taken from this point.

The engineering stress is calculated by dividing the load on the sample by the nominal area of the sample. The nominal area is the area of the nonporous stacked sample, which is the area of the 5 mm diameter circular cross-sectional area.

This process is repeated five times so that a total of five porous and five nonporous saturated stacked samples are tested in compression.

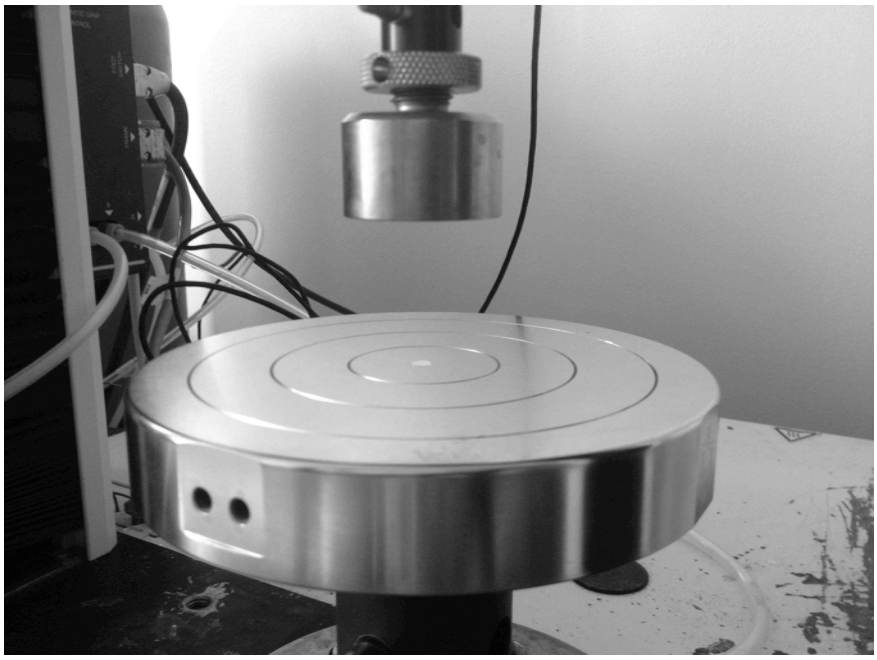

Figure 6.2: Stacked nonporous sample on lower platen before compression testing

6.2.3 Data Analysis

The data are analyzed to test the hypothesis that the micropunching process does not affect the mechanical properties of a porous sample. The engineering stress-engineering strain curves for nonporous (n=5) and porous (n=5) stacked samples are plotted to detect the linear region indicating compressive modulus. A line of best fit is calculated for the first 30 data points of each stress-strain curve and the slope is recorded. The set of 30 points is then shifted by one data point until the line of best fit is determined for every set. Within the elastic region of the stress-strain curve, the greatest slope recorded is considered the Young's modulus, ensuring that the R^2 value is at least 0.9990.

The compressive strength of a material is defined as the highest engineering stress value attained during compression. However, the stress level on a sample at 10% strain is considered the compressive strength if the sample does not yield before 10% strain or does not yield at all [63].

The yield point of the engineering stress-engineering strain curve is then determined. This point is defined by extending the steepest portion of the linear region of the stress-strain curve to the x-axis. A line with the same slope as the steepest portion is plotted and offset by 0.2% strain. The point where this line intersects with the stress-strain curve is the yield point [65]. The engineering strain and engineering stress at this point are recorded as the strain and stress at yield. This process is repeated for the compression data of each nonporous and porous stacked sample.

Two-sample t-tests are performed comparing mechanical properties of nonporous stacked samples and porous stacked samples.

6.3 Results

Compression tests were conducted on five nonporous and porous stacked samples in a saturated state. A typical engineering stress-engineering strain curve obtained from the compression tests on both a nonporous and porous stacked sample is shown in Fig. 6.3.

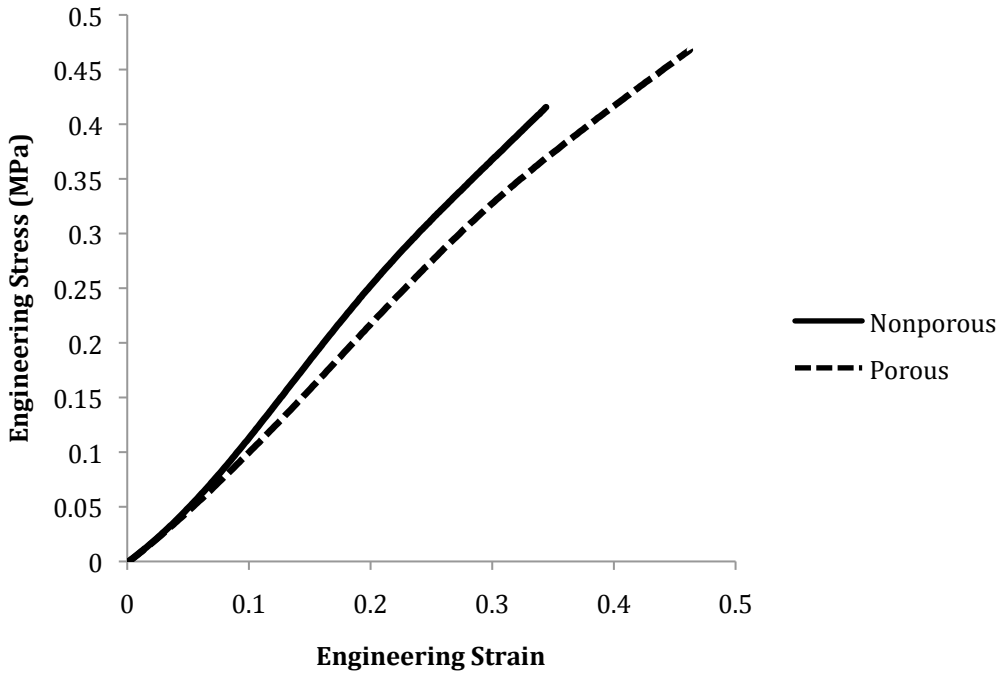

Figure 6.3: Engineering stress-engineering strain curve from compression testing of saturated nonporous and porous stacked samples (4% porosity)

The approximate porosity of the samples was calculated for reference. The average hole diameter was approximately 100.22 μm and the total hole area approximately 0.8045 mm^2. These holes resulted in a porosity of 12.6% in the micropunched region and total porosity of approximately 4%, Fig. 6.4.

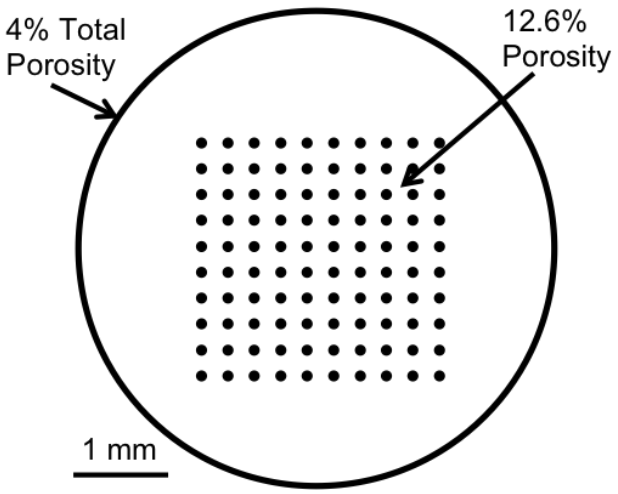

Figure 6.4: Cartilage sample with a diameter of 5 mm and 100 micro-holes of approximately 100 µm diameter punched in a 2.5 mm x 2.5 mm square matrix. Micro-holes create a 12.6% level of porosity in the micropunched region and a total level of porosity of 4%.

Table 6.1: Average Young's modulus and compressive strength for nonporous and porous stacked samples (mean +/- st. dev., n=5). Average thickness of nonporous stacked samples = 298 µm; average thickness of porous stacked samples = 269 µm.

Cartilage Sample	Young's Modulus (MPa)	Compressive Strength (kPa)
Nonporous	1.33 ± 0.25	104.8 ± 30.5
Porous	1.12 ± 0.18	95.7 ± 12.9

The Young's modulus and compressive strength of porous and nonporous samples are presented in Table 6.1. There is no statistically significant difference between the average Young's modulus and compressive strength of nonporous and porous stacked samples. There is however a nearly significant difference when comparing the average Young's modulus ($p = 0.085$). The compressive strength is determined at 10% strain because none of the samples yielded before 10% strain and one nonporous sample did not yield at all.

Table 6.2: Average engineering strain and engineering stress at yield for nonporous and porous stacked samples (mean +/- st. dev.). Average thickness of nonporous stacked samples = 298 μm; average thickness of porous stacked samples = 269 μm.

Cartilage Sample	Strain at Yield	Stress at Yield (MPa)
Nonporous (n=4)[1]	0.24 ± 0.04	0.28 ± 0.03
Porous (n=5)	0.18 ± 0.04	0.19 ± 0.07

[1]One of the five samples compressed did not yield

The average strains and stresses at the calculated yield points are presented in Table 6.2. A significant difference was found between the average strains at yield ($p = 0.044$) and between the average stresses at yield ($p = 0.025$).

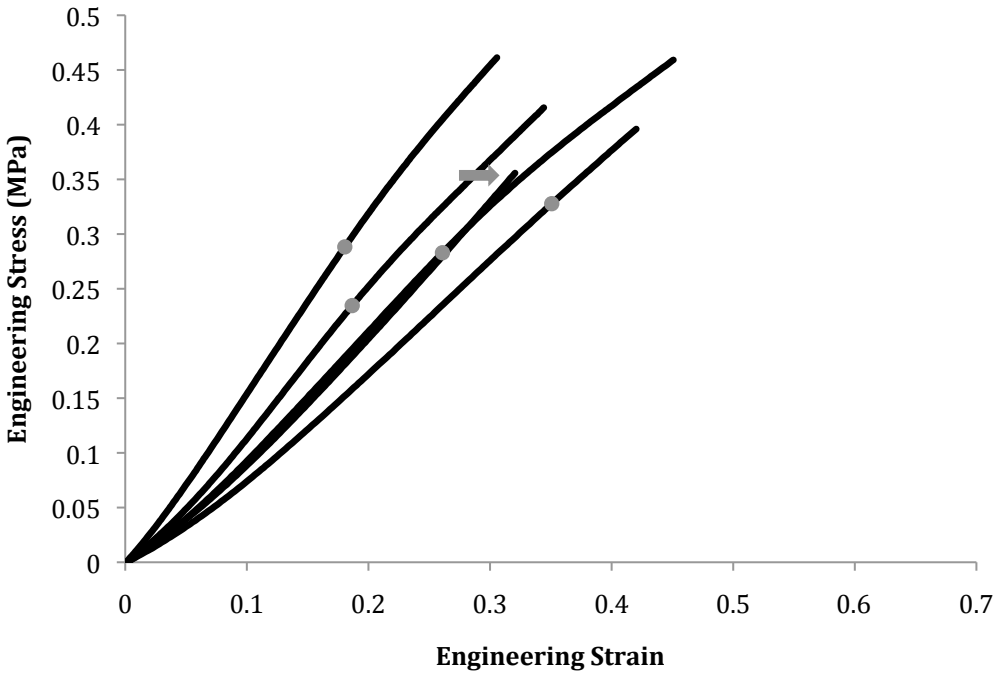

Figure 6.5: Engineering stress-engineering strain curves of five nonporous stacked samples under compression. Grey dots indicate yield point, grey arrow indicates sample that did not yield.

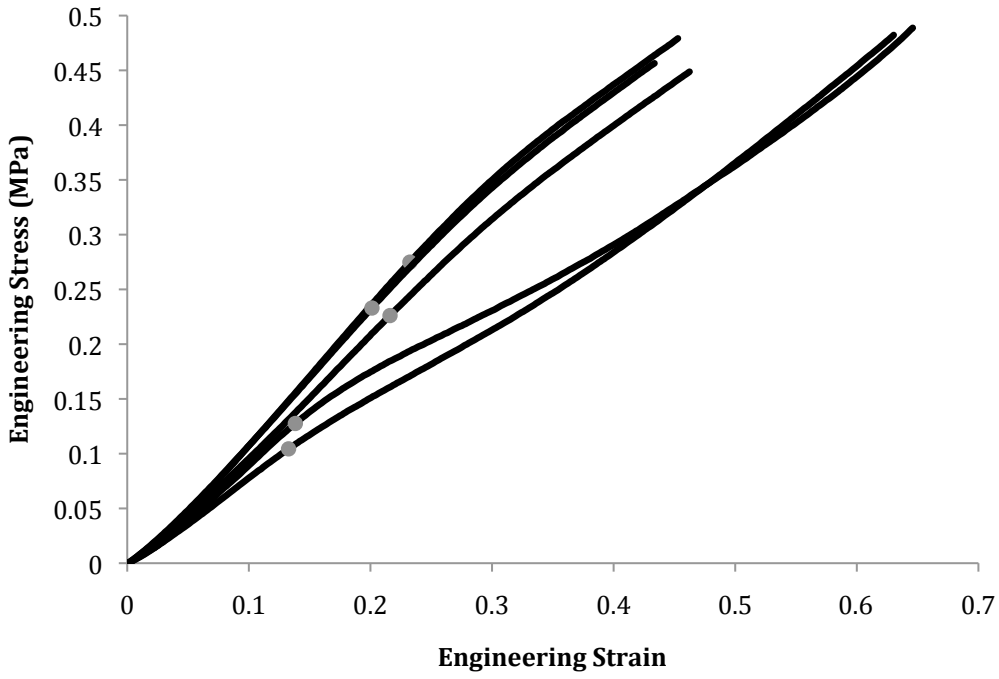

Figure 6.6: Engineering stress-engineering strain curves of five porous stacked samples under compression. Grey dots indicate yield point.

Figures 6.5 and 6.6 show the five compression trials of both nonporous and porous samples so the yield points can be seen on the curves. One of the nonporous samples did not yield and two of the porous samples yielded much earlier than the other three porous samples. The nonporous samples had a high degree of variation in both yield point and Young's modulus. Yet the three porous samples that yielded at a higher stress and strain had very similar yield points and Young's moduli, and the samples that yielded at a lower stress and strain had very similar yield points and Young's moduli.

6.4 Discussion

Compression testing was performed on nonporous and porous stacked cartilage samples, revealing that porosity does not have a significant effect on compressive Young's modulus. Though the porous samples have a decreased surface area, the sample will still occupy the same area in vivo, thus it must support the same amount of force as a

nonporous sample for that area. This is why the nominal nonporous area was used for stress calculations for porous samples.

Young's modulus, compressive strength, and yield point were compared between nonporous and porous stacked samples. No statistically significant difference was found between nonporous and porous samples for Young's modulus and compressive strength. A trend towards decreasing mechanical properties may be present, but at 4% porosity, no significant relationship was found. Thus, levels of porosity around 4% do not appear to have a significant effect on Young's modulus and compressive strength.

The Young's modulus of these stacked samples cannot be compared to cartilage in vivo or cartilage samples that have not been sectioned because the samples used in this research have been fixed in formalin, which could slightly alter the mechanical properties. The Young's modulus of cartilage in vivo has been reported to fall between 0.45 and 0.80 MPa [10], so the values calculated for stacked samples (1.12 – 1.33 MPa) are greater, but within the same order of magnitude.

As compared to nonporous cartilage, porous stacked samples yielded at significantly lower levels of stress and strain. Two of the porous samples yielded at lower strain and stress values than the other three porous samples. The three porous samples that yielded at higher strain and stress values may have had a more connected porous network. If the micro-holes were aligned to allow more connectivity of the pores, the PBS in the samples would be able to escape more easily, reducing the internal hydrostatic stress and allowing the samples to compress more before yielding. It is important to investigate this to determine how the stacking process can affect the yield point of a stacked construct.

Porosity does not appear to have a significant effect on the stiffness of a sample, but it does seem to cause a sample to yield at lower strain and stress values. However, cartilage has been shown to deform between 3% and 6% during various activities in vivo

[66]. In addition, the defined compressive strength is before the yield point in all samples. Thus, the yield point of nonporous and porous samples would not be reached under physiological conditions.

6.5 Conclusion

Both nonporous and porous stacked cartilage samples have been shown to yield at high levels of strain in compression, indicating that under in vivo conditions yield would not occur in the stacked configuration. Therefore, the stiffness of the sample is the most important mechanical property. No significant difference was found between the Young's moduli of nonporous and porous samples at 4% porosity. This indicates that micropunched porous cartilage samples would provide sufficient mechanical properties in vivo for integration, cell differentiation, and mechanical support.

Higher levels of porosity may result in a degradation of mechanical properties and as such the conclusions drawn here should not be extended beyond 4-5% porosity.

7 Cell Seeding in Porous Cartilage Samples

7.1 Introduction

Previous efforts of engineering cartilage through seeding cells in a natural or synthetic scaffold have had varying degrees of success, but to date none of the methods have consistently created a durable articular surface [5]. The challenge is to engineer a cartilage implant that contains living chondrocytes and is capable of integrating and adapting to surrounding native cartilage. The implant must be composed of materials that will promote the formation of cartilage tissue, such as natural extracellular matrix (ECM), and initially contain sufficient micro-vascularity to provide the diffusion of oxygen and nutrients to promote cellular growth [19,40].

Hwang et al. demonstrated that three-dimensional cell cultures promote chondrogenic differentiation of embryonic stem cells more efficiently than two-dimensional cultures [20]. However, Bian et al. showed that chondrocytes cannot survive in the center of three-dimensional constructs (2.34 mm thick) due to nutrient diffusion distances that are too large [40]. Thus, a construct must be developed that is thin enough to allow for adequate nutrient diffusion while still providing a three-dimensional architecture.

Bian et al. has shown that creating microchannels in tissue constructs can decrease diffusion distances during initial culturing when it is critical to provide the cells with nutrients. They found that channels less than 1 mm in diameter were closed with fresh ECM deposited by the cultured cells [40]. Thus, according to Bian et al.'s findings, micro-holes intended for cell seeding created with Schmitt's micropunching machine and a 200 μm diameter punch will close during culture. Finally, Bian et al. determined that the process of punching channels in constructs does not affect cell viability at the cutting

surface or at other areas, making the micro-holes suitable lacunae substitutes for cell culture.

Micropunched, thin, natural cartilage ECM samples provide an attractive alternative to currently used artificial constructs. Thin samples with micro-holes provides short diffusion distances for the cells cultured in all parts of the construct. At the same time, the micro-holes provide a three-dimensional architecture for cell attachment. In addition, constructs made from natural cartilage ECM provide the correct biochemical components for chondrogenic differentiation.

Micropunched cartilage ECM samples are attached to collagen hydrogels to provide a bottom surface during cell seeding and initial culture while the cells produce their own neomatrix. Human mesenchymal stem cells (MSCs) are cultured on the cartilage samples to determine if the MSCs will fall into the micro-holes and be positioned to take advantage of the three-dimensional aspect of the holes with current seeding methods.

7.2 Materials and Methods

7.2.1 Cartilage Sample Preparation

To prepare samples for cell seeding, articular cartilage is scraped from the medial and lateral condyles of the femur of a fresh rear leg of an equine between the 24th and 36th months of age, obtained from the Cummings School of Veterinary Medicine, North Grafton, MA, USA. Samples, approximately 2.0 mm in depth, are taken from both condyles and fixed in 10% formalin for 24 hours. Next, the samples are placed in OCT compound (Embedding Medium for Frozen Tissue Specimens to ensure Optimal Cutting Temperature) (Sakura Finetek USA, Inc., Torrance, CA, USA) and frozen on dry ice for further processing. The samples are then sectioned to an appropriate thickness of 100 μm

with a cryostat-microtome (Leica CM1950, Leica Biosystems, Wetzlar, Germany) and placed in non-sterile PBS baths at 4°C.

An equine sample is placed between two 30 µm thick pieces of wax paper and punched in the micropunching machine with a 201 µm male punch and a 211 µm female die hole, providing 10% clearance. Fifty holes are punched in the sample in a hydrated state, forming a 10x5 matrix, Fig. 7.1.

Once the cartilage sample is punched, it is washed in deionized water at 4°C for 24 hours. A decellularization process is then performed where the sample is soaked in 1% triton X100 at 4°C for 24 hours. Finally, to remove any remaining chemicals and to prepare the sample for cell seeding, it is washed in PBS on a shaker at 37°C for 24 hours.

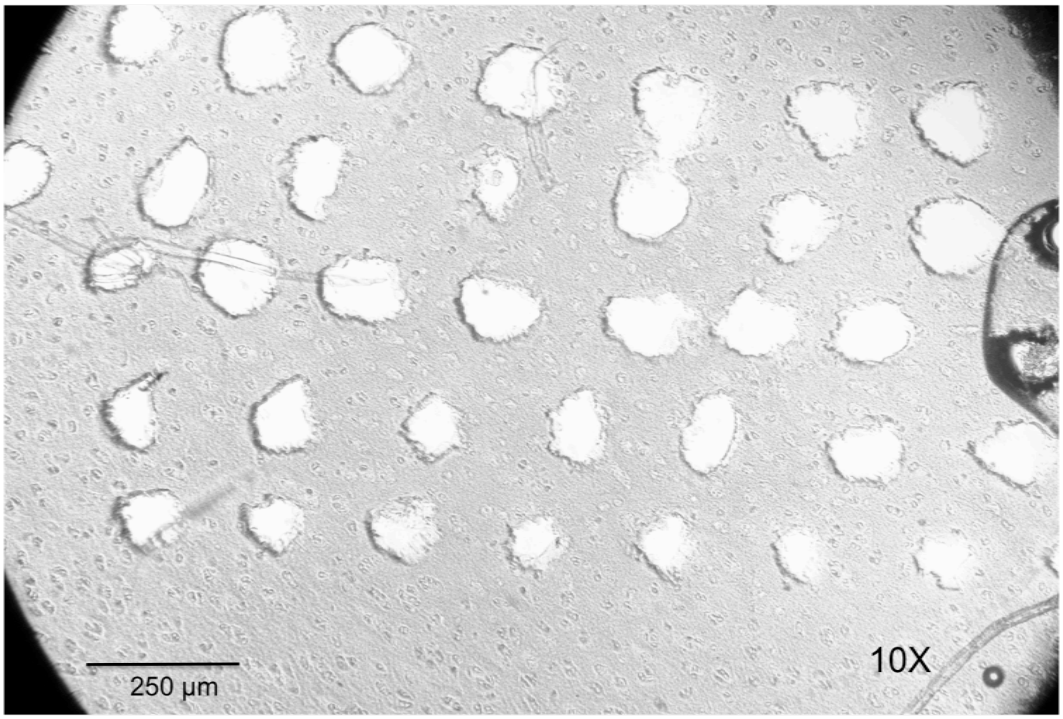

Figure 7.1: Micropunched, formalin fixed, 100 µm thick, equine cartilage sample used for cell seeding

After decellularization and washing, the sample is cut into 4 sections of equal area, two with micro-holes and two without.

7.2.2 Cell Seeding and Culture

The micropunched cartilage ECM samples are placed on collagen type II hydrogels to provide a bottom surface for the seeded cells and prevent them from washing away in the added media. Thin collagen type II hydrogels are cast in the bottom of each well of a four well plate. Immediately, each cartilage sample is then placed on the hydrogel to ensure that the seeded cells do not fall through the micro-holes and wash away. The gels are then allowed to solidify for 10 minutes, adhering the cartilage samples to the hydrogels.

Human MSCs (passage 8, Poietics, Lonza, Basel, Switzerland) are seeded on each cartilage sample at a density of 6.67×10^9 cells/μL in 15 μL of chondrogenic media. The cell suspension is spread evenly over the surface area of each sample. One half of the MSCs are GFP-infected (green fluorescent protein) (Anti-GFP Antibody, Abcam, Cambridge, MA, USA). After seeding all samples, the four well plate is placed in an incubator at 37°C and 5% CO_2 for two hours to allow the cells to attach to the cartilage. Samples are removed from the incubator and 400 μL of media is added to each well. The samples are then placed back in the incubator and cultured statically for 14 days.

7.2.3 Analysis

The position of the seeded cells is determined after 4, 7, and 14 days to determine if the cells successfully utilize the micropunched holes and are positioned to attach to the walls of the fabricated holes. The samples are imaged on Day 4, Day 7, and Day 14. On Day 4 and 7, images are taken with fluorescent imaging and the corresponding bright field; the images are overlayed. On Day 14, the samples are stained with the fluorescent dye 4'-6-diamidino-2-phenylindole (DAPI) to better see where the MSCs are located on the samples. Images are taken with fluorescence microscopy in UV (358 nm) to excite the DAPI, at 480 nm to excite the GFP, and in bright field with a confocal microscopy. The images are overlayed to show the location of the fluorescence on the samples.

7.3 Results

Human mesenchymal stem cells were cultured on four articular cartilage ECM constructs, approximately 100 μm in thickness. Two of the constructs contained micropunched holes and two were unpunched.

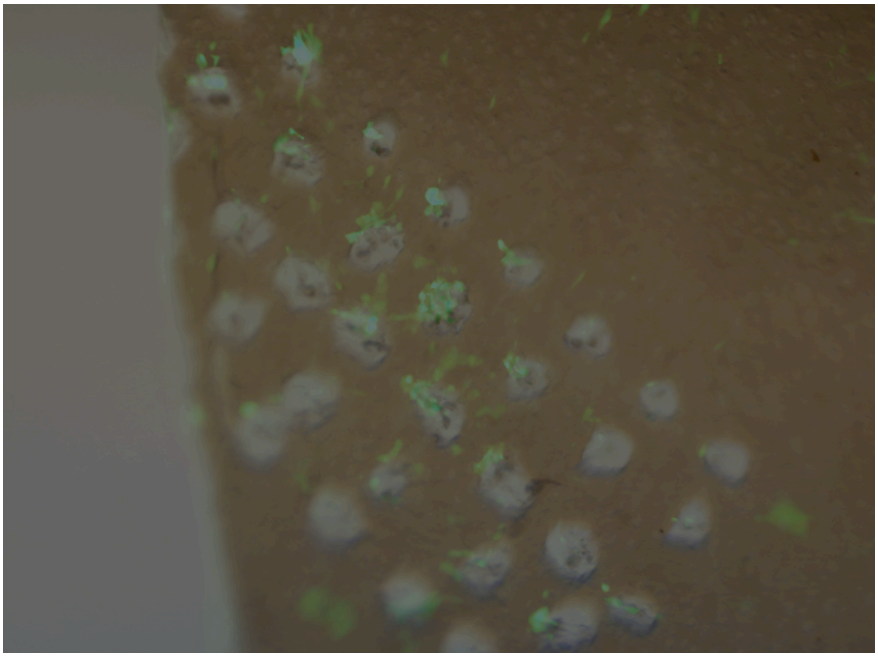

Figure 7.2: Overlay of GFP and bright-field images (Day 4, Sample 2)

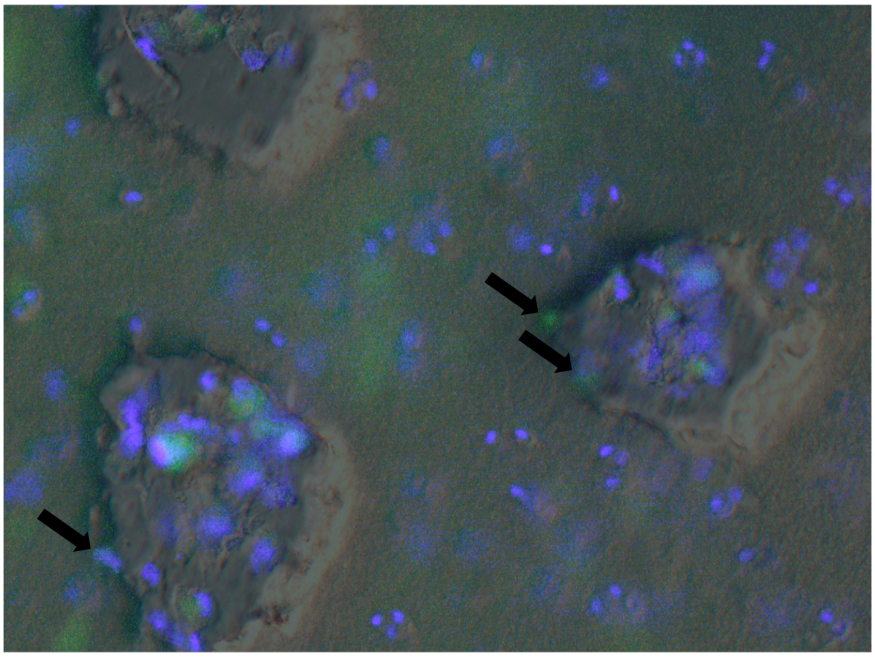

Figure 7.3: Overlay of green fluorescent protein, DAPI, and bright images (Day 14, Sample 2). Arrows show cells growing against wall of micro-hole that was fabricated by micropunching cartilage.

Images taken on Day 4 of culture show that cells are concentrated on the edges of the micropunched holes, Fig. 7.2. Figure 7.3 shows an overlay of fluorescent GFP, DAPI, and bright field images. The DAPI imaging shows many cells growing in the micro-holes as well as on the cartilage ECM surface. The arrows point to the cells that are growing on the walls of the micro-holes, Fig. 7.3.

7.4 Discussion

Human MSCs are cultured on micropunched cartilage samples with the intent of determining if cells will fall into the micro-holes and remain there during the seeding and culture process. Figures 7.2 and 7.3 show cells situated in the micro-holes and along the walls of the micro-holes. This indicates that seeding and static culture were sufficient for a high enough percentage of the cells to fall into the micro-holes and to be positioned within and against the walls of the holes.

The images taken at all three time periods show that the interface between the cartilage samples and the collagen hydrogels successfully contained the MSCs and prevented them from being washed away by the media. The collagen gels provide a bottom surface for the MSCs to attach to while they produce their own neomatrix. The DAPI and GFP imaging on Day 14 also shows that some of the cells are situated against the walls of the micro-holes. This could indicate that the cells have attached to the walls, taking advantage of the three-dimensional architecture provided by micropunching.

In addition to the cells entrapped in the micro-holes, cells are also distributed over the surface of the construct. Though these cells don't benefit from the three-dimensional architecture of the micro-holes, they still have the advantage of the correct biochemical composition and architecture of natural cartilage ECM.

7.5 Conclusion

Micropunched thin slices of articular cartilage ECM appear to be promising constructs for cartilage tissue engineering. This research shows that seeded cells can successfully take advantage of the three-dimensional architecture and the native biochemical composition of natural cartilage ECM.

More extensive culture of cells on micropunched constructs and analysis of cell viability must be compared to contemporary methods to determine if growth in a three dimensional environment is preferable over growth on two dimensional constructs. Future studies will address the speed of processing micropunched cartilage samples, with the goal of creating a punch-die set that creates multiple holes in each stroke of the punch press.

8 Conclusions

The micropunching machine developed by Schmitt et al. [15] was successfully repurposed to create micro-holes in thin cartilage samples. It was determined that die clearance has a significant effect on the maximum punching force (MPF), with MPF increasing as die clearance decreases. For lower die clearances, the male punch is inclined to contact the female die. In addition, the hydration level of the cartilage sample also has a significant effect on the MPF. The MPF increases as the sample dries out. However, the normalized MPF of dry samples is the lowest due to comparative final hole size, indicating that dry samples fracture more easily than saturated and hydrated samples. The hydration level of the cartilage sample also has a significant effect on the final hole size. The hole size of dry samples was determined to be approximately four times larger than that of saturated and hydrated samples. Upon SEM inspection of hole geometry, saturated samples exhibited stretching of collagen fibers, whereas dry samples had a shear surface appearance.

The MPF of dry and hydrated samples was successfully predicted with a modified version of Shergold et al.'s model [46]. This allows the required MPF for a given hydration level and male punch radius to be predicted for cartilage sandwiched between two pieces of wax paper, which is important for the design of die sets and related micropunching equipment.

Young's modulus of porous and nonporous stacked cartilage samples was not found to be significantly different at 4% porosity. In addition, the results of the compression tests indicate that the samples would not yield in vivo. Thus, micropunched porous stacked cartilage samples will maintain their mechanical properties at 4% porosity for cell culture and implantation in vivo.

Finally, initial investigations indicate that thin, micropunched cartilage samples provide a promising construct for cartilage tissue engineering. Seeded cells can take advantage of the three-dimensional properties of the punched micro-holes, in addition to the high nutrient diffusion of thin samples. Micro-punched holes can also be used to create microtubules for enhanced nutrient diffusion in a thick construct during early development.

Micropunched, thin, cartilage extracellular matrix (ECM) samples are promising constructs for culturing mesenchymal stem cells in vitro and for future cartilage tissue engineering applications.

8.1 Future Work

Significant work still remains in the investigation of the use of micropunched cartilage ECM samples for cartilage tissue engineering. The research conducted herein was the first of its kind and as such is preliminary in nature.

8.1.1 Die Sets with Multiple Pins

A die set that includes a constellation of punches must be created to allow for multiple holes to be punched at the same time. This will permit all holes to be punched at the same hydration level and thereby eliminate the issue of samples drying out during punching. The time required to punch samples will also be greatly reduced, eliminating the need to fix the tissue in formalin. Cells could then be cultured on the freshly punched samples. The creation of die sets with multiple punches is necessary for the advancement of all future research on micropunching cartilage samples.

8.1.2 Effect of Hydration on Hole Size

Final hole size has been shown to increase as the cartilage sample dries out. This relationship can be calibrated to determine the approximate resulting hole size based on

the precise level of hydration. Further investigations should be conducted to establish this relationship so that the desired hole sizes can be determined a priori.

8.1.3 Cell Seeding

An extensive cell culture study should be performed to determine the ability of the cartilage samples to promote chondrogenic differentiation and cell proliferation. To allow for cellular growth, the samples must be fresh and unfixed, requiring the time of processing all samples to occur in less than three days.

Micropunched cartilage samples should be tested for the ability to promote chondrogenic differentiation and deposition of cartilage neomatrix. In addition, tests should be conducted to determine whether micro-holes with rough (punched while saturated) or smooth (punched while dry) walls are better for promoting cellular attachment and proliferation.

8.1.4 Stacking Layers

Finally, a system for precise stacking of micropunched cartilage samples must be developed. Samples with cells cultured in micro-holes should be stacked and cultured together once the cells are mature. This will create a thick construct while still taking advantage of the low diffusion distances during early cell culture. A method of ensuring the layers integrate and attach to each other must also be established to ensure the samples do not separate once they encounter shear forces in vivo.

If nutrient diffusion rates are too low once samples are stacked, microtubules can be created in the punching and stacking process. Punching the sample while it is dry can create larger micro-holes with smooth walls. These holes can then be aligned while stacking to create a microvascular network throughout the cartilage sample and increase nutrient diffusion.

References

[1] Sandell, L. J., and Aigner, T. (2001). "Articular Cartilage and Changes in Arthritis: Cell Biology of Osteoarthritis." *Arthritis Research*, 3, 107-113.

[2] Ytrehus, B., Carlson, C. S., Lundeheim, N., Mathisen, L., Reinholt, F. P., Teige, J., and Ekman, S. (2004). "Vascularisation and Osteochondrosis of the Epiphyseal Growth Cartilage of the Distal Femur in Pigs – Development with Age, Growth Rate, Weight and Joint Shape." *Bone*, 34(3), 454-465.

[3] Kurtz, S., Ong, K., Lau, E., Mowat, F., and Halpern, M. (2007). "Projections of Primary and Revision Hip and Knee Arthroplasty in the United States from 2005 to 2020." *Journal of Bone and Joint Surgery*, 89(4), 780–785.

[4] Fisher, M. B., and Mauck, R. L. (2013). "Tissue Engineering and Regenerative Medicine: Recent Innovations and the Transition to Translation." *Tissue Engineering Part B Reviews*, 19(1), 1-13.

[5] Punwar, S., and Wasim K. S. (2011). "Mesenchymal Stem Cell and Articular Cartilage Repair: Clinical Studies and Future Direction." *Open Orthopaedics Journal*, 5(Suppl 2-M11), 296-301.

[6] Peel, S. A. F., Chen, H., Renlund, R., Badylak, S. F., and Kandel, R. A. (1998). "Formation of a SIS-Cartilage Composite Graft *in Vitro* and Its Use in the Repair of Articular Cartilage Defects." *Tissue Engineering*, 4(2), 143-155.

[7] Wainwright, J. M., Czajika, C. A., Patel, U. B., Freytes, D. O., Tobita, K., Gilbert, T. W., and Badylak, S. F. (2010). "Preparation of Cardiac Extracellular Matrix from an Intact Porcine Heart." *Tissue Engineering Part C: Methods,* 16(3), 525-532.

[8] Elder, B. D., Kim, D. H., and Athanasiou, K. A. (2010). "Developing an Articular Cartilage Decellularization Process Toward Facet Joint Cartilage Replacement." *Neurosurgery*, 66(4), 722-727.

[9] Badylak, S. F., Taylor, D., and Uygun, K. (2010). "Whole Organ Tissue Engineering: Decellularization and Recellularization of Three-Dimensional Matrix Scaffolds." *Annual Review of Biomedical Engineering*, 13(1), 27-53.

[10] Mansour, J. (2003). "Biomechanics of Cartilage." In Oatis, C., editor, *Kinesiology: The Mechanics and Pathomechanics of Human Movement*, chapter 5, 66–79. Lippincott Williams and Wilkins, Philadelphia.

[11] Schmitt, E. C., Sagar, A., White, R. D., and James, T. P. (2013). "Tissue Scaffold Engineering by Micro-Stamping." *Proceeding of the Materials Research Society*, 2013 MRS Fall Meeting and Exhibit, Boston, MA, USA, Dec. 1-6.

[12] Schmitt, E. C. (2013). "Design and Development of a Stamping Press Capable of Punching Microscale Holes in Polymer Membranes.," M.S. Thesis, Tufts University, Medford, MA, USA.

[13] Joo, B. Y., Oh, S. I., and Jeon, B. H. (2001). "Development of Micro Punching System." *CIRP Annals – Manufacturing Technology*, 50(1), 191-194.

[14] Joo, B. Y., Rhim, S. H., and Oh, S. I. (2005). "Micro-hole Fabrication by Mechanical Punching Process." *Journals of Materials Processing Technology*, 170(3), 593-601.

[15] Hwang, N. S. (2007). "Cartilage Tissue Engineering: Directed Differentiation of Embryonic Stem Cells in Three-Dimensional Hydrogel Culture." *Methods in Molecular Biology*, 407, 351-373.

[16] Buckwalter, J. A., and Mankin, H. J. (1997). "Articular Cartilage Part II: Degeneration and Osteoarthrosis, Repair, Regeneration, and Transplantation." *Journal of Bone and Joint Surgery,* 79-A(4), 612-632.

[17] Hutmacher, D. W. (2001). "Scaffold Design and Fabrication Technologies for Engineering Tissues – State of the Art and Future Perspectives." *Journal of Biomaterials Science, Polymer Edition*, 12(1), 107-124.

[18] Vacanti, J. P., and Langer, R. (1999). "Tissue Engineering: The Design and Fabricatio of Living Replacement Devices for Surgical Reconstruction and Transplantation." *Lancet*, 354(suppl 1), 32-34.

[19] Badylak, S. F. (2002). "The Extracellular Matrix as a Scaffold for Tissue Reconstruction." *Seminars in Cell and Developmental Biology*, 13(5), 377-383.

[20] Hwang, N. S., Kim, M. S., Sampattavanich, S., Baek, J. H., Zhang, Z., and Elisseeff, J. (2006) "Effects of Three-Dimensional Culture and Growth Factors on the Chondrogenic Differentiation of Murine Embryonic Stem Cells." *Stem Cells*, 24(2), 284-291.

[21] Badylak, S. F. (2004). "Xenogeneic Extracellular Matrix as a Scaffold for Tissue Reconstruction." *Transplant Immunology*, 12(3/4), 367-377.

[22] Badylak, S. F., Arnoczky, S., Plouhar, P., Haut, R., and Mendenhall, V. (1999). "Naturally Occuring Extracellular Matrix as a Scaffold for Musculoskeletal Repair." *Clinical Orthopaedics and Related Research*, 367, S333-S343.

[23] Li, C., Vepari, C., Jin, H. J., Kim, H. J., and Kaplan, D. L. (2006). "Electrospun Silk-BMP-2 Scaffolds for Bone Tissue Engineering." *Biomaterials*, 27(16), 3115-3124.

[24] Reing, J. E., Brown, B. N., Daly, K. A., Freund, J. M., Gilbert, T. W., Hslong, S. X., Huber, A., Kullas, K. E., Tottey, S., Wolf, M. T., and Badylak, S. F. (2010). "The Effects of Processing Methods upon Mechanical and Biological Properties of Porcine Dermal Extracellular Matrix Scaffolds." *Biomaterials*, 31(33), 8626-8633.

[25] Athanasiou, K. A. (1991). "Interspecies Comparisons of in Situ Intrinsic Mechanical Properties of Distal Femoral Cartilage." *Journal of Orthopaedic Research*, 9(3), 330-340.

[26] Buckwalter, J. A., and Mankin, H. J. (1997). "Articular Cartilage Part I: Tissue Design and Chondrocyte Matrix Interactions." *Journal of Bone and Joint Surgery*, 79(4), 600-611.

[27] Chen, S. S., Falcovitz, Y. H., Schneiderman, R., Maroudas, A., and Sah, R. L. (2001). "Depth-Dependent Compressive Properties of Normal Aged Human Femoral Head Articular Cartilage." *Osteoarthritis and Cartilage*, 9, 561-569.

[28] Kempson, G. E. (1979). "Mechanical Properties of Articular Cartilage." In: Freeman MAR, editor. Adult Articular Cartilage. Tunbridge Wells, England: Pitman Medical: 333-414.

[29] Eyre, D. R. (1991). "The Collagens of Articular Cartilage." *Seminars in Arthritis and Rheumatism*, 21(Suppl 2), 2-11.

[30] Jeffery, A.K., Blunn, G. W., Archer, C. W., and Bentley, G. (1991). "Three-Dimensional Collagen Architecture in Bovine Articular Cartilage." *Journal of Bone and Joint Surgery*, 73-B(5), 795-801.

[31] Maroudas, A., Bullough, P., Swanson, A. V., and Freeman, M. A. R. (1968). "Permeability of Articular Cartilage." *Journal of Bone and Joint Surgery*, 50-B(1), 166-177.

[32] Shapiro, F., Koide, S., and Glimcher, M. J. (1993). "Cell Origin and Differentiation in the Repair of Full-Thickness Defects of Articular Cartilage." *Journal of Bone and Joint Surgery*, 75-A(4), 532-553.

[33] Cicuttini, F. M., Baker, J. R., and Spector, T. D. (1996). "The Association of Obesity with Osteoarthritis of the Hand and Knee in Women: A Twin Study." *Journal of Rheumatology*, 23, 1221-1226.

[34] Peyron, J. G. (1986). "Osteoarthritis: The Epidemiologic Viewpoint." *Clinical Orthopaedics and Related Research*, 213, 13-19.

[35] Oddis, C. V. (1996). "New Perspectives on Osteoarthritis." *American Journal of Medicine*, 100, 10S-15S.

[36] Peyron, J. G. (1991). "Clinical Features of Osteoarthritis, Diffuse Idiopathic Skeletal Hyperostosis." *Current Opinion on Rheumatology*, 3, 653-661.

[37] Cukierman, E., Pankov, R., Stevens, D. R., and Yamada, K. M. (2001). "Taking Cell-Matrix Adhesions to the Third Dimension." *Science*, 294(5547), 1708-1712.

[38] Cukierman, E., Pankov, R., and Yamada K. M. (2002). "Cell Interactions with Three-Dimensional Matrices." *Current Opinion in Cell Biology*, 14(5), 633-640.

[39] Zorlutuna, P., Annabi, N., Camci-Unal, G., Nikkhah, M., Cha, J. M., Nichol, J. W., Manbachi, A., Bae, H., Chen, S., and Khademhosseini, A. (2012). "Microfabricated Biomaterials for Engineering 3D Tissues." *Advanced Materials*, 24, 1782-1804.

[40] Bian, L., Angione, S. L., Ng, K. W., Lima, E. G., Williams, D. Y., Mao, D. Q., Ateshian, G. A., and Hung, C. T. (2008). "Influence of Decreasing Nutrient Path Length on the Development of Engineered Cartilage." *Osteoarthritis and Cartilage*, 17(5), 677-685.

[41] Choi, N. W., Cabodi, M., Held, B., Gleghorn, J. P., Bonassar, L. J., and Stroock, A. D. (2007). "Microfluidic Scaffolds for Tissue Engineering." *Nature Materials*, 6, 908-915.

[42] Radisic, M., Park, H., Chen, F., Salazar-Lazzaro, J. E., Wang, Y., Dennis, R., Langer, R., Freed, L. E., and Vunjak-Novakovic, G. (2006). "Biomimetic Approach to Cardiac Tissue Engineering: Oxygen Carriers and Channeled Scaffolds." *Tissue Engineering*, 12(8), 2077-2091.

[43] Freytes, D. O., Badylak, S. F., Webster, T. J., Geddes, L. A., and Rundell, A. E. (2004). "Biaxial Strength of Multilaminated Extracellular Matrix Scaffolds." *Biomaterials*, 25(12), 2353-2361.

[44] Livingston, D. I., Yeh, G. S., Rohall, P., and Gehman, S. D. (1961). "Visco-Elastic Factors in the Strength of Elastomers Under Complex Stress by a Puncture Method." *Journal of Applied Polymer Science*, 5(16), 442-451.

[45] Shergold, O. A., and Fleck, N. A. (2005). "Experimental Investigation Into the Deep Penetration of Soft Solids by Sharp and Blunt Punches, With Application to the Piercing of Skin." *Journal of Biomechanical Engineering*, 127, 838-848.

[46] Shergold, O. A., and Fleck, N. A. (2004). "Mechanisms of Deep Penetration of Soft Solids, with Application to the Injection an Wounding of Skin." *Proceedings of the Royal Society of London. Series A, Mathematical and Physical Sciences*, 460, 3037-3058.

[47] Wright, S. C., Huang, Y., and Fleck, N. A. (1992). "Deep Penetration of Polycarbonate by a Cylindrical Punch." *Mechanics of Materials*, 13(4), 277-284.

[48] Azar, T., and Hayward, V. (2008). "Estimation of the Fracture Toughness of Soft Tissue from Needle Insertion." *Lecture Notes in Computer Science*, 5104, 166-175.

[49] Stevenson, A., and Abmalek, K. (1994). "On the Puncture Mechanics of Rubber." *Rubber Chemistry and Technology*, 67(5), 743-760.

[50] Purslow, P. P. (1983). "Measurement of the Fracture Toughness of Extensible Connective Tissues." *Journal of Material Sciences*, 18(12), 3591-3598.

[51] Ogden, R. W., Saccomandi, G., and Sgura, I. (2004). "Fitting Hyperelastic Models to Experimental Data." *Computational Mechanics*, 34, 484-502.

[52] Twizell, E. H., and Ogden, R. W. (1983). "Non-Linear Optimization of the Material Constants in Ogden's Stress-Deformation Function for Incompressible Isotropic Elastic Materials." *Journal of the Australian Mathematical Society*, 24B(4), 424-434.

[53] Frick, T. B., Marucci, D. D., Cartmill, J. A., Martin, C. J., and Walsh, W. R. (2001). "Resistance Force Acting on Suture Needles." *Journal of Biomechanics*, 34(10), 1335-1340.

[54] Figge, F. H., and Barnet, D. J. (1948). "Anatomic Evaluation of a Jet Injection Instrument Designed to Minimize Pain and Inconvenience of Parenteral Therapy." *American Practitioner and Digest of Treatment*, 3, 197-206.

[55] Brett, P. N., Parker, T. J., Harrison, A. J., Thomas, T. A., and Carr, A. (1997). "Simulation of Resistance Forces Acting on Surgical Needles." *Proceedings of the Institution of Mechanical Engineers*, 211, 335-347.

[56] Chin-Purcell, M. V., Lewis, J. (1996). "Fracture of Articular Cartilage." *Journal of Biomechanical Engineering*, 118, 545-556.

[57] Shergold, O. A., and Fleck, N. A. (2006). "The Uniaxial Stress versus Strain Response of Pig Skin and Silicone Rubber at Low and High Strain Rates." *International Journal of Impact Engineering*, 32(9), 1384-1402.

[58] Ogden, R.W. (1972). "Large Deformation Isotropic Elasticity – On the Correlation of Theory and Experiment for Incompressible Rubberlike Solids." *Proceedings of the Royal Society of London. Series A, Mathematical and Physical Sciences*, 326, 565-584.

[59] Mow, V. C., Kuei, S. C., Lai, W. M., and Armstrong, C. G. (1980). "Biphasic Creep and Stress Relaxation of Articular Cartilage in Compression? Theory and Experiments." *Journal of Biomechanical Engineering*, 102, 73-84.

[60] Sanjeevi, R., Somanathan, N., and Ramaswamy, D. (1982). "A Viscoelastic Model for Collagen Fibres." *Journal of Biomechanics*, 15(3), 181-183.

[61] Hayes, W. C., and Mockros, L. F. (1971). "Viscoelastic Properties of Human Articular Cartilage." *Journal of Applied Physiology*, 31, 562-568.

[62] Xu, J., Guo, B., Wang, C., and Shan, D. (2012). "Blanking Clearance and Grain Size Effects on Micro Deformation Behavior and Fracture in Micro-Blanking of Brass Foil." *International Journal of Machine Tools & Manufacture*, 60, 27-34.

[63] ASTM Standard D1621-10, 2010, "Standard Test Method for Compressive Properties of Rigid Cellular Plastics," ASTM International, West Conshohocken, PA, 2010, www.astm.org.

[64] Bobyn, J. D., Mortimer, E. S., Glassman, A. H., Engh, C. A., Miller, J. E., Brooks, C. E. (1992). "Producing and Avoiding Stress Shielding: Laboratory and Clinical Observations of Noncemented Total Hip Arthroplasty." *Clinical Orthopaedics and Related Research*, 274, 79-96.

[65] ASTM Standard D695-10, 2010, "Standard Test Method for Compressive Properties of Rigid Plastics," ASTM International, West Conshohocken, PA, 2010, www.astm.org.

[66] Eckstein, F., Lemberger, B., Gratzke, C., Hudelmaier, M., Glaser, C., Englmeier, K. H., and Reiser, M. (2005). "In Vivo Cartilage Deformation after Different Types of Activity and its Dependence on Physical Training Status." *Annals of Rheumatic Diseases*, 64(2), 291-295.

Appendix A – Matlab Code for Punching Force Data Analysis

```
F = dlmread('1Forces.csv');                %Load force data
cal_factor = 21.57592093;                  %Calibration factor to convert data to Newtons
Fx = cal_factor*F(:,1);
Fy = cal_factor*F(:,2);
Fz = cal_factor*F(:,3);
f = 500;                                   %Frequency at which data was collected
dt = 1/f;                                  %Seconds
T = dt*length(F);                          %Total time that data was collected for
t = 0:dt:T-dt;
Fzz = smooth(Fz,11,'lowess');              %Filter function to smooth data
zero_corr = min(Fzz);
Fzz = Fzz - zero_corr;                     %Zeroing force
Fz = Fz - zero_corr;
figure(1);                                 %Plot raw and filtered data
plot(t,Fz)
hold on
plot(t,Fzz,'r')
grid on
xlabel('Time (s)')
ylabel('Force (N)')
figure(2)                                  %Plot only filtered data
plot(t,Fzz,'r')
grid on
xlabel('Time (s)')
```

```
ylabel('Force (N)')
P_L = [0.158 0.05347];                          %Point one on drifting data
P_H = [2.916 0.1286];                           %Point two on drifting data
Fzz_c = Drift_Correction(t,Fzz,P_L,P_H);        %Drift correction
figure(3);                                      %Plot filtered and drift corrected data
plot(t,Fzz,'r')
hold on
plot(t,Fzz_c)
grid on
xlabel('Time (s)')
ylabel('Force (N)')
Fzz_c_zero_c = Fzz_c - mean(Fzz_c(1:501));      %Zero data after drift correction
figure(4)
plot(t,Fzz_c_zero_c)
grid on
xlabel('Time (s)')
ylabel('Force (N)')
```

Drift Correction

```
function F_c = drift_correction(t,F,P_L,P_H)
m = (P_H(2)-P_L(2))/(P_H(1)-P_L(1));            %Calculate slope of drift
del_F = m*(t'-P_L(1));                          %How much to subtract from each point
F_c = F - del_F;                                % Drift correction
end
```

Appendix B – Maximum Punching Force Measurements at each Hydration Level

Table B.1: Data from force measurements of saturated cartilage samples between wax paper (201 µm punch, 216 µm die, 7.34% nominal die clearance, n=5)

Maximum Punching Force (N)	Final Hole Radius (µm)[1]	Normalized Max Force (N/mm)[2]
2.3545	18.505	20.250
1.8861	23.300	12.883
2.4291	36.245	10.666
2.8699	24.175	18.894
2.7655	26.000	16.929

[1]Measured in a saturated state
[2]Normalized Max Force = Maximum Punching Force/Hole Circumference

Table B.2: Data from "two-punch tests" for hydrated cartilage samples between wax paper (201 µm punch, 216 µm die, 7.47% nominal die clearance, n=10)

Maximum Punching Force (N)	Second Stroke Punch Force (N)	Final Hole Radius (µm)[1]	Normalized Mean Max Force (N/mm)[2]
3.7771	0.4067	19.925	30.170
3.014	0.2948	36.265	13.227
2.6149	0.6589	30.26	13.753
3.1030	0.3964	27.495	17.962
2.9126	0.7195	26.710	17.355
2.4889	0.3314	22.490	17.613
3.1739	0.3317	18.435	27.401
4.4965	0.8016	29.625	24.157
3.6214	0.6524	23.990	24.025
2.5590	0.8760	15.965	25.511

[1]Measured in a saturated state
[2]Normalized Max Force = Maximum Punching Force/Hole Circumference

Table B.3: Data from two-punch tests for dry cartilage samples between wax paper (201 µm punch, 216 µm die, 11.71% nominal die clearance, n=10)

Maximum Punching Force (N)	Second Stroke Punch Force (N)	Final Hole Radius (µm)[1]	Normalized Max Force (N/mm)[2]
3.6187	0.2821	94.930	6.0669
3.5473	0.1989	98.440	5.7352
4.5044	0.2791	99.540	7.2021
4.1722	0.2990	95.655	6.9419
3.4433	0.2451	86.355	6.3461
4.3170	0.3384	89.425	7.6832
4.3329	0.2725	92.290	7.4721
4.1209	0.3028	100.390	6.5331
3.9000	0.2769	99.615	6.2310
4.1808	0.2483	101.530	6553.7

[1]Measured in a dry state

[2]Normalized Max Force = Maximum Punching Force/Hole Circumference

Appendix C – Derivation of Punching Force Prediction Equation

$$F_{total}\delta h = 2\pi b J_{IIC}\delta\ell + \frac{\partial S_H}{\partial \ell}\delta\ell + \frac{\partial S_C}{\partial \ell}\delta\ell \tag{C.1}$$

where F_{total} is the total punching force on the punch, δh is the increment by which the head of the punch is advanced, b is the radius of the hole after the punch has been removed, J_{IIC} is the fracture toughness of the material, $\delta\ell$ is the instantaneous vertical distance of the advancement of the column of compressed material, $\frac{\partial S_H}{\partial \ell}$ is the energy stored in the solid, radially around the hole, and $\frac{\partial S_C}{\partial \ell}$ is the work done per unit length to compress a column of the material below the head of the punch.

$\frac{\partial S_C}{\partial \ell}\delta\ell$ is neglected because the sample thickness is small so its contribution is negligible. Thus, the equation becomes,

$$F_{total}\delta h = 2\pi b J_{IIC}\delta\ell + \frac{\partial S_H}{\partial \ell}\delta\ell \tag{C.2}$$

Both sides are divided by $\pi\mu R^2$, where R is the radius of the punch and μ is the shear modulus of the solid:

$$\frac{F_{total}\delta h}{\pi\mu R^2} = \left[\frac{2bJ_{IIC}\delta\ell}{\mu R^2} + \frac{\delta\ell}{\pi\mu R^2}\left(\frac{\partial S_H}{\partial \ell}\right)\right] \tag{C.3}$$

The equation is non-dimensionalized by dividing both sides by δh. $\delta\ell$ is also factored out of the parentheses on the right hand side of the equation and the two values are converted to a derivative of ℓ with respect to h:

$$\frac{F_{total}}{\pi\mu R^2} = \left[\frac{2bJ_{IIC}}{\mu R^2} + \frac{1}{\pi\mu R^2}\left(\frac{\partial S_H}{\partial \ell}\right)\right]\frac{\partial \ell}{\partial h} \tag{C.4}$$

The first term on the right side of Eq. (C.4) is rewritten to factor out $\frac{2b}{R}$

$$\frac{F_{total}}{\pi\mu R^2} = \left[\frac{2b}{R}\frac{J_{IIC}}{\mu R} + \frac{1}{\pi\mu R^2}\left(\frac{\partial S_H}{\partial \ell}\right)\right]\frac{\delta\ell}{\delta h} \tag{C.5}$$

Since the sample is thin and the column of compressed material is neglected, it can be assumed that $\ell \approx h$ and therefore $\frac{\delta\ell}{\delta h} \approx 1$,

$$\frac{F_{total}}{\pi\mu R^2} = \left[\frac{2b}{R}\frac{J_{IIC}}{\mu R} + \frac{1}{\pi\mu R^2}\frac{\partial S_H}{\partial \ell}\right] \tag{C.6}$$

From Shergold et al. [46],

$$\frac{\partial S_H}{\partial \ell} = \pi R^2 \int_1^{\infty} \frac{2\mu}{\alpha^2} g\left(\eta, \tfrac{b}{R}\right) d\eta \tag{C.7}$$

where α is the strain hardening exponent of the solid, and

$$g\left(\eta, \tfrac{b}{R}\right) = \left(1 - \frac{1-\left(\frac{b}{R}\right)^2}{\eta}\right)^{\alpha/2} + \left(1 - \frac{1-\left(\frac{b}{R}\right)^2}{\eta}\right)^{-\alpha/2} - 2 \tag{C.8}$$

where

$$\eta = \left(\frac{r}{R}\right)^2, \tag{C.9}$$

which is introduced to normalize the equation.

When (C.8) is substituted into (C.7), which is then combined with (C.6), πR^2 cancels out. The $\frac{2\mu}{\alpha^2}$ is a constant so it is brought out of the integral. The leading μ cancels with the μ in the denominator in front of $\frac{\partial S_H}{\partial \ell}$. Thus, the governing equation becomes,

$$\frac{F_{total}}{\pi\mu R^2} = \left[\frac{2b}{R}\frac{J_{IIC}}{\mu R}\right] + \left[\frac{2}{\alpha^2}\int_1^{\infty}\left[\left(1 - \frac{1-\left(\frac{b}{R}\right)^2}{\eta}\right)^{\alpha/2} + \left(1 - \frac{1-\left(\frac{b}{R}\right)^2}{\eta}\right)^{-\alpha/2} - 2\right] d\eta\right] \tag{C.10}$$

Appendix D – Derivation of Predicted Stress from Strain Energy Equation

By definition, the stress is related to strain energy density, ϕ, by

$$\sigma_z = \frac{d\phi}{d\lambda_z} - p \tag{D.1}$$

where p is the hydrostatic pressure, which is assumed to be negligible, resulting in,

$$\sigma_z = \frac{d\phi}{d\lambda_z} \tag{D.2}$$

And ϕ is the strain energy density function from Ogden according to,

$$\phi = \frac{2\mu}{\alpha^2}\left(\lambda_x^\alpha + \lambda_y^\alpha + \lambda_z^\alpha - 3\right) \tag{D.3}$$

Since the material is assumed to be incompressible, the product of the stretch ratios is unity,

$$\lambda_x\lambda_y\lambda_z = 1 \tag{D.4}$$

Therefore,

$$\lambda_x = \lambda_y = \frac{1}{\sqrt{\lambda_z}} \tag{D.5}$$

Substitution of (D.5) into (D.3) results in,

$$\phi = \frac{2\mu}{\alpha^2}\left(\frac{1}{\lambda_z^{\alpha/2}} + \frac{1}{\lambda_z^{\alpha/2}} + \lambda_z^\alpha - 3\right) \tag{D.6}$$

can be further simplified,

$$\phi = \frac{2\mu}{\alpha^2}\left(\frac{2}{\lambda_z^{\alpha/2}} + \lambda_z^\alpha - 3\right) \tag{D.7}$$

Distributing across the parentheses gives,

$$\phi = \frac{4\mu}{\alpha^2}\lambda_z^{-\alpha/2} + \frac{2\mu}{\alpha^2}\lambda_z^\alpha - \frac{6\mu}{\alpha^2} \tag{D.8}$$

and differentiating with respect to λ_z results in,

$$\frac{d\phi}{d\lambda_z} = -\frac{4\mu}{2\alpha}\lambda_z^{-\alpha/2-1} + \frac{2\mu}{\alpha}\lambda_z^{\alpha-1} + 0 \tag{D.9}$$

Finally, factoring out $\frac{2\mu}{\alpha}$ results in the equation for stress employed in this research,

$$\sigma_z = \frac{d\phi}{d\lambda_z} = \frac{2\mu}{\alpha}\left(\lambda_z^{\alpha-1} - \lambda_z^{-1-\alpha/2}\right) \tag{D.10}$$

Appendix E – Calculating the Shear Modulus and Strain Hardening Exponent

From a least squares error equation for the calculated stress,

$$S = \left(\sigma_z - \hat{\sigma}_z\right)^2 \tag{E.1}$$

where σ_z is the measured stress in the direction of compression and $\hat{\sigma}_z$ is the calculated stress in the direction of compression. The calculated stress is derived from the strain energy density function,

$$\sigma_z = \frac{d\phi}{d\lambda_z} = \frac{2\mu}{\alpha}\left(\lambda_z^{\alpha-1} - \lambda_z^{-1-\alpha/2}\right) \tag{E.2}$$

Substituting this calculated stress into the least squares error equating gives

$$S = \left[\sigma_z - \frac{2\mu}{\alpha}\left(\lambda_z^{\alpha-1} - \lambda_z^{-1-\frac{\alpha}{2}}\right)\right]^2 \tag{E.3}$$

where the values of μ and α are determined from compression test date by minimizing S and selecting results in the admissible range.

Appendix F – Deriving the Fracture Toughness Equation

The components of the force measured when punching cartilage are

$$F_{total,1} = F_C + F_f + F_S \tag{F.1}$$

where F_C is the force required to create and propagate the crack in the material, F_f is the friction on the punch as it advances through the material, and F_S is the force required to stretch the diameter of the hole to the size of the punch.

From the fracture toughness, the work required to create and propagate the crack is

$$W_C = J_{IIC} dA \tag{F.2}$$

where A is the cylindrical area of the inside of the hole in the sample. Thus,

$$dA = (2\pi b) dz \tag{F.3}$$

where b is the radius of the final hole in the sample after the punch has been removed and dz is the instantaneous depth of the punch head. Therefore, the work required to create and propagate the crack is

$$W_C = J_{IIC}(2\pi b) dz \tag{F.4}$$

The work required to overcome friction as the punch advances is

$$W_f = F_f dz \tag{F.5}$$

The change in the stored internal recoverable strain energy potential due to the stretching of the hole to the diameter of the punch is $d\Delta$. Therefore, the work required to punch a hole in the cartilage sample is

$$W_{total,1} = F_{total,1} dz = J_{IIC}(2\pi b) dz + F_f dz + d\Delta \tag{F.6}$$

The second trial of the two-punch test is in the same location as the first trial. Therefore, the force of the second trial will be identical to that of the first trial, except the punch will not have to create or propagate a crack. Thus, the work required to advance the punch in the second trial will be

$$W_{total,2} = F_{total,2} dz = F_f dz + d\Delta \tag{F.7}$$

By subtracting the work on the punch during Trial 2 from the work on the punch in Trial 1, the remaining contribution to the work is only from the crack formation and propagation:

$$W_{total,1} - W_{total,2} = \left(F_{total,1} - F_{total,2}\right)dz = J_{IIC}(2\pi b)dz \tag{F.8}$$

By integrating both sides over the compressed distance,

$$\int_{z_0}^{z_1}\left(F_{total,1} - F_{total,2}\right)dz = \int_{z_0}^{z_1}\left(J_{IIC}\,2\pi b\right)dz \tag{F.9}$$

where z_0 is the depth of the punch at the moment that the punch breaks through the first surface (when the crack is formed) and z_1 is depth of the punch at the moment that the punch breaks through the second surface.

The term $J_{IIC}\,2\pi b$ on the right side of (F.9) can be moved outside of the integral because it is a constant,

$$\int_{z_0}^{z_1}\left(F_{total,1} - F_{total,2}\right)dz = J_{IIC}\,2\pi b\int_{z_0}^{z_1} dz \tag{F.10}$$

By dividing by $2\pi b\int_{z_0}^{z_1} dz$,

$$J_{IIC} = \left(\frac{1}{2\pi b}\right)\left[\frac{\int_{z_0}^{z_1}\left(F_{total,1} - F_{total,2}\right)dz}{\int_{z_0}^{z_1} dz}\right] \tag{F.11}$$

The integral in the numerator can be estimated by trapezoidal integration and the integral in the denominator can be simplified to $z_1 - z_0$:

$$J_{IIC} = \frac{\left\{\dfrac{\sum_{z_0}^{z_1}\left[z(t) - z(t-1)\right]\left[F_{total,1}(t) - F_{total,2}(t) + F_{total,1}(t-1) - F_{total,2}(t-1)\right]}{2}\right\}}{2\pi b\left[z_1 - z_0\right]} \tag{F.12}$$

which simplifies to

$$J_{IIC} = \frac{\sum_{z_0}^{z_1}\left[z(t) - z(t-1)\right]\left[\left(F_{total,1} - F_{total,2}\right)(t) + \left(F_{total,1} - F_{total,2}\right)(t-1)\right]}{4\pi b\left[z_1 - z_0\right]} \tag{F.13}$$

However, if both surfaces of the material crack simultaneously, and there is only one peak in the force profile, the numerator simplifies to the difference in the max forces of the two trials and the $\left[z_1 - z_0\right]$ drops out of the denominator, resulting in

$$J_{IIC} = \frac{F_{total,1} - F_{total,2}}{2\pi b} \tag{F.14}$$

Appendix G – Summary of Shear Modulus and Strain-Hardening Exponent Data

Table G.1: Calculated shear modulus (μ) and strain-hardening exponent (α) from compression testing of hydrated and dry samples of cartilage between wax paper

Trial	Hydrated		Dry	
	μ	α	μ	α
1	0.13784445	1.41970256	0.95989776	2.39488763
2	0.16653272	1.62818663	0.43830985	4.76387433
3	0.18696857	1.68085606	0.33352685	1.76534675
4	0.12194216	1.26644618	0.29928771	1.57130301
5	0.14303965	1.45533334	0.43726608	1.7684658
Average	0.15126551	1.49010495	0.49365765	2.4527755